2006

External Cavity Multiwavelength Semiconductor Mode-locked Laser Gain Dynamics

Luis Archundia-Berra
University of Central Florida

EXTERNAL CAVITY MULTIWAVELENGTH SEMICONDUCTOR MODE-LOCKED LASER GAIN DYNAMICS

by

LUIS CARLOS ARCHUNDIA-BERRA
B.S. Instituto Tecnológico de Puebla, Mexico, 1994
M.S. INAOE, Mexico, 1998
M.S. University of Central Florida, 2000

A dissertation submitted in partial fulfillment of the requirements
for the degree of Doctor of Philosophy
in the College of Optics and Photonics / CREOL & FPCE
at the University of Central Florida
Orlando, Florida

Fall Term
2006

Major Professor: Peter J. Delfyett, Jr.

ABSTRACT

External cavity semiconductor mode-locked lasers can produce pulses of a few picoseconds. The pulses from these lasers are inherently chirped with a predominant linear chirp component that can be compensated resulting in sub-picosecond pulses. External cavity semiconductor mode-locked lasers can be configured as multiwavelength pulse sources and are good candidates for time and wavelength division multiplexing applications. The gain medium in external cavity semiconductor mode-locked lasers is a semiconductor optical amplifier (SOA), and passive and hybrid mode-locked operation are achieved by the introduction of a saturable absorber (SA) in the laser cavity. Pump-probe techniques were used to measure the intracavity absorption dynamics of a SA in an external cavity semiconductor mode-locked laser and the gain dynamics of a SOA for the amplification of diverse pulses. The SOA gain dynamics measurements include the amplification of 750 fs pulses, 6.5 ps pulses, multiwavelength pulses and the intracavity gain dynamics of an external cavity multiwavelength semiconductor mode-locked laser. The experimental results show how the inherent chirp on pulses from external cavity semiconductor mode-locked lasers results in a slow gain depletion without significant fast gain dynamics. In the multiwavelength operation regime of these lasers, the chirp broadens the temporal pulse profile and decreases the temporal beating resulting from the phase correlation among wavelength channels. This results in a slow gain depletion mitigating nonlinearities and gain competition among wavelength channels in the SOA supporting the multiwavelength operation of the laser. Numerical simulations support the experimental results.

To my sons Pepe and Luis, my wife Ana and my parents Carlos and Nicolasa.

ACKNOWLEDGMENTS

I want to express my gratitude to my advisor Dr. Peter Delfyett for his guidance and support. His encouragement carried me on through difficult times and his insights and suggestions keep me going on the right direction.

Thanks to the Ultrafast Photonics group members, Myoung-Taek Choi, Chris DePriest, Jenifer Evans, Hossein Izadpanah, Ji-Myoung Kim, Leonard Kisimbi, Shinwook Lee, Wankuen Lee, Dimitrios Mandridis, Brian Mathason, Shan Mitra, Ikuko Nitta, Max Obando, Sarper Ozharar, Eric Park, Scott Rozzo, Robert Stegeman, Erica Wells and Tolga Yilmaz and specially Sangyoun Gee, Kyungbum Kim, Franklyn Quinlan and Bojan Resan for their help and support during my graduate studies.

I would like to thank the professors than contributed to my academic formation, the CREOL staff members who helped me during my graduate years and the members of my dissertation committee, Dr. Patrick L. LiKamWa, Dr. George I. Stegeman and Dr. Florencio E. Hernandez, for their interest and suggestions.

I must recognize the efforts of my parents who made me the person I am and who worked hard to support my former education. I also thank my wife for her support and my two sons who are my biggest motivation.

TABLE OF CONTENTS

LIST OF FIGURES

CHAPTER ONE:
INTRODUCTION

1.1 Motivation

Semiconductor lasers are compact, efficient, reliable and inexpensive and can be electrically biased and modulated. These qualities make semiconductor lasers attractive for a broad range of applications including CD and DVD players, metrology equipment, fiber optic communication systems and high power pump sources for solid state and fiber lasers.

Laser action in a semiconductor material was first demonstrated in 1962 [1-4] and it was immediately seen as a breakthrough that would revolutionize the industry. The development of double-heterostructure semiconductor lasers by 1970 reduced the continuous wave emission threshold and allowed the operation of these lasers at room temperature. Advancements in metalorganic chemical vapor deposition and molecular beam epitaxy enabled the fabrication of quantum well lasers by 1975 [7] and quantum dot lasers more recently [8].

The broad optical bandwidth of semiconductors suggested they could support pulses shorter than 100 fs and investigation of pulse generation from laser diodes began soon after the invention of the laser diode [9]. An important advance in the generation of ultra short pulses from semiconductor lasers was achieved with the first active mode-locking external cavity semiconductor laser [10], followed by its extensive investigation experimentally [11-12] and theoretically [13-16].

Passive mode-locking of semiconductor lasers has also been extensively investigated. In its beginnings, defects were created in the semiconductor laser introducing saturable absorption by optical damage to achieve passive mode-locking operation [17-19]. These lasers produced pulses from several hundred femtoseconds to a few picoseconds, but as a result of the degradation of the diode due to the defects, the lifetimes were limited to several hours of operation. The use of proton bombarded multiple quantum well saturable absorbers in external cavity semiconductor lasers allowed the passive mode-locked operation of these lasers without the need of the introduction of defects in the diode [20]. Further work with external cavity semiconductor mode-locked lasers lead to the achievement of 200 fs pulses after dispersion compensation and 185 fs pulses from a dispersion managed ring laser [21, 22].

Time division multiplexing (TDM) and wavelength division multiplexing (WDM) are techniques used to exploit the information transmission capabilities of optical fiber communication systems, reaching terabits per second transmission rates [23-25]. The availability of compact, reliable and cost effective multiwavelength pulse sources is of great importance for these systems. Light from superluminescent diodes [26, 27], spontaneous emission from fiber amplifiers [28], super-continuum generation from fiber [29-31], and femtosecond lasers [32-34], are examples of sources that have been spectrally sliced to be used as multiwavelength sources. An alternative to the spectral slicing of broad band sources is the use of multiwavelength lasers, where multiple wavelength channels are produced directly from one laser source.

External cavity semiconductor mode-locked lasers have been configured as multiwavelength lasers, and have proven to be attractive candidates for TDM and WDM applications [35-38]. Up to 168 wavelength channels at 6 GHz have been obtained from a single external cavity semiconductor laser yielding an aggregate pulse rate of 1 THz, [38]. Furthermore,

the availability of semiconductor lasers at all the optical communications transmission windows and its compatibility with existing communications systems place semiconductor lasers in a strategic position for applications in optical communications.

In order to continue improving the performance of external cavity semiconductor mode-locked lasers it is necessary to understand the pulse evolution and the gain dynamics of these lasers. Pump-probe techniques were used to measure the absorption dynamics of a multiple quantum well saturable absorber, the gain dynamics of a semiconductor optical amplifier (SOA) for the amplification of short pulses, long pulses and multiwavelength pulses and the intracavity gain dynamics of an external cavity semiconductor mode-locked laser under multiwavelength operation, revealing the mechanisms that support the mode-locked operation of semiconductor lasers. The conclusions derived from this dissertation can be used to overcome the difficulties encountered and improve the performance of these lasers.

1.2 Dissertation overview

This section briefly describes the content of each chapter and provides a general overview of this dissertation.

Chapter Two describes the semiconductor optical amplifiers (SOAs) and the saturable absorbers (SAs) employed in the experiments presented in this dissertation; these two elements are the heart of external cavity semiconductor mode-locked lasers. Active, passive and hybrid mode-locking operation of external cavity semiconductor lasers are described and the main considerations for passive mode-locking operation are reviewed. This chapter also shows the

configuration of a double pass dual grating dispersion compensator used to compress the pulses from the external cavity semiconductor mode locked lasers by linear dispersion compensation.

Pump-probe techniques were used for all the SOA gain dynamics measurement as well as for the SA absorption measurements presented in this dissertation.

In Chapter Three the main gain dynamics of SOAs are reviewed, the experimental results for the measurement of the gain dynamics of a SOA for the amplification of 750 fs and 6.5 ps are presented and the evolution of the pulses in an external cavity semiconductor hybrid mode-locked laser is analyzed. Carrier heating, carrier cooling and a subsequent self-phase modulation are observed for the amplification of 750 fs pulses and it is shown how these effects decrease when the longer 6.5 ps pulses are amplified.

Chapter Four presents the experimental results of the measurement of the absorption dynamics of a multiple quantum well saturable absorber. The saturable absorber absorption dynamics was measured using sub-picosecond pump and probe pulses obtained from an external cavity semiconductor mode-locked laser. The intracavity saturable absorber absorption dynamics of an external cavity semiconductor mode-locked laser was also measured; in this case, the saturable absorber under test is used to mode-locked the laser and the pulses from this laser are compressed and used as a probe to measure the saturable absorber absorption dynamics without disturbing the laser operation.

The fifth chapter introduces the multiwavelength operation of external cavity semiconductor mode-locked lasers and presents the experimental results of the measurements of the gain dynamics of a SOA for the amplification of multiwavelength pulses and the experimental results of the measurements of the intracavity gain dynamics of an external cavity semiconductor hybrid mode-locked laser under multiwavelength operation. The multiwavelength

pulses used for the measurements of the SOA gain dynamics for the amplification of multiwavelength pulses were obtained by spectrally slicing the pulses from an external cavity semiconductor mode-locked laser and the measurements were made for pulses containing the chirp of the pulse source and dispersion compensated pulses. The intracavity gain dynamics measurements of the external cavity semiconductor hybrid mode-locked laser under multiwavelength operation reveal a temporal skew among pulses corresponding to different wavelength channels and a slow depletion of the SOA gain with no significant nonlinearities, supporting the multiwavelength operation of the laser.

The results of the numerical simulations of the gain dynamics of a SOA for the different experimental cases analyzed in this dissertation are presented in Chapter Six. The numerical simulations agree well with the experimental results and support the conclusions derived from this work. The MATLAB programs used for the simulations are included in the Appendix.

The last chapter (Chapter Seven) summarizes and concludes this dissertation.

CHAPTER TWO:
EXTERNAL CAVITY SEMICONDUCTOR MODE-LOCKED LASERS

2.1 Introduction

There have been huge advances in the performance of external cavity semiconductor mode-locked lasers, from the first active semiconductor mode-locked laser [10], to the generation of 185 fs from a breathing mode semiconductor mode-locked ring lasers [22] and the multiwavelength operation of semiconductor mode-locked lasers [38]. In this chapter, the main elements of external cavity semiconductor mode-locked lasers are reviewed, and passive, active and hybrid mode-locking operation regimes are described.

2.2 Gain media

The gain media of external cavity semiconductor mode locked lasers is a semiconductor optical amplifier (SOA) or superluminescent diode (SLD). A SOA or SLD is a laser diode with suppressed facet reflectivity that can amplify an injected optical signal by means of stimulated emission [39, 40]. The effective reflectivity of the facets is reduced by antireflection coatings and the tilting of the active stripe to prevent the coupling of the residual light reflected on the facets back into the active area. Residual effective facet reflectivity results in a modulation of the SOA spontaneous emission spectrum due to the Fabry-Perot etalon formed by the SOA facets [41].The

high SOA gain amplifies the reflected light coupled back into the SOA and enhances the spectral modulation, thus a very low facet reflectivity is required.

The SOAs used in the experiments reported in this dissertation were provided by Sarnoff Corporation and are AlGaAs based double heterostructure devices. The SOAs are 350 μm long, antireflection coated and the active area is tilted 5º respect to the facets normal [40]. Figure 2.1 shows the layer structure and composition of one of these SOAs.

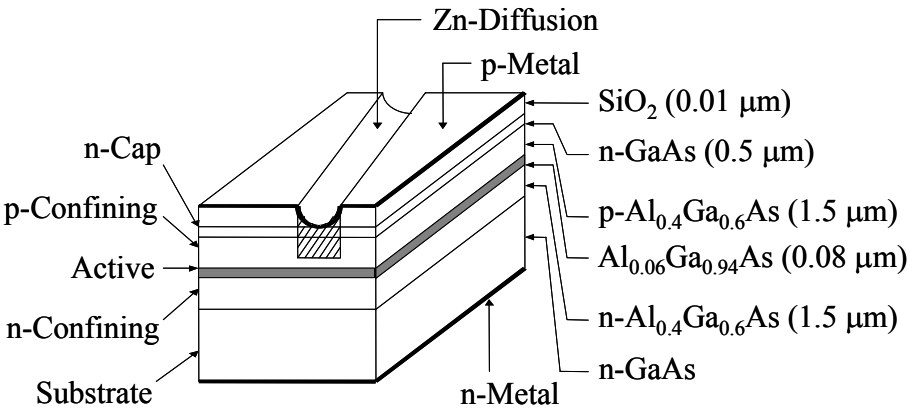

Figure 2.1: Semiconductor optical amplifier (SOA).

Figure 2.2 shows a picture of a mounted SOA. The SOA is soldered p-side down in a gold coated copper stud for a good heat dissipation and electrical conduction. The thickness of the copper stud must closely match the length of the SOA. If the SOA is longer than the stud, overheating on the SOA ends may lead to its damage and if the SOA is shorter than the stud, the light emitted by the SOA may be partially blocked by the stud. A ceramic stand with gold coatings on the top and bottom is also soldered on the stud. A gold wire of 25 μm diameter connects the top of the ceramic stand and the n-side of the SOA. The SOA is biased with a

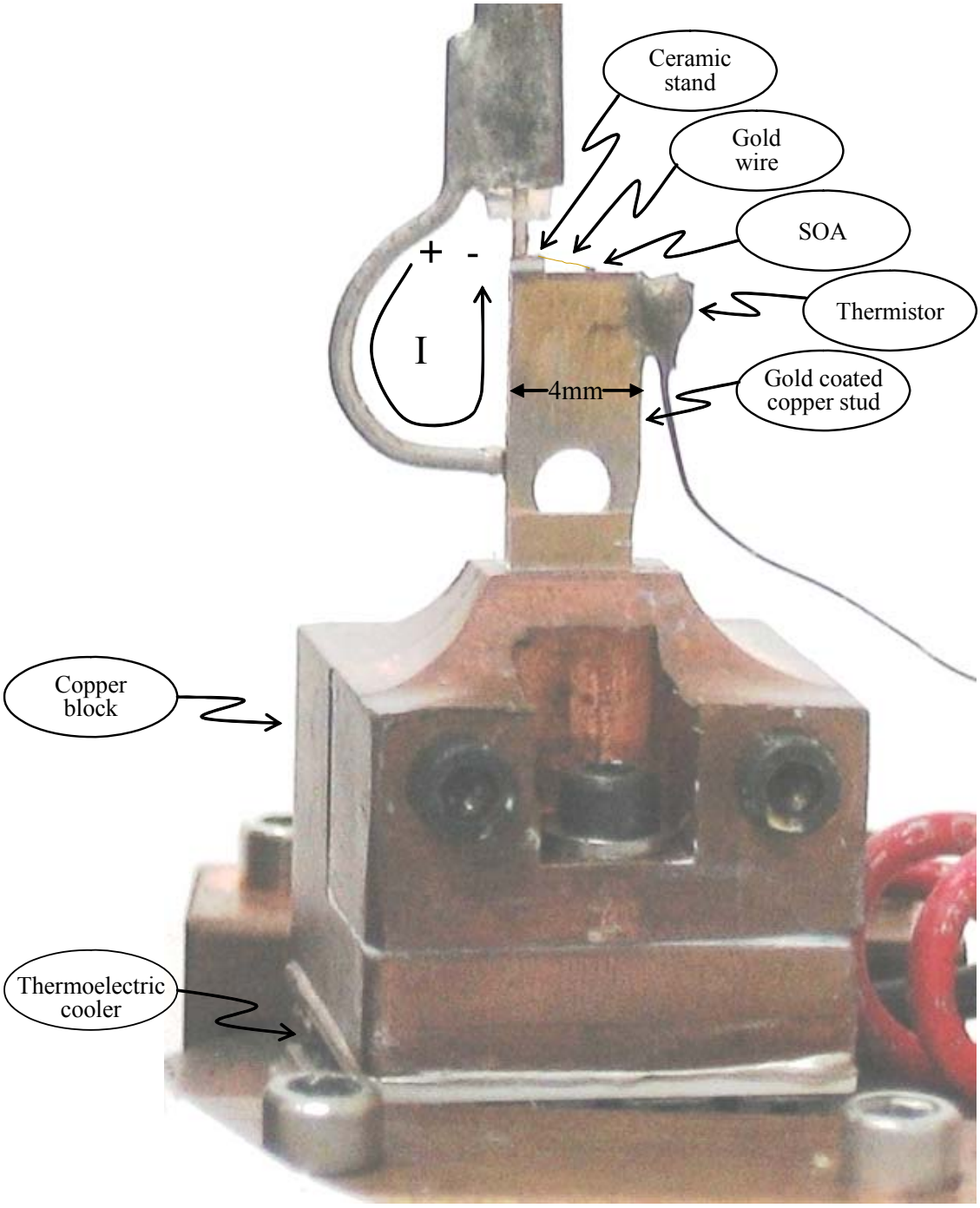

Figure 2.2: Picture of a mounted SOA

current source and electrical contact is made with the stud (SOA p side) and the top of the ceramic stand (SOA n side). The ceramic stand avoids mechanical contact with the SOA preventing its damage. The copper stud is attached to a copper block glued on top of a thermoelectric cooler using silver epoxy. The temperature of the stud is monitored with a thermistor. A temperature controller biases the thermoelectric cooler and keeps the stud temperature constant a few degrees below room temperature with a temperature stability better than 0.1º C.

Figure 2.3 shows the SOA light-current curve (L-I) and the SOA spontaneous emission spectrum measured for a DC bias of 200 mA. The L-I curve shows a typical exponential spontaneous emission power increase as a function of the biased current and the small modulation of the spontaneous emission spectrum is a result of the residual facet reflectivity.

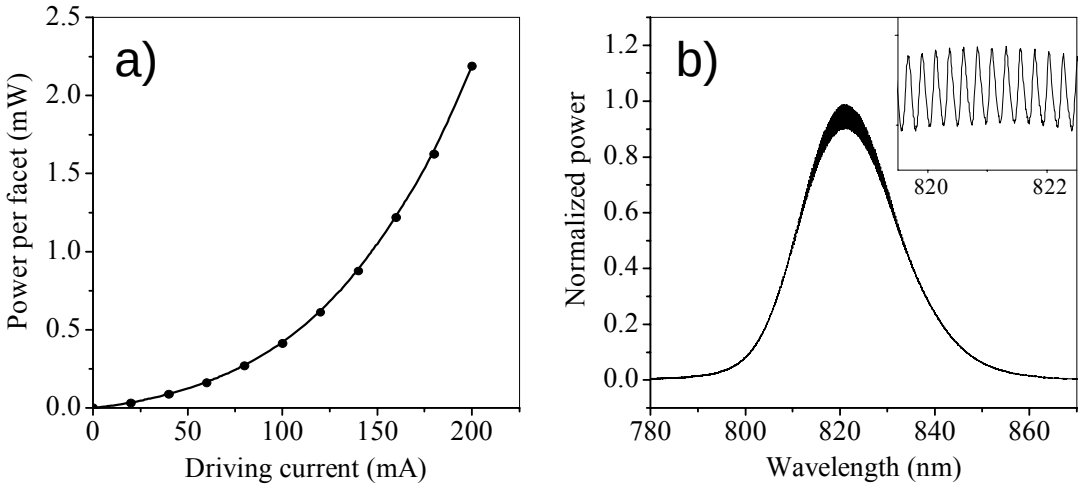

Figure 2.3: L-I curve and spontaneos emission spectrum.

2.3 Saturable absorber

Multiple quantum well saturable absorbers were used to passively or hybridly mode-lock the external cavity semiconductor mode-locked lasers in the experiments presented in this dissertation. The mechanism used to passively or hybridly mode-lock these lasers is the bleaching of the saturable absorber by the saturation of the quantum wells exitons [42, 43]. The multiple quantum well saturable absorbers used were fabricated by growing a series of multiple quantum wells on a mirror stack or by eliminating the substrate from a multiple quantum well structure, then attaching the quantum wells on a gold mirror by Van Der Waals bonding [44,45]. The saturable absorbers were designed to have an exitonic absorption peak around 830 nm and the position of the exitonic absorption peak is a function of the quantum well thickness. An exitonic absorption peak around 830 nm at room temperature corresponds to a well thickness of 70 Å. The spontaneous emission spectrum of a SOA was used as a reference to measure the reflection spectrum of two of these saturable absorber mirrors and the measured spectra are shown in Figure 2.4. The first saturable absorber (SA1) contains 100 periods of 70 Å GaAs wells separated by AlGaAs barriers of 100 Å grown on a mirror stack. The second saturable absorber (SA2) contains GaAs wells of 70, 75, and 80 Å separated by 100 Å AlGaAs barriers obtaining a broader absorption band by changing the well thickness [46]. All the saturable absorbers used in the experiments presented in this dissertation are proton implanted with a single dose of 200 KeV protons with a density of aproximately$10^{13}/cm^2$, creating recombination centers and

decreasing the saturable absorber recovery time from approximately 30 ns to a few hundred picoseconds [47].

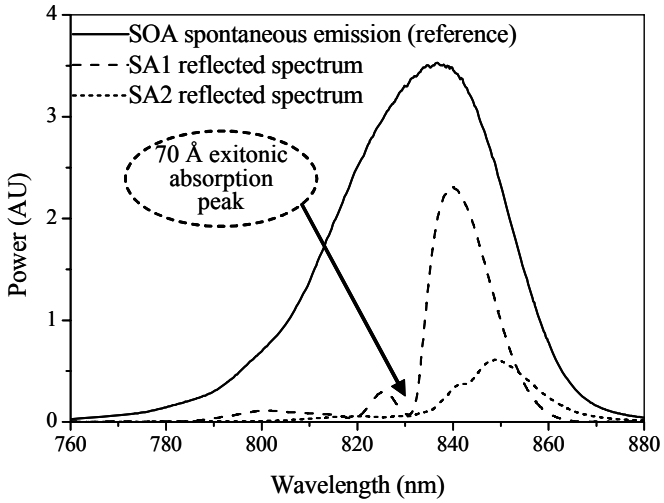

Figure 2.4: SOA spontaneous emission reference spectrum (──), SA1reflected spectrum (---) and SA2 reflected spectrum (….).

2.4 Active, passive and hybrid mode-locking of external cavity semiconductor lasers

In its basic form an external cavity semiconductor mode-locked laser includes a semiconductor optical amplifier (SOA), an output coupler and a back mirror or saturable absorber mirror. Figure 2.5 shows a diagram of a basic external cavity semiconductor laser. The SOA is the gain media and two lenses are used to collimate the light emitted by it. Two more lenses are used to focus the light on the back mirror and the output coupler adding cavity stability.

The laser can be actively mode-locked by DC biasing the SOA close to threshold and then modulating the DC bias with a radio frequency (RF) signal. The DC and the RF bias are

combined using a bias tee. The period of the radio frequency signal must match the cavity round trip time (fundamental mode-locking) or divide the cavity round trip time by an integer number (harmonic mode-locking). For fundamental mode-locking operation there is only one pulse in the laser cavity at any time and for harmonic mode-locking operation there are as many pulses in the cavity as the ratio between the cavity round trip and the period of the RF signal.

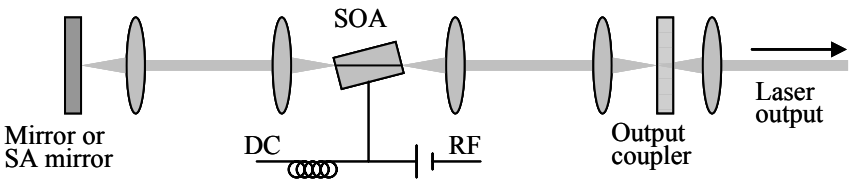

Figure 2.5: Basic external cavity semiconductor mode-locked laser.

Passive mode-locking is achieved by substituting the back mirror of Figure 2.5 for a saturable absorber mirror and biasing the SOA at the proper DC level. Active mode-locking is more stable than passive mode-locking due to the active modulation of the bias current, but passive mode-locking yields pulses with a better organized chirp allowing for sub-picosecond pulses after linear dispersion compensation [48].

The laser can be hybridly mode-locked combining active and passive mode-locking techniques. Typically the laser is passively mode-locked first; then, a RF signal at the repetition rate of the laser is combined with the DC bias using a bias tee adding stability to the laser.

External cavity semiconductor mode-locked lasers produce chirped pulses with a predominately linear chirp, pulse durations typically longer than 5 ps and average output powers of a few milliwatts [48]. The linear chirp of these pulses can be compensated resulting in sub-picosecond pulses. Figure 6 shows a typical spectrum and autocorrelation of an external cavity

semiconductor hybrid mode-locked laser, where Figure 2.6b shows the autocorrelation of the pulses directly from the laser and after linear dispersion compensation.

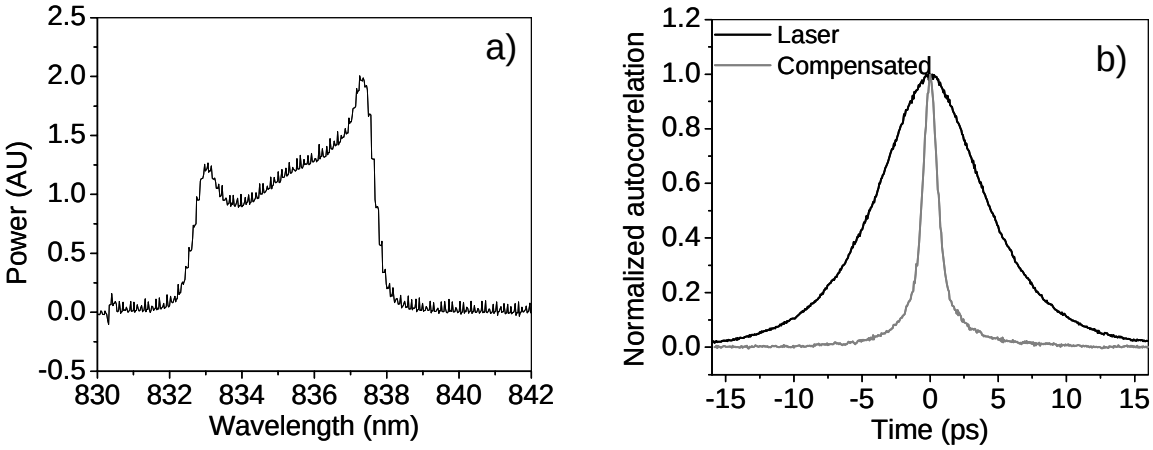

Figure 2.6: Typical spectrum and autocorrelation of an external cavity semiconductor hybrid mode-locked laser

2.5 Passive mode-locking general considerations

Two conditions must be satisfied for passive mode-locking operation of external cavity semiconductor mode-locked lasers. The saturation intensity of the gain media (SOA) must be larger than the saturation intensity of the saturable absorber and the recovery time of the gain media must be longer than the recovery time of the saturable absorber [49]. Since the intensity saturation of the exitons is approximately ten times smaller than the saturation intensity of band to band absorption, the first condition is satisfied. The second condition is satisfied by the reduction of the recovery time of the saturable absorbers after proton implantation and keeping a

small beam size on the saturable absorber using a tight focusing lens also helps to decrease the SA recovery time by carrier diffusion [47].

When the laser is passively mode-locked, the intracavity pulse is amplified when it passes through the SOA depleting the SOA. When this amplified pulse reaches the saturable absorber mirror, the pulse leading edge is absorbed, bleaching the saturable absorber and allowing the rest of the pulse to be reflected. The combination of the gain depletion and the bleaching of the saturable absorber open a time window that allows the pulse formation [47, 50]. By the time the intracavity pulses completes a cavity round trip the SOA gain has recovered and the saturable absorber has returned to its unbleached state.

The repetition rate of the laser depends on the cavity length and the recovery time of the SOA. If the cavity round trip is longer than the recovery time of the SOA the laser will produce more than one pulse per cavity round trip (harmonic mode-locking).

Another important consideration for passive mode-locking is the match of the SOA spectral gain peak and the saturable absorber spectral absorption peak. If the peak of the SOA gain does not match well with the exitonic absorption peak, the laser can not be passive mode-locked and it will continuous wave lase (CW lase) at the minimum loss (maximum gain) wavelength. In general, each element in the laser cavity has its own spectral response and the combination of all the cavity elements defines the overall gain spectrum. Figure 2.7 shows the laser cavity, the pulse spectrum and the pulse autocorrelation of an external cavity semiconductor passive mode-locked laser for which a spectral filter had to be introduced to shift the spectral gain peak to the absorption band of the saturable absorber. Without the filter, the laser CW lases on the long wavelength side of the spectrum.

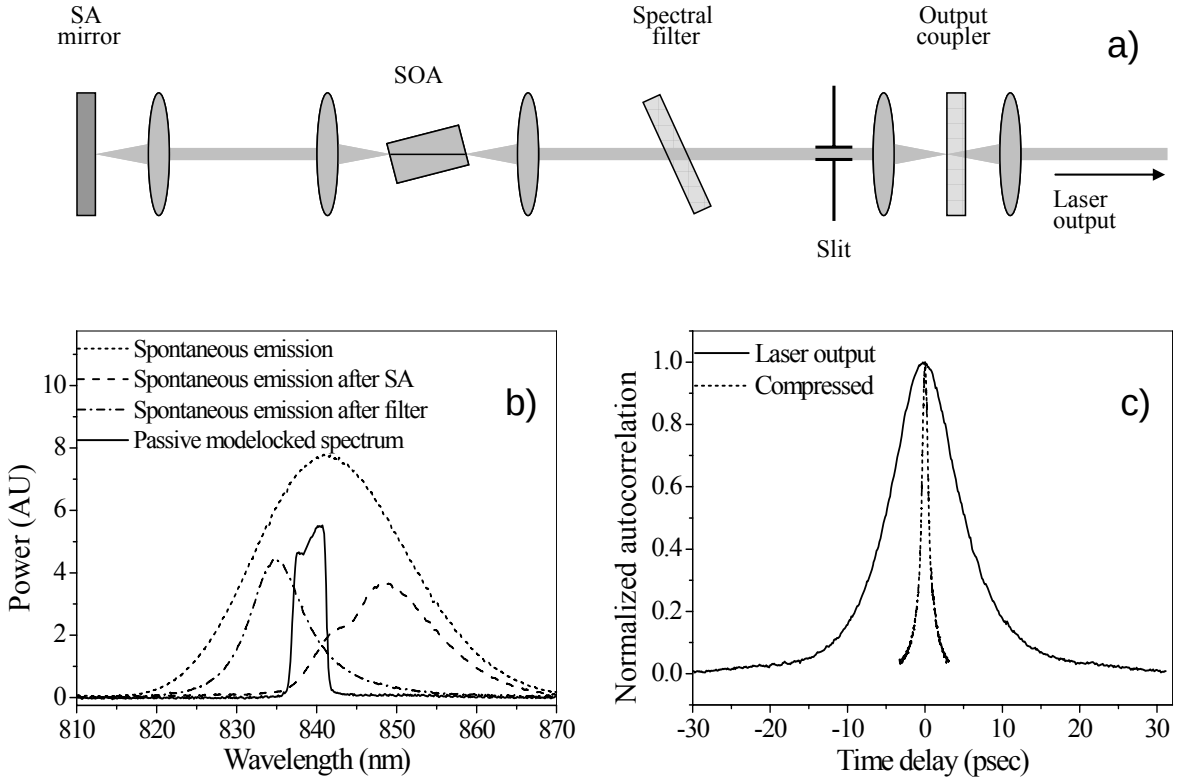

Figure 2.7: External cavity semiconductor passive mode-locked laser cavity, pulse spectrum and autocorrelation

Figure 2.7b shows the spectrum of the SOA spontaneous emission, the spectrum of the SOA spontaneous emission reflected by the saturable absorber mirror, the spectrum of the SOA spontaneous emission transmitted by the spectral filter and the spectrum of the pulses once the laser is passively mode-locked. It is clear from the plot of the spectrum of the SOA spontaneous emission reflected by the saturable absorber mirror that the laser can not operate at wavelengths shorter than the exitonic absorption band due to the high absorption of the multiple quantum well saturable absorber at those wavelengths. If the spectral filter is not used in the laser cavity, the high reflectivity of the saturable absorber mirror at wavelengths longer than the exitonic

absorption band results in the CW lasing of the laser in this spectral region. The introduction of the spectral filter forces the laser to operate on the exitonic absorption band, bleaching the saturable absorber and attaining passive-mode-locked operation. The pulses from this laser are approximately 7 ps long and are highly chirped and far from Fourier transform limited. The laser pulses were compressed to approximately 800 fs by the compensation of the linear chirp of the pulses. Figure 2.7c shows the autocorrelation of the pulses obtained directly from the laser and after dispersion compensation.

For all the experimental results presented in this dissertation, the duration of the pulses is calculated from the measured pulse autocorrelations assuming squared secant hyperbolic pulses.

2.6 Dispersion compensation

The dispersion compensators used in the experiments reported in this dissertation are dual grating double pass dispersion compensators [51, 52] with a one-to-one telescope. Figure 2.8 depicts one of these dispersion compensators. The two lenses in the dispersion compensator are separated by a distance equal to twice the focal length *f*, forming a one-to-one telescope and creating an inverted image of the input beam on the first grating at a distance *f* to the right of the second lens (zero dispersion point). This is equivalent to have the first grating parallel to the second one located at the zero dispersion point. The dispersion introduced by the dual grating dispersion compensator is proportional to the distance between the second grating and the zero dispersion point and the configuration used allows the addition of positive or negative dispersion to the pulses being dispersion compensated. Negative dispersion is added by moving the second

grating to the right of the zero dispersion point and positive dispersion is added by moving the second grating to the left. A roof mirror is used after the second grating to translate the beam up and reflect the pulses back to the dispersion compensator allowing the separation of the input and output beams and double passing the pulses through the dispersion compensator. The double pass configuration prevents the distortion of the pulses and doubles the dispersion introduced by the dispersion compensator [53]. The configuration of the dispersion compensator also allows the spectral filtering of the pulses being dispersion compensated, the first grating disperses the input beam in the horizontal plane and the first lens focuses each wavelength into a point along a line at a distance *f* from this lens. Spectral filtering can be done at this plane (Fourier plane) using a spatial filter.

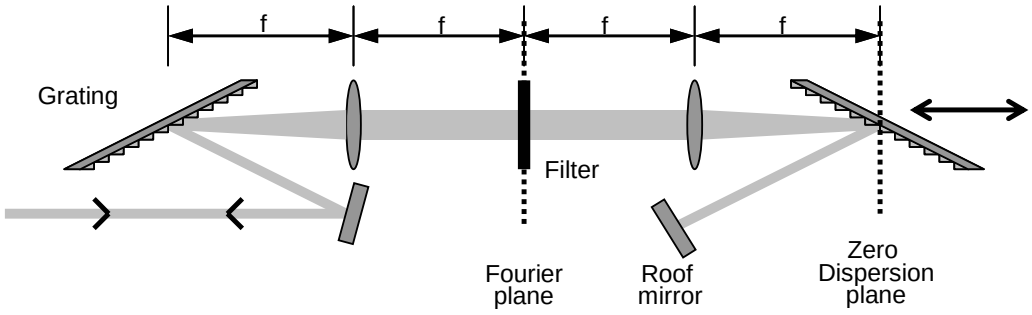

Figure 2.8: Dual grating dispersion compensator and spectral filter (top view).

Two grating dispersion compensators were built. The first uses 1800 lines/mm gratings and 30 cm focal length lenses and has an input angle of 42.2º with respect to the grating normal, yielding a dispersion of approximately 0.58 ps/(nm.cm). The second dispersion compensator uses 2000 lines/mm gratings and 15 cm focal length lenses and has an input angle of 50.1º with

respect to the grating normal yielding a dispersion of 1.2 ps/(nm.cm). Both dispersion compensators were aligned for a center wavelength of 835 nm.

CHAPTER THREE:
INTRACAVITY PULSE DYNAMICS

3.1 Introduction

In this chapter the main gain dynamics for the amplification of pulses from external cavity semiconductor mode-locked laser are presented, as well as the results of the measurements of the absorption dynamics of a saturable absorber mirror.

3.2 Semiconductor optical amplifier gain dynamics

From a simple point of view a semiconductor optical amplifier (SOA) is a laser diode with suppressed facet reflection which operates as a light amplifier or gain media. Electrons are pumped from the valence band to the conduction band by DC biasing the SOA, creating a carrier population inversion. When an optical pulse is coupled into a biased SOA, the exited electrons in the conduction band are depleted by stimulated amplification of the injected pulse decreasing the SOA gain. The SOA gain and index of refraction are coupled through the Kramers-Kronig relations such that a decrease of the SOA gain results in an increase of the index of refraction and vice versa. Figure 3.1 illustrates qualitatively the amplification of an optical pulse in a SOA. The electrical current flowing through the SOA pumps electrons to the conduction band and the SOA gain recovers in a nanosecond time scale [48].

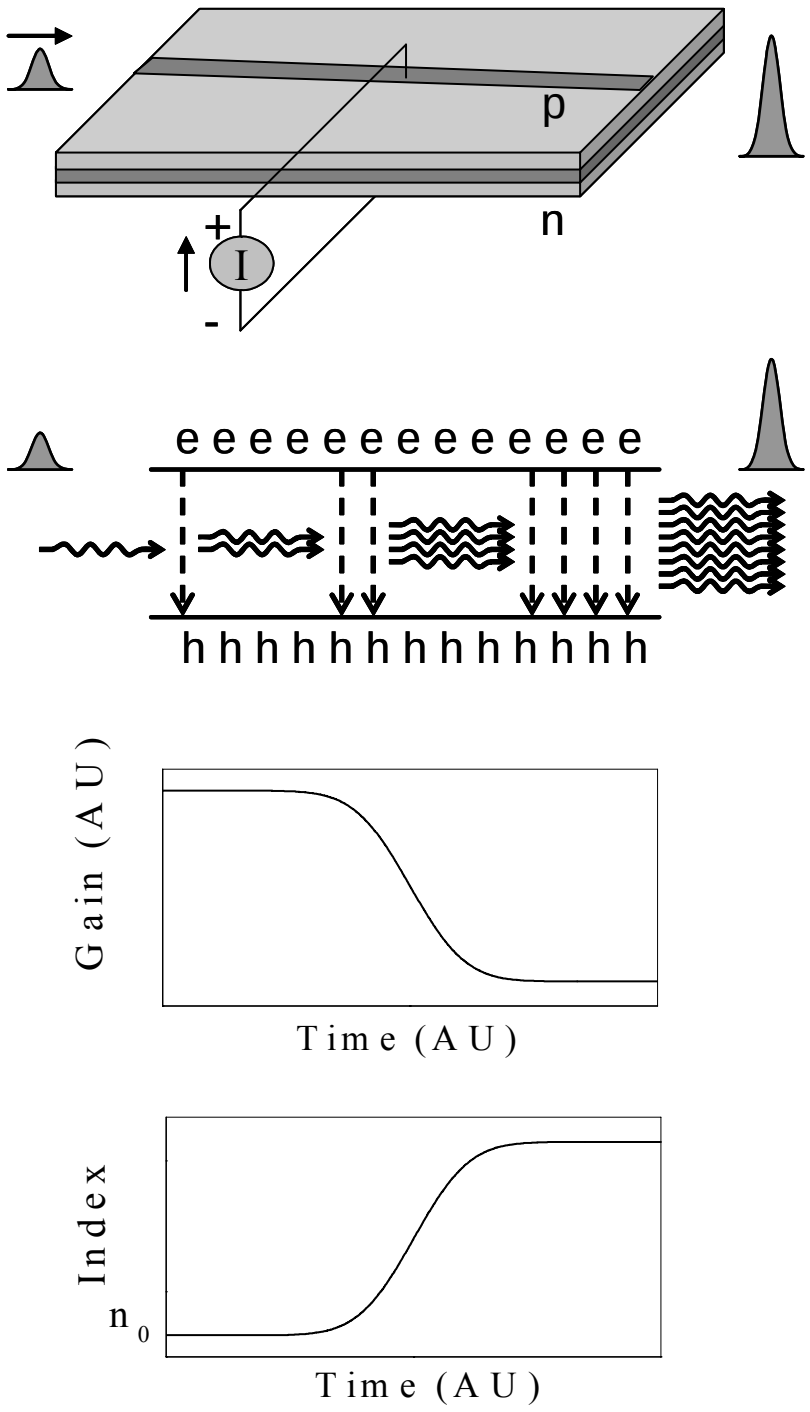

Figure 3.1: Qualitative illustration of the amplification of an optical pulse in a SOA.

The amplification of pulses longer than approximately 2 ps in a SOA follows the gain dynamics described above, but when shorter pulses are amplified, the SOA gain and index of refraction are modified by free carrier absorption, two photon absorption and stimulated transitions resulting in spectral hole burning, carrier heating, carrier cooling and carrier density changes [48, 54-56]. The absorption of photons by free electrons or holes promotes carrier high up into the band and these energetic carriers heat up (carrier heating) the carrier distribution, two photon absorption also changes the carrier distributions resulting in carrier density changes and carrier heating and stimulated emission causes carrier density changes, spectral hole burning and carrier heating. Figure 3.2 shows the qualitative evolution of the carrier distribution in a SOA induced by an ultra short pulse.

The gain and index changes due to intra-band dynamics increase as the duration of the amplified pulse decreases and the importance of the ultra fast carrier dynamics depends on the time scale of the amplified pulses. The duration of the pulses from external cavity semiconductor mode-locked lasers involved in the experiments reported in this dissertation range from a few hundred femtoseconds to hundreds of picoseconds and a result, spectral hole burning and carrier scattering are not observed.

When a pulse of light is amplified in a SOA, the pulse induces a dynamic gain change in the SOA and consequently a dynamic index of refraction, modulating the temporal phase of the pulse (self phase modulation). This phase modulation leads to an instantaneous frequency proportional to the negative derivative of the index of refraction with respect to time ($\omega_{inst}(t) \propto -\partial n(t)/\partial t$) [57, 58].

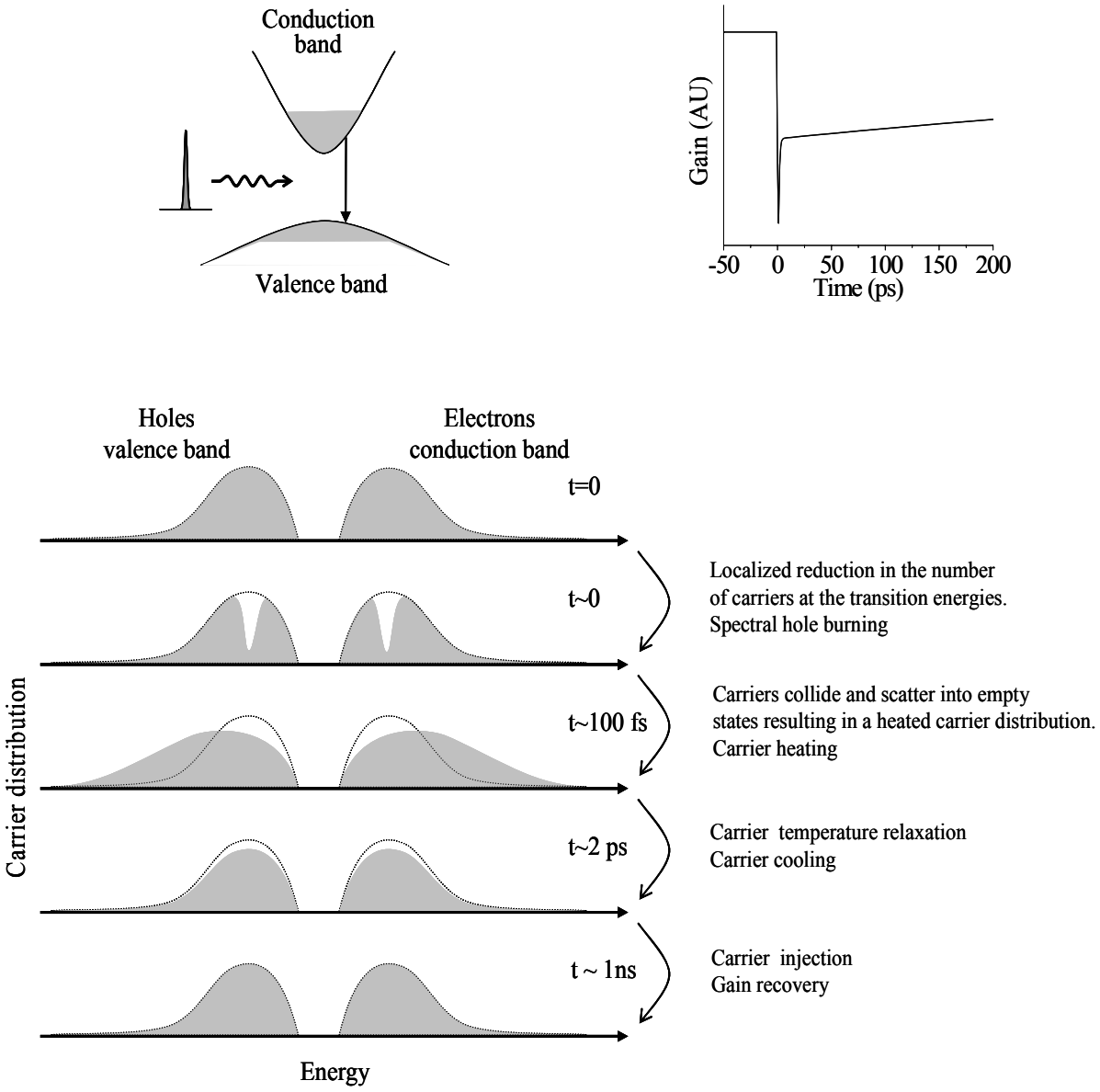

Figure 3.2: Carrier distribution evolution in a SOA induced by the amplification of an ultra short pulse.

If long pulses are amplified in a SOA, the gain is slowly depleted increasing the index of refraction, resulting in an instantaneous frequency shifted to low frequencies modifying the pulse

spectrum and temporal profile. A pulse is considered long if its temporal duration is longer than the SOA carrier cooling time (approximately one to two picoseconds). If pulses shorter than the SOA carrier cooling time are amplified, an additional instantaneous gain reduction due to carrier heating is observed. As the hot carriers cool back to equilibrium, the gain partially recovers, resulting in an instantaneous frequency shifted to high frequencies. Thus, for the amplification of pulses shorter than the SOA carrier cooling time, the instantaneous frequency moves from low frequencies to high frequencies as the short pulses are amplified. Figure 3.3 summarizes the self-phase modulation effects in SOAs for the amplification of pulses longer and shorter than the carrier cooling time constant.

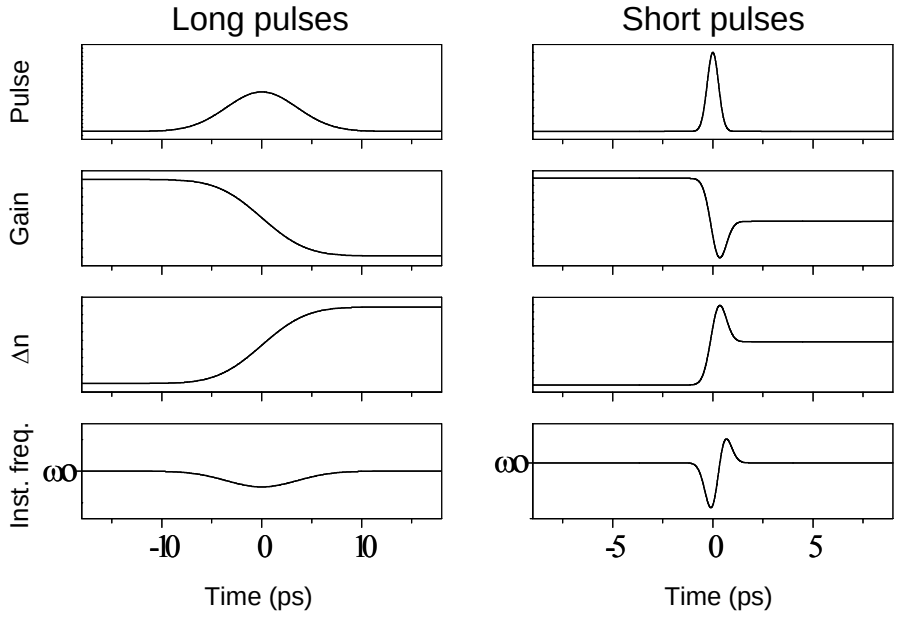

Figure 3.3: Self-phase modulation effects in SOAs for the amplification of pulses longer and shorter than the SOA carrier cooling time.

3.3 Measurement of the gain dynamics of a SOA for the amplification of pulses shorter and longer than the SOA carrier cooling time constant

The gain dynamics of a SOA were measured for the amplification of 750 fs and 6.5 ps pulses using pump-probe techniques. The pump-probe experimental setup is shown in Figure 3.4. An external cavity semiconductor mode-locked laser was used as the pulse source for the pump and the probe and is sketched in Figure 3.5a. This laser produces pulses of approximately 6.5 ps with a predominantly linear up chirp at a repetition rate of 270 MHz and with 4 mW of average output power.

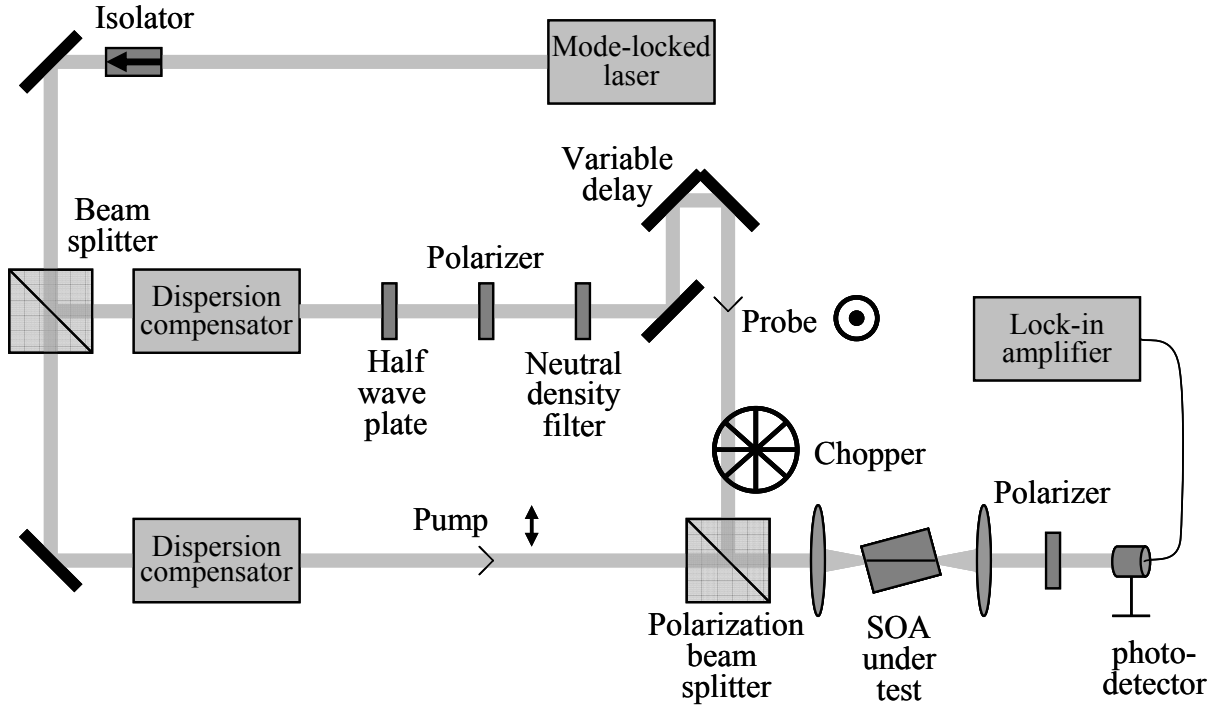

Figure 3.4: Experimental setup used for the measurement of the gain dynamics of a SOA for the amplification of 6.5 ps and 750 fs pulses.

The laser output is split in two beams, 90% of the laser power is used for the pump and the rest for the probe. The probe pulses are compressed to approximately 750 fs using a dual grating dispersion compensator like the one shown in Figure 2.8. Figures 3.5b and 3.5c show the spectrum and autocorrelation of the probe pulses after linear dispersion compensation. The probe polarization is rotated 90^{o} and a variable filter is used to decrease its power. The probe power is such that no significant gain changes are induced on the SOA under test by the probe.

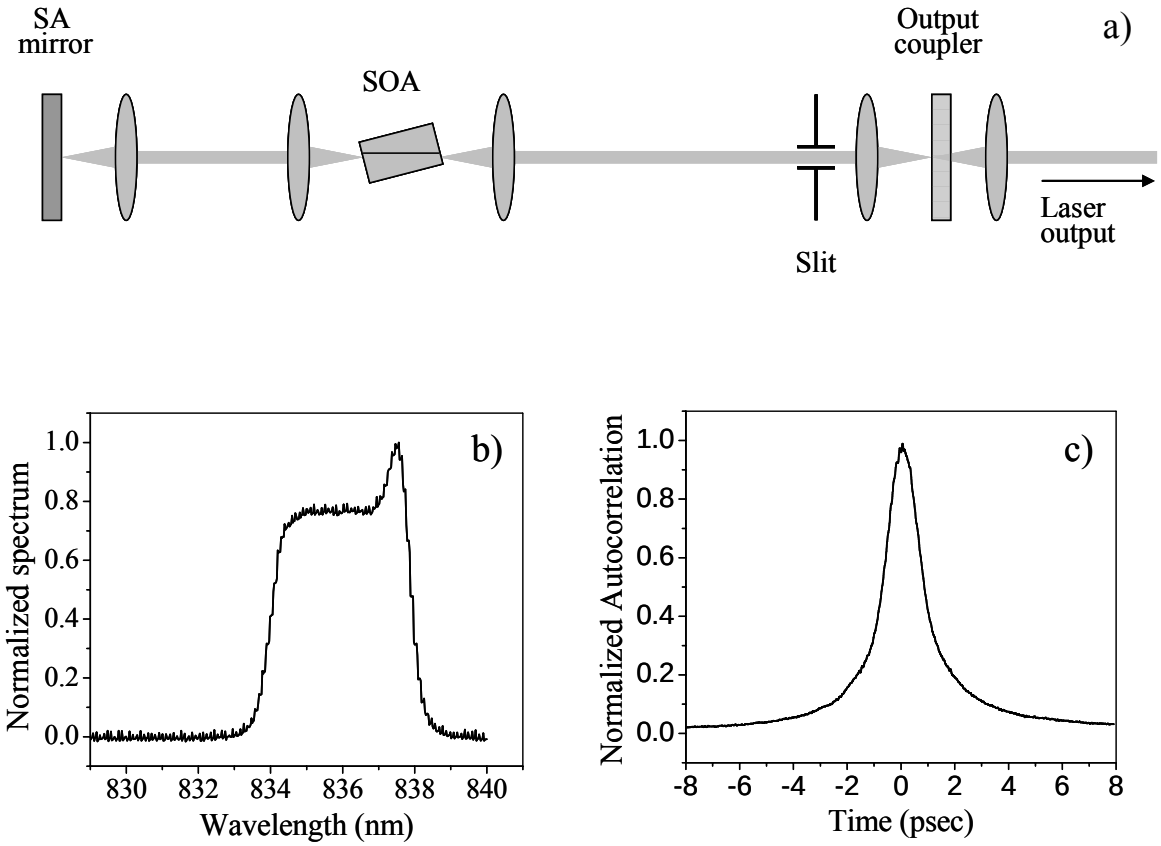

Figure 3.5: Mode-locked laser used as the pulse source for the pump-probe measurements of the gain dynamics of an SOA a), probe spectrum b) and probe pulse autocorrelation c).

The pump pulses were compressed to 750 fs for the measurement of the gain dynamics of the SOA for the amplification of 750 fs pulses and left uncompressed for the measurement of the gain dynamics of the SOA for the amplification of longer, 6.5 ps pulses. A variable delay stage is used to delay the probe with respect to the pump and a chopper is used on the probe. The cross polarized pump and probe are recombined using a polarization beam splitter and coupled into the SOA under test. The weak short probe pulses sense the SOA gain changes induced by the strong pump pulses. A polarizer blocks the amplified pump pulses and let the probe pulse pass and a slow photo-detector and a lock-in amplifier measure the probe power as a function of the delay. Even though the pump and probe are cross polarized, there is a small coupling between them when amplified in the SOA, resulting is a small pump component at the probe polarization leading to interference effects for small delays between pump and probe. The interference effects were washed out by dithering the delay station around each measurement point.

Figure 3.6 shows the results for the amplification of the 6.5 ps pulses, where Figures 3.6a and 3.6b show the spectrum of the 6.5 ps up chirped pulses before and after amplification. The enhancement on the long wavelength side of the spectrum after amplification is a result of the combination of the SOA gain and the instantaneous frequency shifted to low frequencies associated with the gain depletion as explained in the previous section. Figure 6.5c plots the pulse autocorrelation before and after amplification showing no significant pulse distortion introduced during the amplification. Figure 4d represents the temporal evolution of the SOA gain. The relatively long pump pulses induce a smooth gain depletion by stimulated amplification with a gain recovery in a nanosecond time scale.

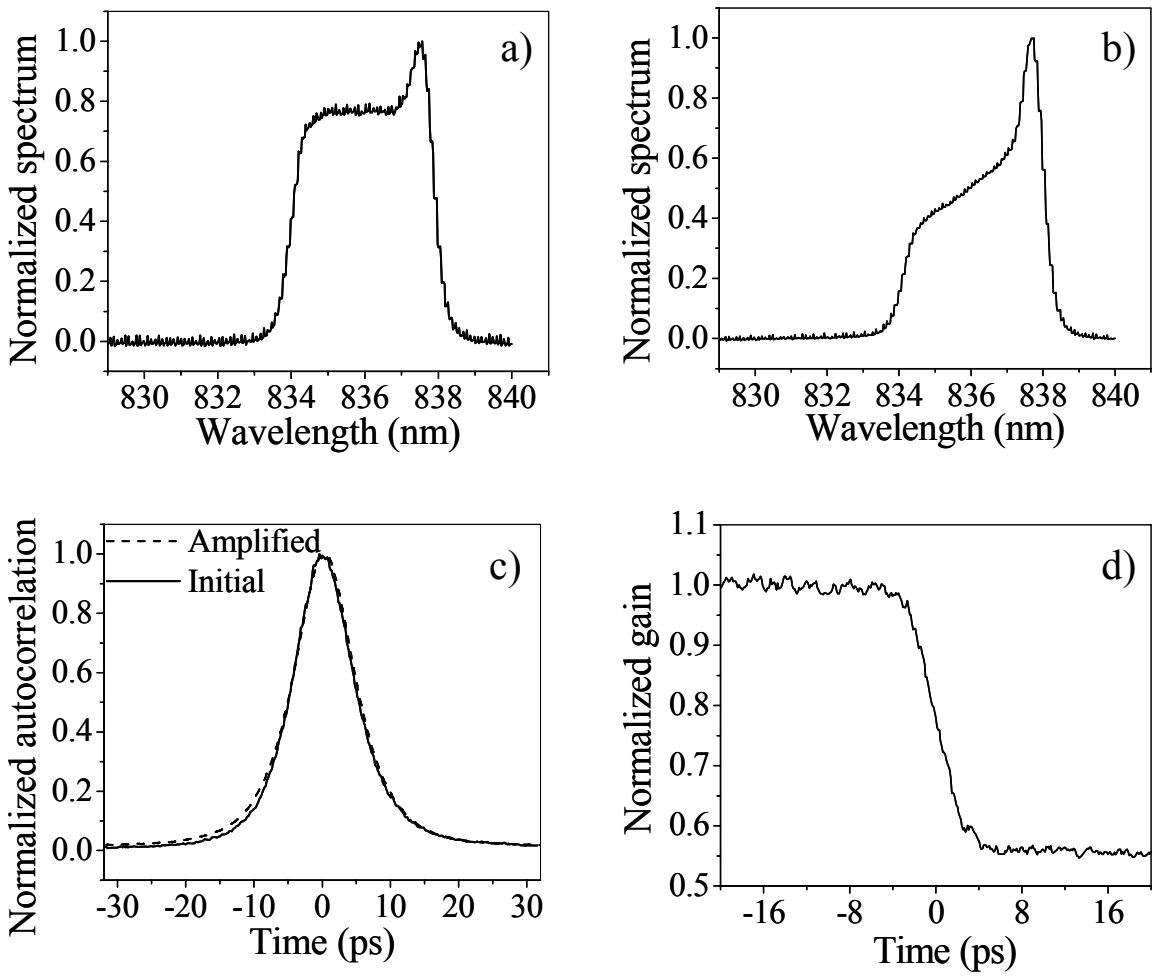

Figure 3.6: Amplification of 6.5 ps pulses in a SOA. Pulse spectrum before amplification a), pulse spectrum after amplification b), pulse autocorrelation before (—) and after (---) amplification c), and time resolved gain dynamics d).

The experimental results for the amplification of the 750 fs dispersion compensated pump pulses are shown in Figure. 3.7. This Figure shows the pump pulse spectra and autocorrelations before and after amplification and the measured SOA gain dynamics. The SOA gain dynamics in this case is significantly different compared with the gain dynamics observed for the

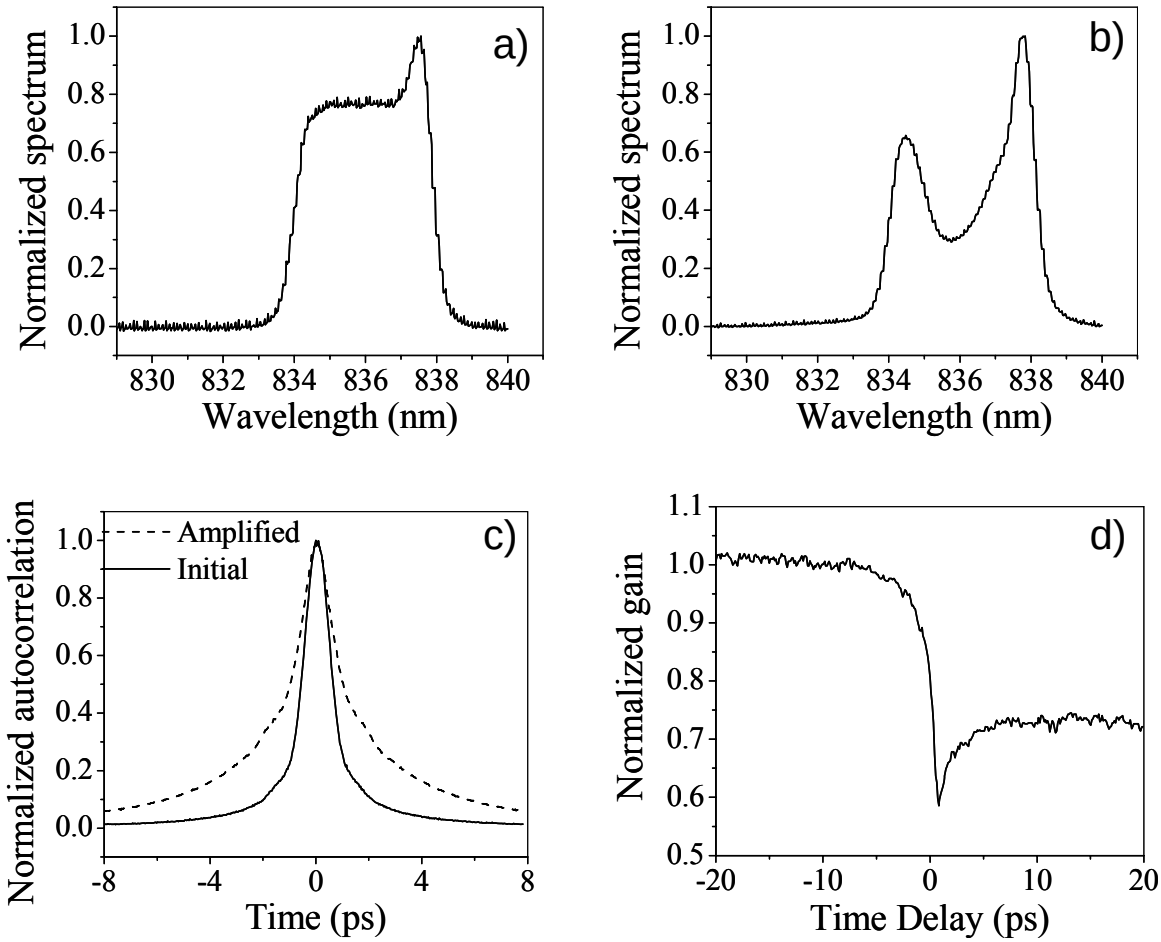

Figure 3.7: Amplification of 750 fs pulses in a SOA. Pulse spectrum before amplification a), pulse spectrum after amplification b), pulse autocorrelation before (—) and after (---) amplification c), and time resolved gain dynamics d).

amplification of the 6.5 ps pump pulses shown above. In this case an enhancement of the long wavelength side and the short wavelength side of the amplified pulse spectrum are present as observed in Figure 3.7b. Figure 3.7d reveals a fast gain depletion followed by a fast partial gain recovery. The enhancement of the long wavelength side of the amplified pulse spectrum is a result of the low frequency instantaneous frequency associated with the fast gain depletion and

the enhancement of the short wavelength side of the spectrum is a result of the high frequency instantaneous frequency associated with the partial gain recovery. The partial gain recovery is a result of the cooling of hot carriers back to equilibrium as explained in the previous section. Another important observation is the significant pulse broadening of the amplified pulses as observed in Figure 3.7a.

The experimental results obtained clearly show that external cavity semiconductor mode-locked lasers can not support short pulse operation. The amplification of short pulses induces fast SOA gain changes imparting a nonlinear pulse chirp and broadening the pulses, thus destroying the short pulse. Instead, the combination of the dispersion of the cavity elements and the gain dynamics of the SOA and the SA results in the production of long pulses with a predominant linear chirp, avoiding fast gain dynamics and nonlinearities in the SOA, allowing for a stable mode-locking operation [58].

3.4 Intracavity pulse evolution

In this section an external cavity semiconductor hybrid mode-locked laser in a linear configuration is used to describe the intracavity pulse modifications induced by the different cavity elements. Figure 3.8 shows the laser diagram containing a SOA, a SA mirror, an 80% reflecting output coupler, a slit and a pellicle beam splitter. The slit is used to assure single transverse mode operation and the pellicle beam splitter is used to take out a small portion of the intracavity power to measure the pulse spectrum before and after the saturable absorber. The SOA is located approximately one third of the cavity length from the saturable absorber and the

intracavity pulse pass through the SOA twice per cavity round trip. This SOA position is favorable for hybrid mode-locked operation at the fundamental repetition rate and twice the fundamental repetition rate (second harmonic). For hybrid mode-locking in this configuration, the pulses do not pass through the SOA when the RF signal is at a maximum, instead, the pulses pass through the SOA when the gain is approximately equal for each pass [59].

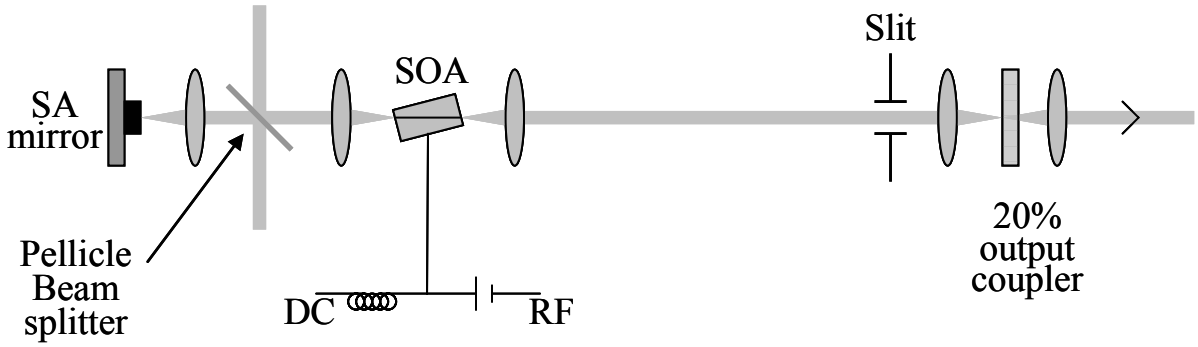

Figure 3.8: External cavity semiconductor hybrid mode-locked laser used to measure the pulse spectrum evolution.

Figure 3.9 show the relation between the RF signal and the pulses in the laser cavity for fundamental and second harmonic hybrid mode-locked operation. The cavity round trip time is T=c/(2L), where c is the sped light and L is the effective cavity length. For fundamental mode-locked operation, the period of the RF applied to the SOA must match the cavity round trip (T) and for second harmonic operation the period of the RF applied to the SOA must be half of the cavity round trip time.

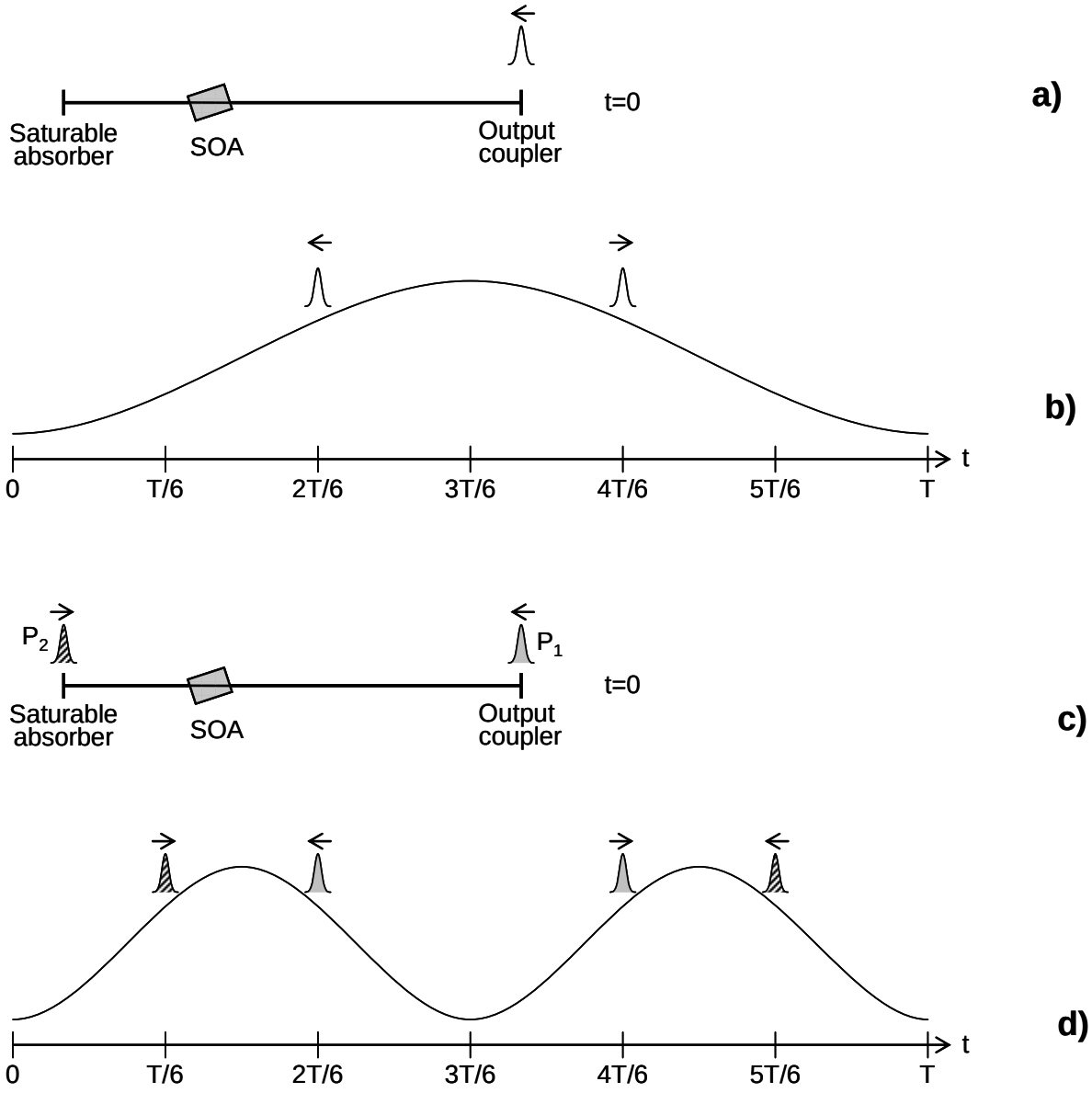

Figure 3.9: Relation between the RF signal and the pulse position in the laser cavity for fundamental [a) and b)] and second harmonic [c) and d)] hybrid mode-locking operation with the SOA located at one third of the laser cavity.

For fundamental mode-locked operation there is only one pulse oscillating in the laser cavity. Let's assign time t=0 to the time when the pulse is at the output coupler as depicted in Figure 3.9a. As mentioned above, the pulse pass through the SOA when the gain (RF bias signal

power) is equal for each pass, then at t=0, the radio frequency signal applied to the SOA must be at a minimum. Figure 3.9b shows the RF signal and the times at which the pulse passes through the OSA. The arrow indicates the direction of the pulse at that time. At time t=2T/6 the pulse passes through the SOA traveling to the left, at t= 3T/6 the pulse reaches the saturable absorber mirror, at t=4T/6d the pulse passes through the SOA traveling to the right and at t=6T/6 the pulse reaches the output coupler completing a cavity round trip. It is observed in Figure 3.9b that the times for which the pulse passes through the SOA are symmetric respect to the RF signal peak and have the same gain. If a small counter propagating pulse is considered to be produced each time the pulse passes through the SOA, the counter propagating pulses will come back to the SOA at times for which the RF is at a minimum, preventing the build up of these pulses in the laser cavity. This is why placing the SOA at one third of the laser cavity is favorable for hybrid mode-locking at the fundamental repetition rate in a linear cavity configuration.

For second harmonic operation there are two pulses spaced by half of the cavity round trip time oscillating in the laser cavity. If time t=0 corresponds to the time for which one pulse (P_1) is at the output coupler, the other pulse (P_2) must be at the saturable absorber and the RF signal must be at a minimum as shown in Figures 3.9c and 3.9d. At time t=T/6, P_1 is between the output coupler and the SOA traveling to the left and P_2 is passing through the SOA traveling to the right. At time t=2T/6, P_1 is passing through the SOA traveling to the left and P_2 is between the SOA and the output coupler traveling to the right, at time t=3T/6, P_1 is at the saturable absorber and P_2 is at the output coupler, at time t=4T/6, P_1 is passing through the SOA traveling to the right and P_2 is between the output coupler and the SOA traveling to the left, at time t=5T/6, P_1 is between the SOA and the output coupler traveling to the right and P_2 is passing through the SOA traveling to the left, and at time t=6T/6=T, P_1 is at the output coupler and P_2 is

at the saturable absorber, completing one cavity round trip. Figure 3.9d shows the RF signal indicating the time and direction at which each pulse passes thru the SOA. If a small counter propagating pulse is considered each time that the pulses are amplified by the SOA, the counter propagating pulses will come back to the SOA at times for which the RF signal is at a minimum, preventing the build up of these pulses in the laser cavity.

The laser of Figure 3.8 was hybridly mode-locked at 624 MHz (second harmonic) with a DC bias current of 125 mA and 14 dBm of RF power, yielding approximately 1mW of averaged output power. Figure 3.10 shows the evolution of the pulse spectrum in the laser cavity. The pulse autocorrelations measured directly from the laser output and after pulse compression are shown in Figure 3.10b and the pulse spectra measured at three different cavity locations are shown in Figures 3.10c, 3.10d and 3.10e. The laser output pulses where compressed by adding negative linear dispersion using a dual grating dispersion compensator. The FWHM of the measured pulse autocorrelations are 11 ps for the laser pulses and 700 fs for the compressed pulses, corresponding to pulses of 7.1 ps and 450 fs respectively assuming square hyperbolic secant pulses. The high compression ratio and the sign of the linear dispersion added indicate that the pulses from the mode-locked laser are highly up-chirped with a predominant linear component.

To describe the pulse evolution in the laser cavity lets start with a pulse between the SOA and the output coupler traveling towards the output coupler. When the pulse reaches the output coupler, 20% of the pulse power is transmitted (laser output) and 80 % is reflected without pulse distortion and the reflected pulse travels towards the SOA. Figure 3.10c shows the spectrum of the output pulses. When the reflected pulse passes through the SOA, the pulse is amplified,

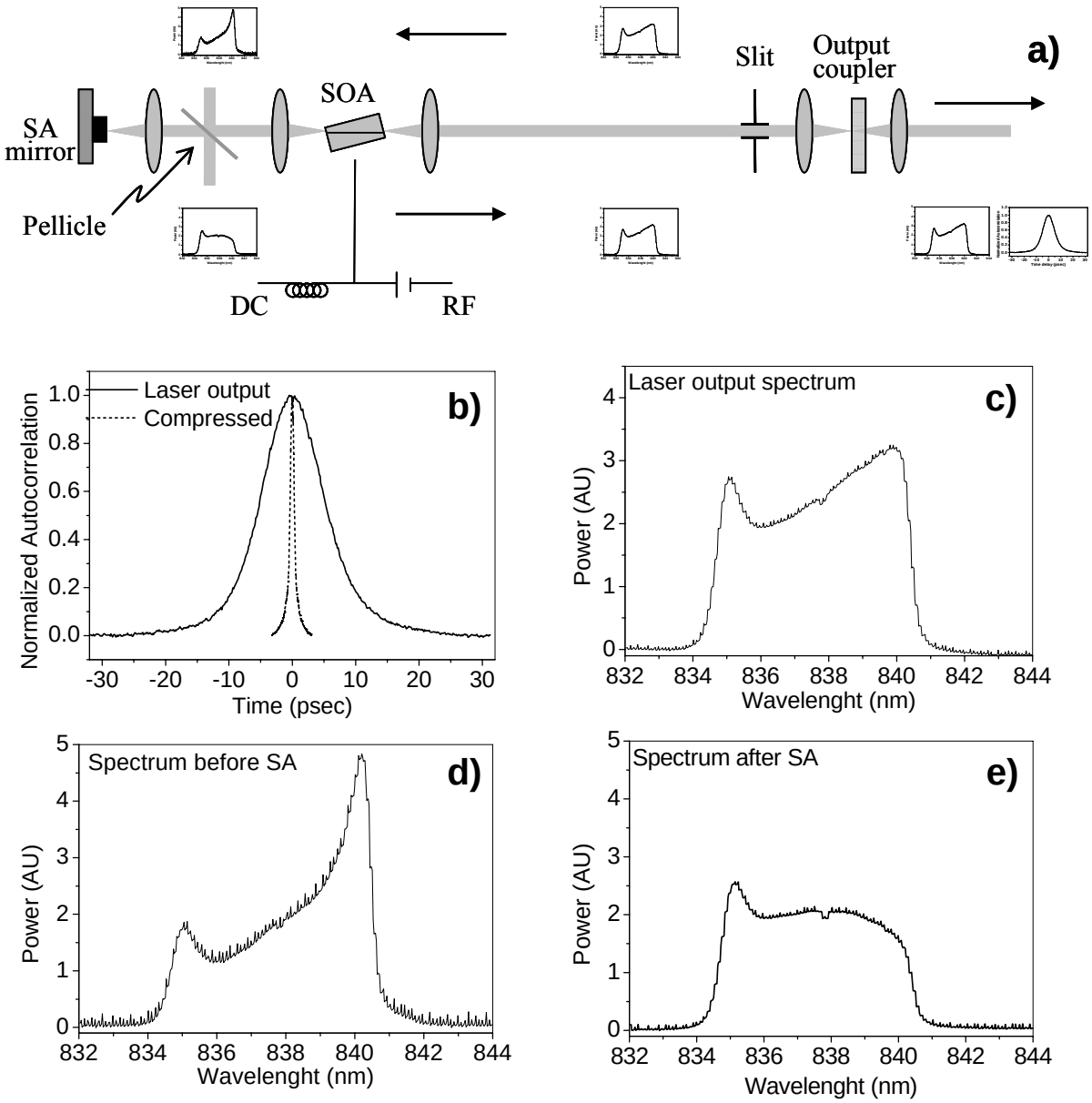

Figure 3.10: External cavity hybrid mode-locked laser pulse spectrum evolution. Laser diagram a), output pulse autocorrelation before and after linear dispersion compensation b), output pulse spectrum c), pulse spectrum before saturable absorber d) and pulse spectrum after saturable absorber.

depleting the SOA gain. As a result, the leading edge of the pulse experiences a higher gain than the trailing one, and since the pulse is up-chirped, this corresponds to a higher amplification on the long wavelength side of the spectrum. Furthermore, as explained in Section 3.2, a time decreasing gain results in a low frequency instantaneous frequency, contributing to the enhancement of the long wavelength side of the spectrum. The measured spectrum after amplification is shown in Figure 10d, where an enhancement of the long wavelength side of the spectrum is clearly observed. When the amplified pulse reaches the saturable absorber mirror, the leading edge of the pulse is absorbed bleaching the saturable absorber mirror and the remaining pulse is reflected and travels towards the SOA. The pulse spectrum of the reflected pulse is shown in Figure 3.10e, where the long wavelength side of the spectrum (leading portion of the pulse) is significantly reduced by the saturable absorber mirror. By the time the pulse reaches the SOA, the SOA gain is recovered and the pulse is amplified one more time. Once again, the long wavelength side of the spectrum is enhanced due to the pulse up-chirp and the self phase modulation. The amplified pulse duplicates the initial pulse (steady state) and travels towards the output coupler completing a cavity round trip.

From the evolution of the pulse spectra and the pulse chirp, it can be observed that the intracavity pulses in external cavity semiconductor hybrid mode-locked lasers undergo through a significant temporal and spectral reshaping as they pass though the SOA and the SA.

CHAPTER FOUR:
SATURABLE ABSORBER ABSORPTION DYNAMICS

4.1 Introduction

A description of the saturable absorbers used in the experiments presented in this dissertation was given in Section 2.3., Experimental results of the absorption dynamics measurements of a multiple quantum well saturable absorber using pump-probe techniques are presented in this chapter. Two different measurements were made, one is the absorption dynamics measurement of a multiple quantum well saturable absorber mirror using 500 ps pulses as pump and probe and the other is the absorption dynamics measurement of a multiple quantum well saturable absorber mirror in an operating external cavity semiconductor hybrid mode-locked laser using the compressed laser output pulses as the probe.

4.2 Saturable absorber mirror absorption dynamics measured using subpicosecond pulses as the pump and probe

The saturable absorber under test contains 100 periods of 70 Å GaAs wells separated by AlGaAs barriers of 100 Å grown on a mirror stack and is proton implanted to decrease its recovery time as described in Chapter Two. The spontaneous emission light of a SOA was used as a reference to measure the reflection spectrum of the saturable absorber mirror. Figure 4.1 shows the spectrum of the SOA spontaneous emission and the spectrum of the SOA spontaneous

emission reflected by the saturable absorber mirror showing a saturable absorber exitonic absorption peak around 830nm.

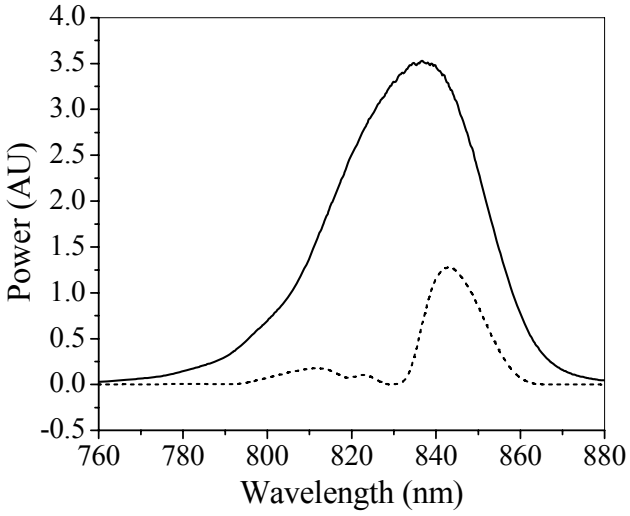

Figure 4.1: 70 Å multiple quantum well saturable absorber. SOA spontaneous emission reference spectrum (──) and saturable absorber mirror reflected spectrum (….).

The experimental setup used for the pump-probe measurement of the absorption dynamics of the saturable absorber mirror is shown in Figure 4.2. An external cavity semiconductor mode-locked laser and a double pass dual grating dispersion compensator are used to obtain the pump and probe. The laser produces pulses of approximately 7 ps at a repetition rate of 624 MHz (second harmonic) with an averaged output power of 0.5 mW. A SOA biased at a constant current of 200 mA amplifies the laser output to 15 mW of average power. The amplified pulses are compressed to approximately 500 fs by the compensation of the linear dispersion using the dispersion compensator as shown in Figure 4.2.

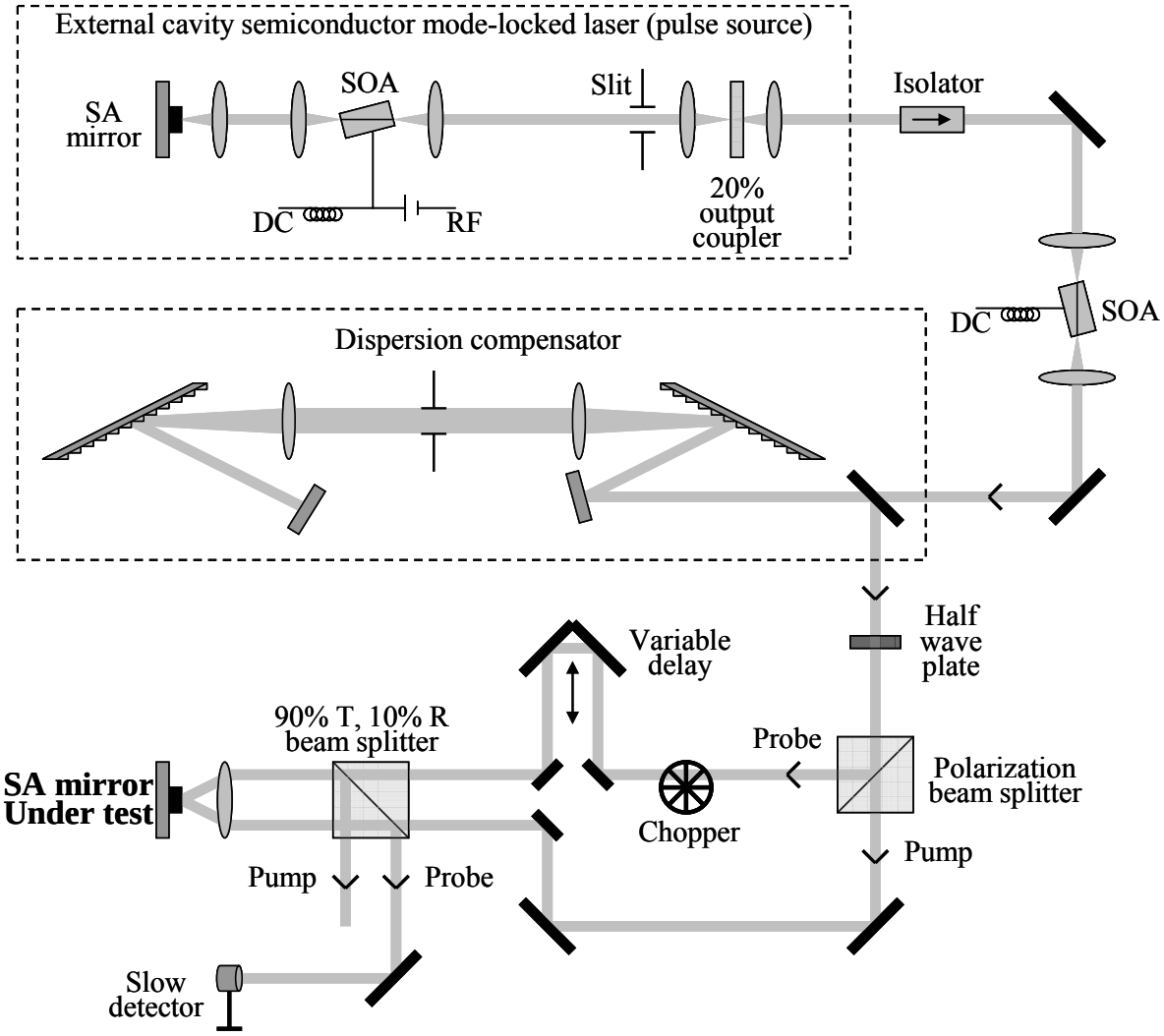

Figure 4.2: Experimental setup for the measurement of the SOA absorption dynamics.

Figure 4.3 shows the pulse spectrum and the pulse autocorrelation directly from the laser and after dispersion compensation. The compressed pulses pass through a halve wave plate and a polarization beam splitter. The beam splitter separates the input beam in cross polarized pump and probe and the power ratio between pump and probe is adjusted by rotating the halve wave

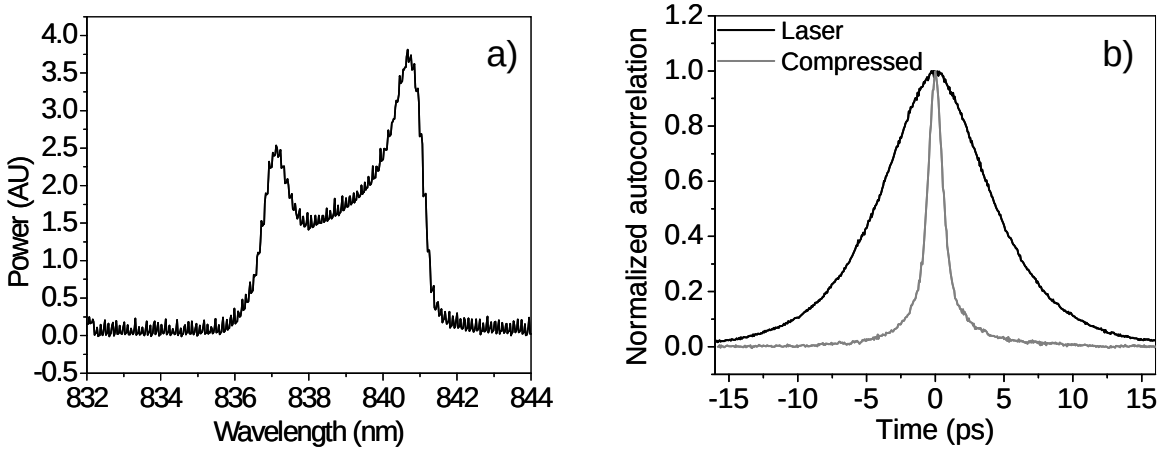

Figure 4.3: Laser spectrum and autocorrelation.

plate. A variable delay stage and a chopper are used on the probe. The pump and probe beams are aligned parallel to each other and pass trough a 90% transmitting (10% reflecting) beam splitter. An 8mm focal length lens tightly focuses the pump and probe beams on the saturable absorber mirror. The short pump pulses bleach the saturable absorber mirror and the probe senses the absorption change induced by the pump and is partially reflected. The beam splitter located in front of the saturable absorber mirror allows the measurement of the 10 % of the reflected probe. The probe power is measured a function of the delay between pump and probe with a slow detector and a lock-in amplifier. Although the pump and probe are cross polarized and spatially separated, there is a small coupling between pump and probe in the saturable absorber mirror, resulting in interference effects. The interference is observed as a spectral modulation of the measured probe with a frequency proportional to the delay between pump and probe [60]. The frequency of the spectral modulation changes very fast with respect to the delay between pump and probe and is observed only for small delays. The interference effects were

washed of by dithering the probe delay stage around each measurement point. The delay station used for this experiment moves in steps of 1.58 μm corresponding to a change on the probe path length of 3.17 μm or 10.58 fs. The delay station was dithered around each measuring point by moving the delay stage back and fort 5 steps at a speed of 200 steps/s satisfactorily eliminating the interference effects. The probe power measured as a function of the delay between pump and probe is plotted in Figure 4.4, where an increase in the measured probe power represents a decrease of the saturable absorber absorption and vice versa.

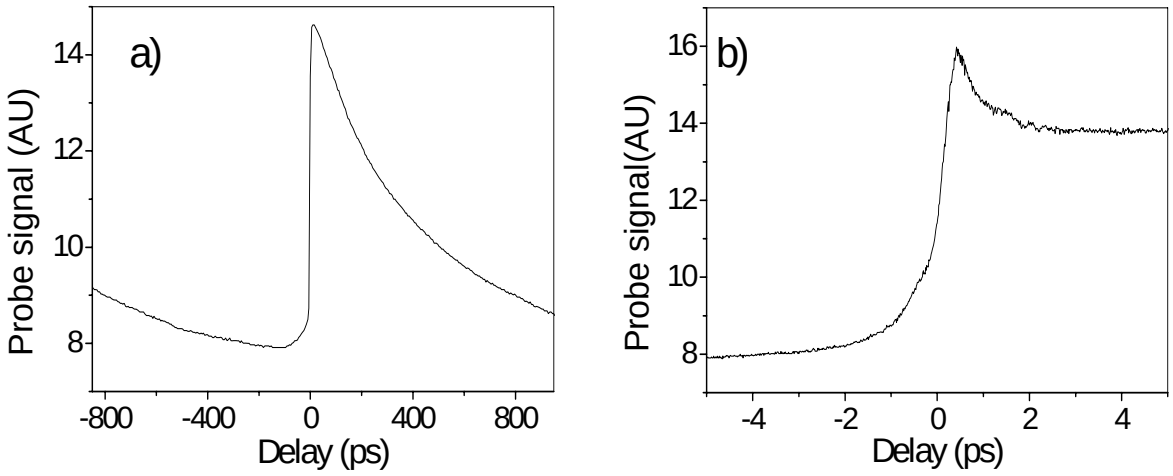

Figure 4.4: Saturable absorber absorption dynamics.

Figure 4.4a shows an initial decrease of the probe power as the saturable absorber absorption recovers from the bleaching of the last pulse and returns to its unbleached state. When the next pulse reaches the saturable absorber, the pulse bleaches the saturable absorber (fast probe signal increase) and the saturable absorber recovers with a time constant of 350 ps measured from the fitting of Figure 4.4a to an exponential decay. Figure 4.4b shows a closer look of the probe signal for small delays, where a fast bleaching followed by a partial fast

recovery is observed. This fast absorption dynamic is due to the excess exitonic population created by resonant ultra short excitation, with a thermal ionization time of exitons at room temperature of approximately 300 fs in GaAs [61, 62].

The spectrum of the probe was measured for delays ranging from -2 ps to 2 ps and the measured spectra are plotted in Figure 4.5. This plot shows the evolution of the absorption bleaching of the saturable absorber mirror over the probe bandwidth. One of the goals of this measurement was to observe spectral changes induced by self-phase modulation effects on the saturable absorber originating from the absorption change and the corresponding index of refraction change in the semiconductor saturable absorber as explained in Section 3.2. However, only spectral changes due to the evolution of the saturable absorber absorption bleaching are observed without significant spectral changes due to self phase modulation.

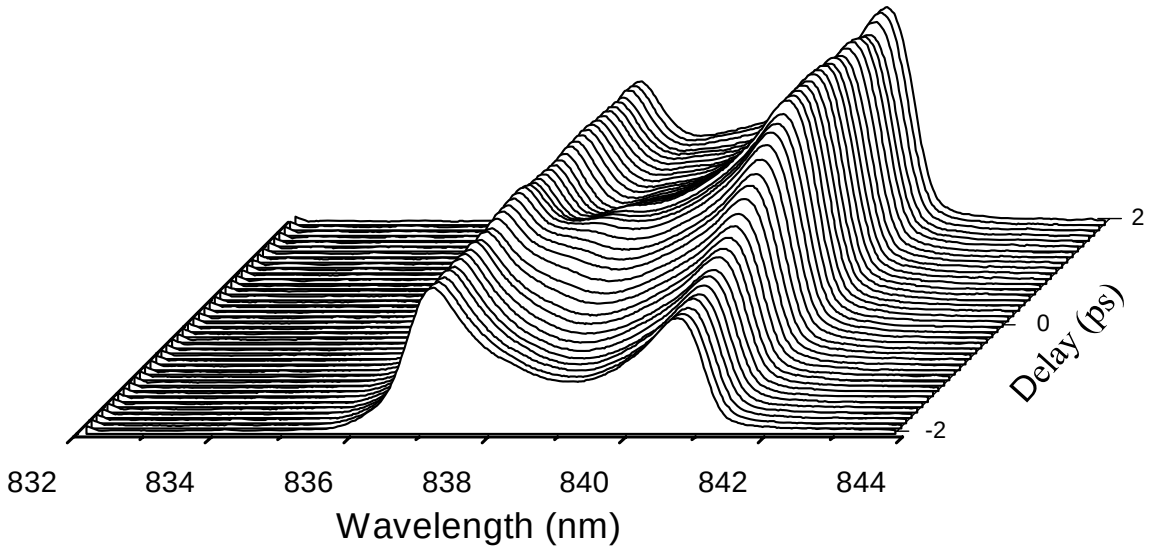

Figure 4.5: Probe spectrum measured as a function of delay between pump and probe.

4.3 Intracavity saturable absorber absorption dynamics

The absorption dynamics of a saturable absorber mirror in an external cavity semiconductor laser were measured. The measurements were made while the laser was hybridly mode-locked without disturbing its operation. The experimental setup is shown in Figure 4.6. The external cavity semiconductor mode-locked laser has a ring cavity configuration and the saturable absorber mirror used in the laser is similar to the saturable absorber under test in the previous section.

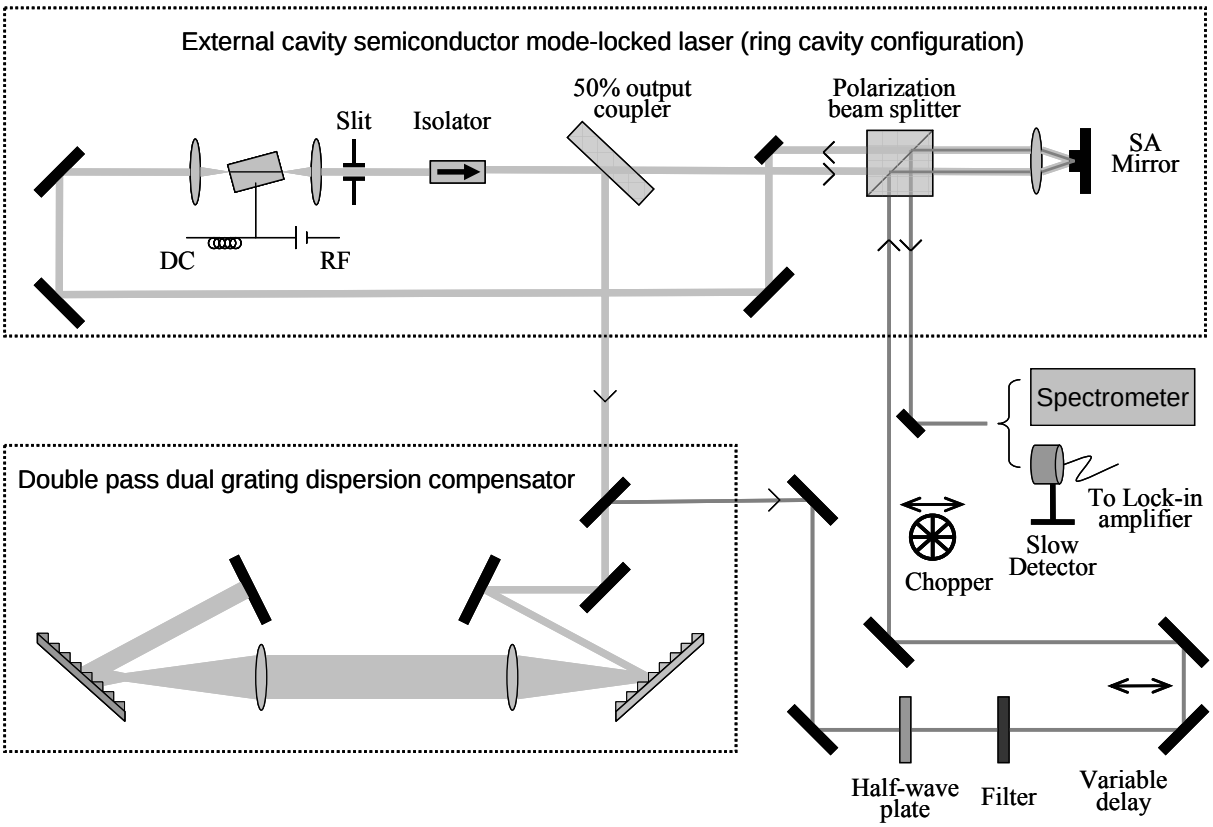

Figure 4.6: Experimental setup used to measure the intracavity absorption dynamics of a saturable absorber mirror.

Figure 4.7 shows the spontaneous emission spectrum of a SOA used as reference and the spectrum of the SOA spontaneous emission reflected by the saturable absorber mirror, showing an exitonic absorption peak around 835 nm.

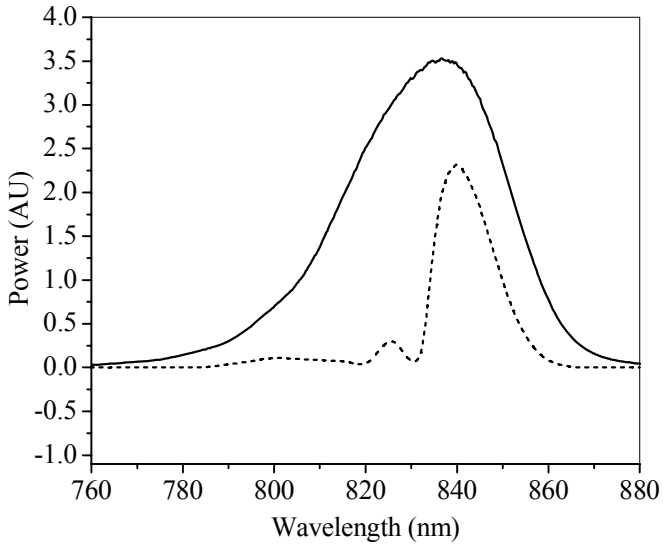

Figure 4.7: Multiple quantum well saturable absorber. SOA spontaneous emission reference spectrum (──) and saturable absorber mirror reflected spectrum (….).

The laser operates at 266 MHz (fundamental repetition rate) for a SOA driving current of 260 mA, with an average output power of 5 mW and a pulse duration of approximately 7 ps. The pulses are compressed to approximately 900 fs by linear dispersion compensation using a double pass dual grating dispersion compensator. Figure 4.8 shows the pulse spectrum and the pulse autocorrelations before and after dispersion compensation. The dispersion compensated pulses are used as a probe to measure the gain dynamics of the saturable absorber mirror in the laser cavity. The polarization of the probe is rotated using a halve wave plate and a polarization beam splitter is used to introduce the probe in the laser cavity as shown in Figure 4.8. The probe is

carefully aligned and focused at the same spot on the saturable absorber as the intracavity pulses. The probe power is attenuated to a few microwatts using a neutral density filter to avoid disturbing the laser operation. The polarization beam splitter also serves to take the probe pulses out of the laser cavity after measuring the absorption dynamics of the SA. A variable delay stage changes the relative delay between the intracavity pulses and the probe pulses and a chopper and a lock-in amplifier are used on the probe to measured the probe power as a function of the delay. The probe power measured as a function of the delay is shown in Figure 4.9. An increase of the measured probe power indicates a decrease in the saturable absorber absorption and vice versa. Figure 4.9a plots the probe signal measured for time delays from -1000 ps to 800 ps measured in 5 ps steps and Figure 4.9b plots the probe signal measured for time delays from -25 ps to 225 ps measured in 0.5 ps steps.

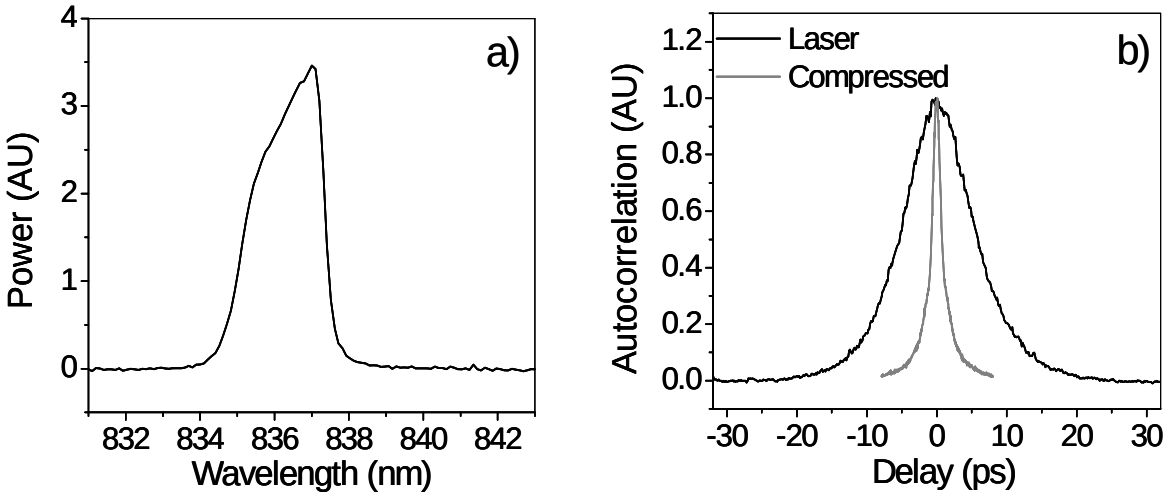

Figure 4.8: Laser spectrum a) and pulse autocorrelation before and after compression by dispersion compensation b).

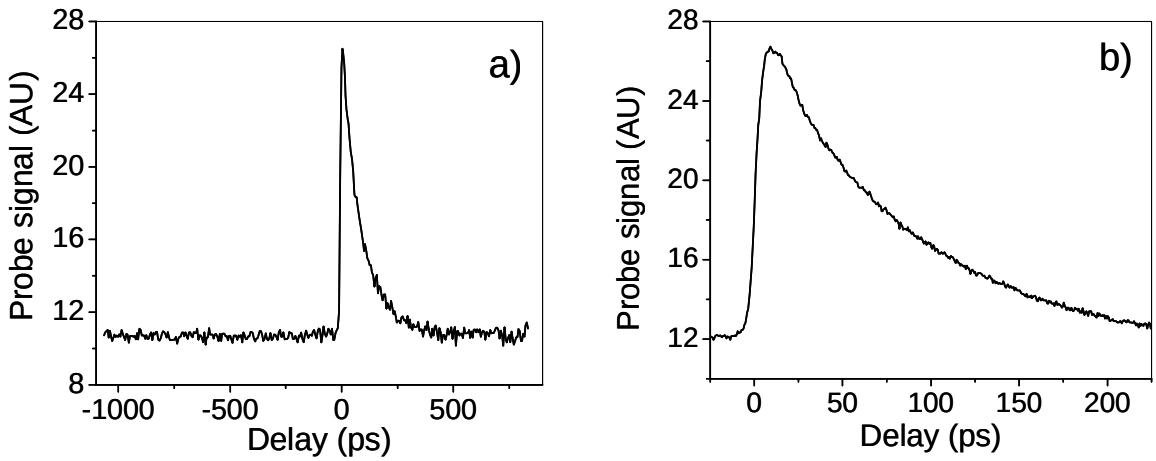

Figure 4.9: Probe power measured as a function of the delay between intracavity pulses and probe.

Figure 4.9 clearly shows a fast increase on the probe signal as the intracavity pulse bleaches the saturable absorber mirror increasing its reflectivity. The saturable absorber absorption recovers with a recovery time of approximately 90 picoseconds measured from the fitting of the experimental data to an exponential decay. The fast absorption dynamics observed in the measurement of the saturable absorber absorption dynamics of Section 4.2 is not observed here since the pulses bleaching the saturable absorber in this case are longer, thus avoiding fast dynamics. The spectrum of the probe signal was measured for each one of the measurement points in Figure 4.9b and is plotted in Figure 4.10. Note the fast absorption bleaching follow by a slow recovery without spectral changes induced by self phase modulation.

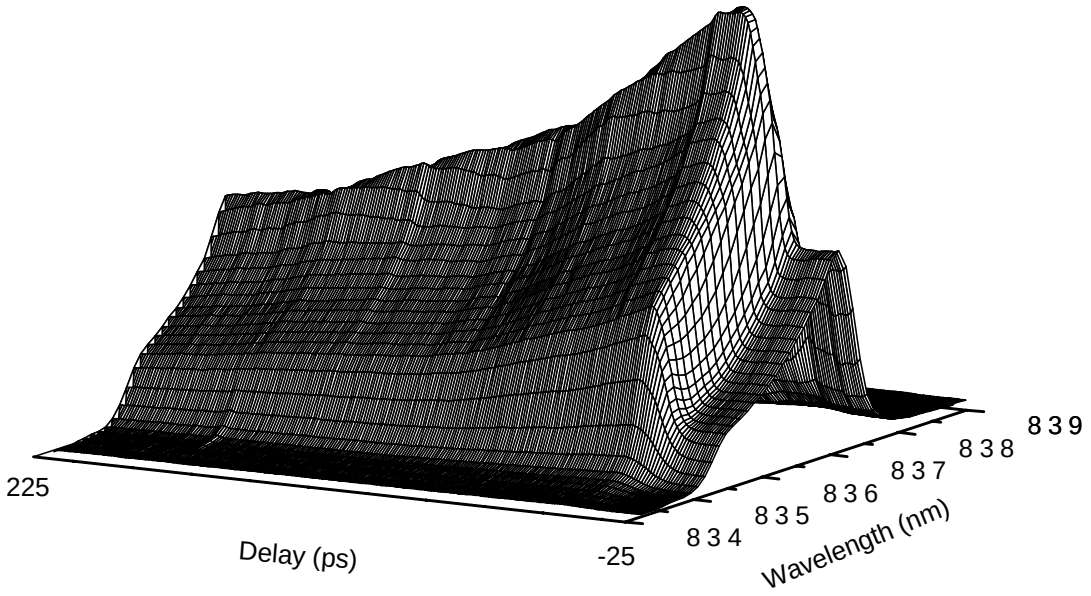

Figure 4.10: Probe spectrum measured as a function of delay between intracavity pulses and probe.

CHAPTER FIVE:
MULTIWAVELENGTH EXTERNAL CAVITY SEMICONDUCTOR MODE-LOCKED LASERS

5.1 Introduction

As mentioned in Chapter One, external cavity semiconductor mode-locked lasers have been successfully configured as multiwavelength pulse sources obtaining up to 160 wavelength channels from a single laser [38]. Two of the main concerns about this kind of laser are the gain competition between different wavelength channels and the nonlinearities in the gain media (SOA).

In this chapter, external cavity semiconductor mode-locked lasers are introduced, then the experimental results for the measurement of the gain dynamics of a SOA for the amplification of dispersion compensated multiwavelength pulses and multiwavelength pulses containing the chirp from the pulse source are presented. The intracavity gain dynamics measurement of an external cavity multiwavelength semiconductor mode-locked laser is also presented. The experimental results reveal how external cavity semiconductor mode-locked lasers avoid nonlinearities and support multiwavelength operation.

5.2 External cavity multiwavelength semiconductor mode-locked lasers

An external cavity semiconductor mode-locked laser can be configured as a multiwavelength laser by introducing a periodic frequency filter in the laser cavity. A Fabry-Perot etalon is a simple way to implement a periodic frequency filter with a transmission function following the formula:

$$T_e = \frac{(1-R)^2}{1+R^2-2R\cos(\delta)} \tag{5.1}$$

where R is the reflectance of the two reflecting surfaces forming the etalon and δ is equal to:

$$\delta = (\frac{2\pi}{\lambda})2nl\cos(\theta) \tag{5.2}$$

where λ is the wavelength, n is the index or refraction of the etalon material, l is the etalon thickness and θ is the angle of incidence measured respect to the normal to the surfaces forming the etalon. The ratio of the separation between transmission peaks to the FWHM of one transmission peak is defined as the finesse of the etalon and is given by the formula:

$$f = \frac{\pi}{2\arcsin(\frac{1-R}{2\sqrt{R}})} \tag{5.3}$$

Figure 5.1 plots the transmission of a 2mm tick solid glass etalon with 70% reflection surfaces at normal incidence plotted around 835 nm.

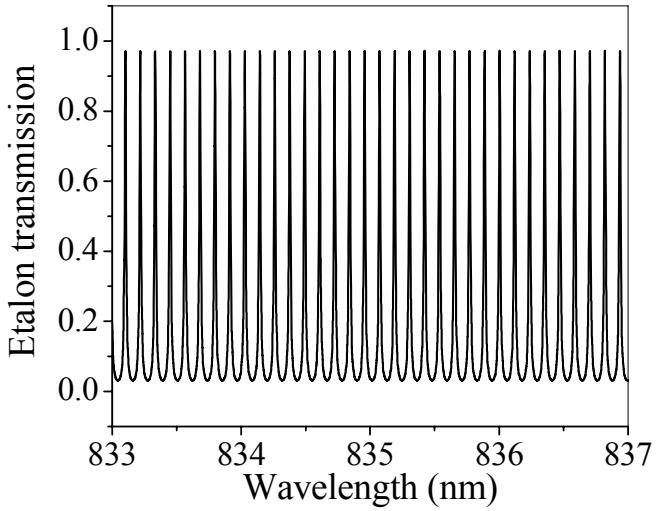

Figure 5.1: Etalon transmission of a 2 mm solid glass etalon with 70% reflecting surfaces at normal incidence around 835 nm.

Another way to implement a periodic spectral filter is the array of a grating, a lens and a mirror, separated a distance equal to the lens focal length. This array generates a Fourier plane on the mirror and a spatial filter can be used to physically select the desired wavelengths as depicted in Figure 5.2. Since the Fourier plane is located at the mirror surface, the spatial filter should be located as close as possible to the mirror.

Figure 5.3 shows the diagram of an external cavity semiconductor mode-locked laser with the SOA located at one third of the laser cavity. An etalon and a spectral filter are included in the laser cavity to achieve multiwavelength operation. The etalon provides a periodic frequency filter and the spectral filter allows the selection of the center wavelength and the number of wavelength channels oscillating in the laser. Multiwavelength operation can also be achieved by using a periodic mask as the spatial filter in the spectral filter instead of the etalon.

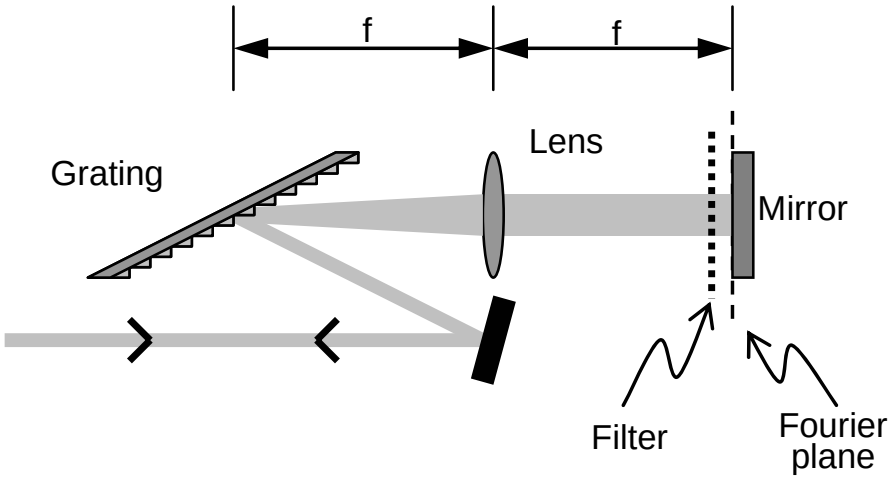

Figure 5.2: spectral filter.

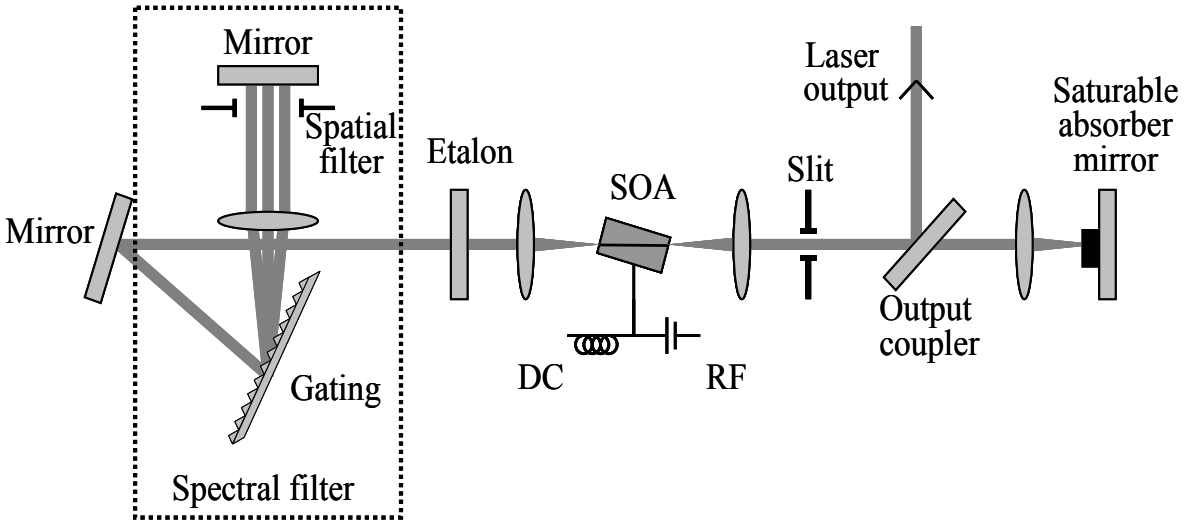

Figure 5.3: External cavity multiwavelength semiconductor mode-locked laser.

The etalon used in the laser is a 2mm tick solid glass etalon with 70% reflecting surfaces. The separation between consecutive etalon transmission peaks is 0.16 nm at a central wavelength

of 835 nm (Figure 5.1). The laser was actively and hybridly mode-locked obtaining 160 and 100 wavelength channels respectively and Figures 5.4 and 5.5 show the corresponding spectra and sampling scope images. To actively mode-locked the laser, the saturable absorber mirror in the laser cavity was temporarily substituted by a dielectric mirror. The sampling scope traces in Figures 5.4b and 5.5b were measured using a 15 GHz bandwidth photo-detector. Note that the measured pulses are inverted and appear as negative pulses. The positive signal observed after the pulses is an artifact of the impulse response of the photo-detector.

In order to maximize the number of wavelength channels oscillating in the laser cavity, the overall gain spectrum, resulting from the combination of all the cavity elements, must be flat over a broad bandwidth and the alignment of the laser plays an important role in this gain flattening. The lenses in the laser cavity have some chromatic dispersion and tweaking the lenses position helps to flatten the gain spectrum and the alignment of the grating in the intracavity spectral filter also contributes to the spectral gain flattening. The saturable absorber used to hybridly mode-lock the laser adds an extra element modifying the overall spectral gain making the gain flattening over a broad spectrum harder to achieve. Additional gain flattening can be achieved using a spatial filter close to the Fourier plane attenuating the wavelength channels with higher gain [63], or introducing a customized Fabry-Perot etalon in the laser cavity to flatten the gain [64].

Multiwavelength active mode-locking allows for a higher number of wavelength channels than hybrid mode-locking, but the mode partition noise due to the gain competition between wavelength channels has been studied in our research group [65] and it has been proven that hybrid mode-locking is less sensitive to gain competition between wavelength channels.

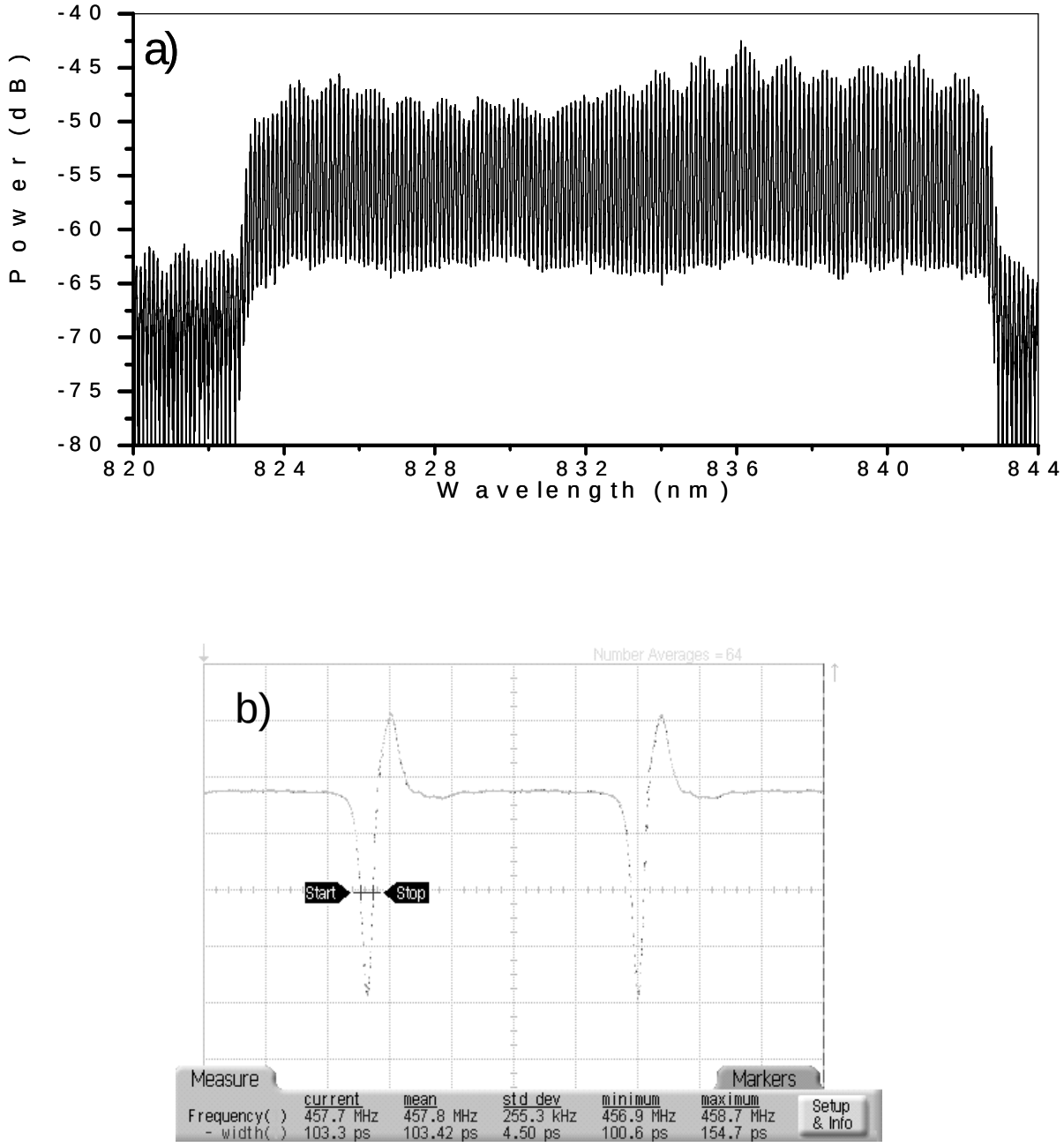

Figure 5.4: Multiwavelength active mode-locking spectrum and sampling scope trace.

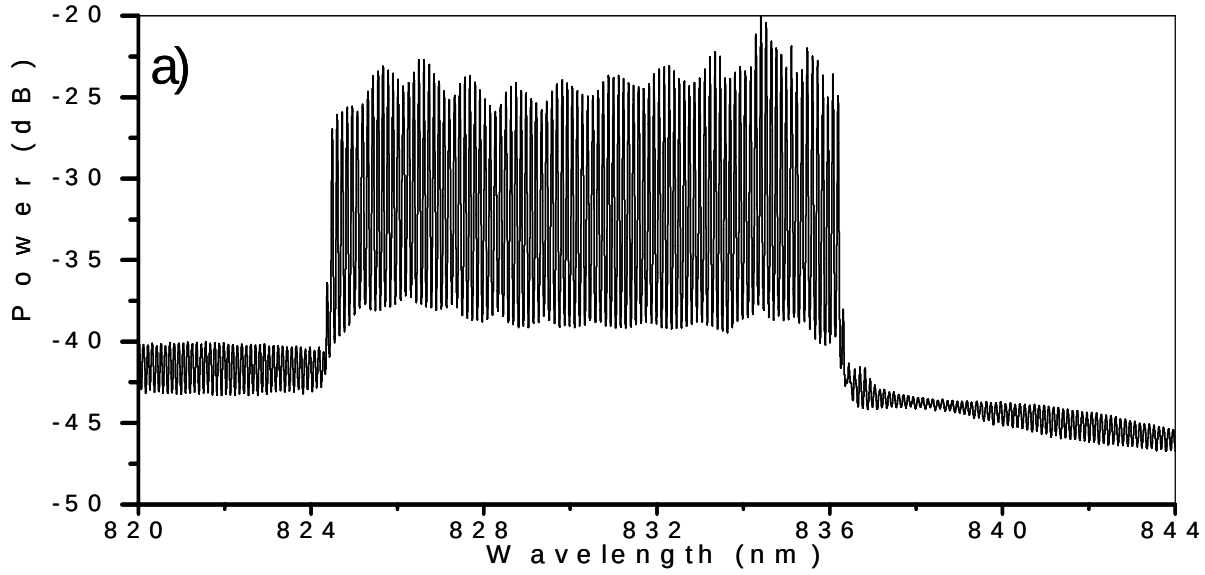

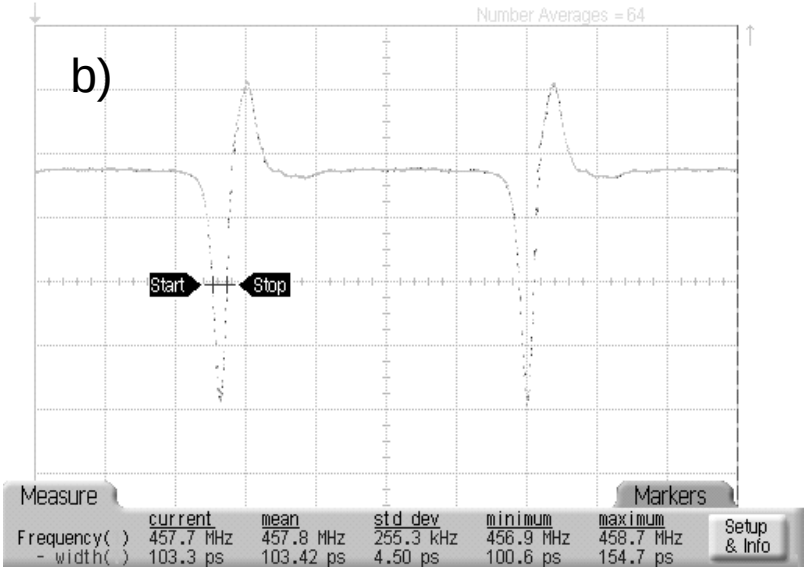

Figure 5.5: Multiwavelength hybrid mode-locking spectrum and sampling scope trace.

5.3 Multiwavelength pulse amplification gain dynamics

The gain dynamics of a semiconductor optical amplifier were measured for the amplification of multiwavelength pulses using pump-probe techniques. An external cavity semiconductor mode-locked laser in a ring cavity configuration was used as the source for the pump and probe pulses. The laser setup is sketched in Fig. 5.6. The isolator guarantees unidirectional operation and the slit limits the beam profile assuring single mode operation. A 50% reflection output coupler is located right after the SOA, where the intracavity power is the highest to extract as much power as possible. Passive mode-locking was achieved at the cavity fundamental repetition rate of 271 MHz for a SOA DC bias of 260 mA, and hybrid mode-locking was achiever by adding 10 mW of radio frequency power to the bias current.

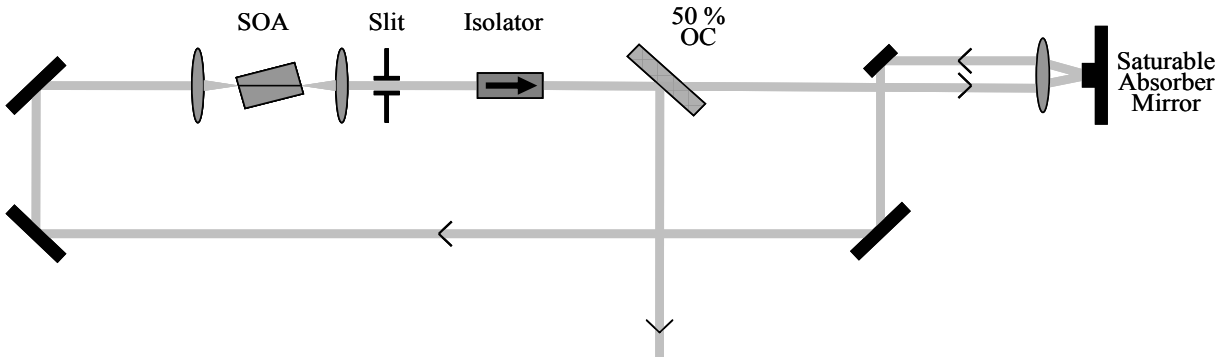

Figure 5.6: External cavity semiconductor mode-locked laser used as pulse source for pump-probe measurements.

The laser produces optical pulses of approximately 6 picoseconds in duration with a spectral bandwidth of 4 nm centered at 835 nm and an average output power of 4mW. The spectrum and autocorrelation of the laser pulses are shown in Fig. 5.7.

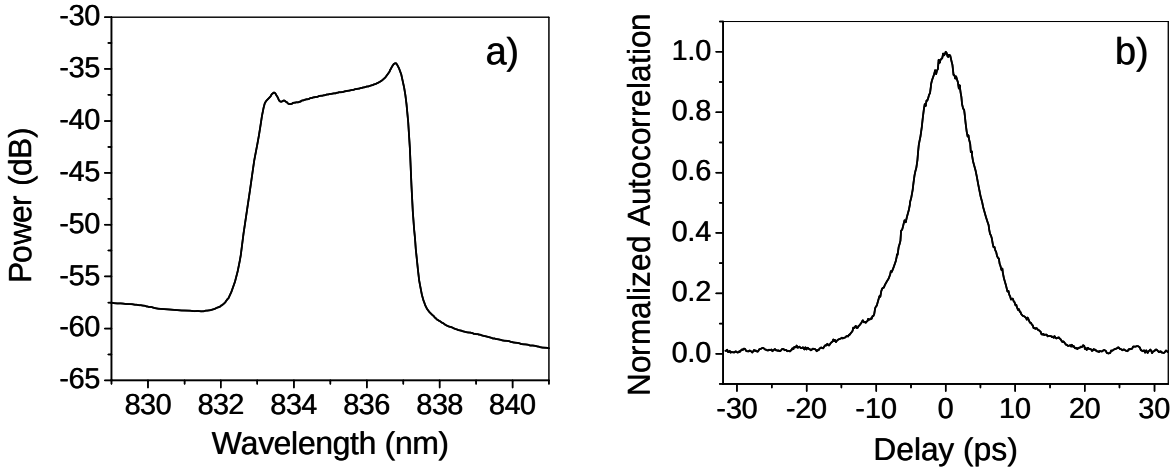

Figure 5.7: Laser source pulse spectrum and autocorrelation.

The experimental setup used for the pump-probe measurement of the gain dynamics of a semiconductor optical amplifier under multiwavelength pulse amplification is shown in Figure 5.8. The pulses from the external cavity semiconductor mode-locked laser described above were divided unequally to obtain the pump and the probe pulses, such that only a small part was used for the probe. The probe pulse duration was reduced to approximately 750 fs after linear dispersion compensation using a dual grating dispersion compensator. The probe spectrum and pulse autocorrelation are shown in Figure 5.9. The probe polarization was rotated 90 degrees, a variable neutral density filter was used to attenuate the probe power and a variable delay stage was used to delay the probe with respect to the pump. The pump was obtained by passing the laser pulses through another dual grating dispersion compensator, where the linear chirp was compensated and the spectrum was spectrally sliced using a spatial filter in the Fourier plane of the dispersion compensator. The sliced spectrum contains three wavelength channels of approximately 0.5nm FWHM each, with a 1.4 nm channel to channel separation. Since the pump

is comprised of three phase correlated wavelength channels, the temporal profile is a burst of short pulses under a broad envelope. The temporal duration of a single pulse within the pulse burst is inversely proportional to the full spectral width encompassing all the wavelength channels, while the temporal duration of the pulse burst is inversely proportional to the spectral bandwidth of a single wavelength channel and the separation between pulses within the pulse burst is inversely proportional to the separation between wavelength channels.

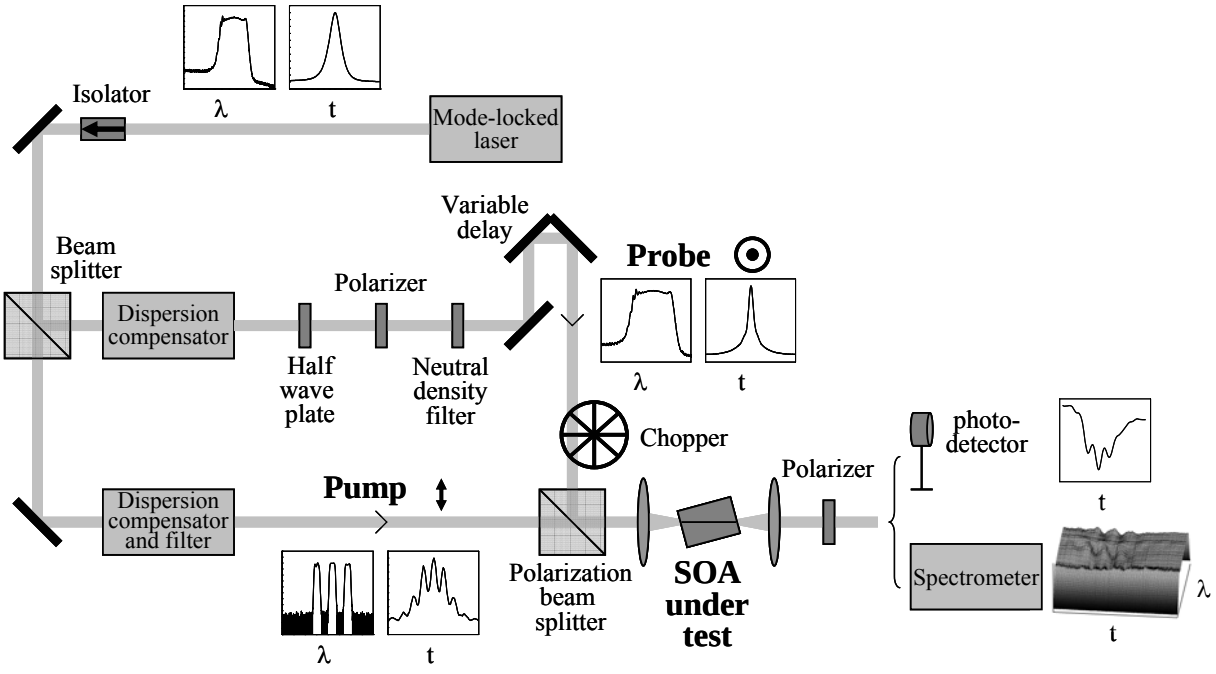

Figure 5.8: Experimental setup for the pump-probe measurement of the gain dynamics of a semiconductor optical amplifier under multiwavelength pulse amplification.

The cross polarized pump and probe are recombined using a polarization beam splitter and coupled into the SOA under test. The strong pump pulses induce changes in the SOA gain, and the short probe pulses measure the gain change as a function of the delay between the pump and probe pulses. A polarizer is used to separate the pump and probe signals after amplification

in the SOA under test and the amplified probe power and spectrum are measured as a function of the delay between pump and probe. When measuring the probe power as a function of the delay, a chopper and a lock-in amplifier are used on the probe to obtain clean measurements. There is a small coupling between pump and probe in the SOA resulting in interference effects on the measured probe. The delay station was dithered around each measurement point to wash out the interference effects in the same way as described in Chapter Four.

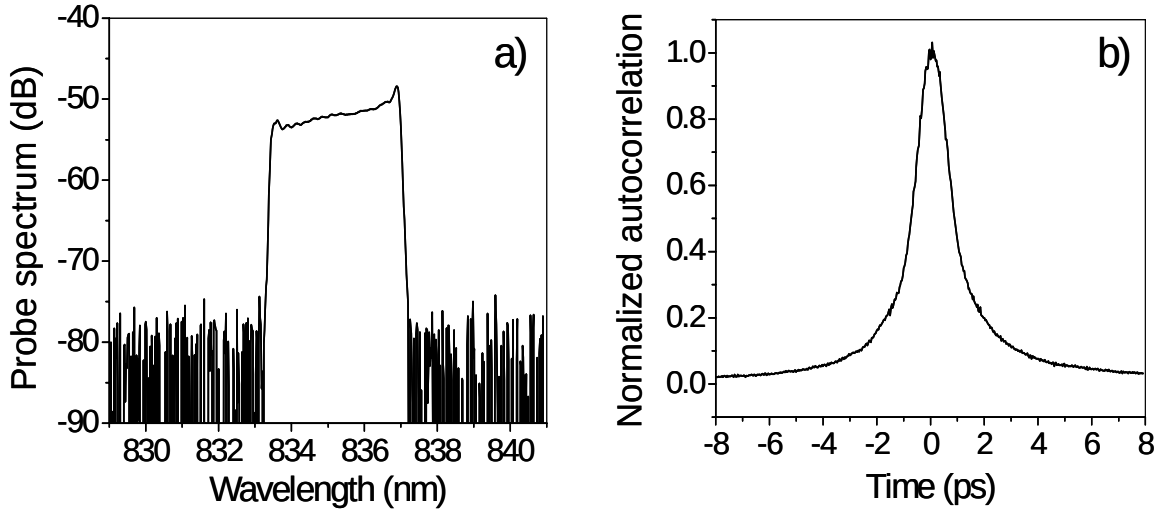

Figure 5.9: Probe spectrum and autocorrelation.

The experimental results for the measurement of the SOA gain dynamics for the amplification of the dispersion compensated multiwavelength pulses are shown in Figure 5.10. Figures 5.10a and 5.10b show the pump spectrum before and after amplification, where the salient feature of Figure 5.10b is the additional wavelength channels generated by the multiwavelength pump via four-wave mixing in the SOA [66-68], suggesting the interchange of

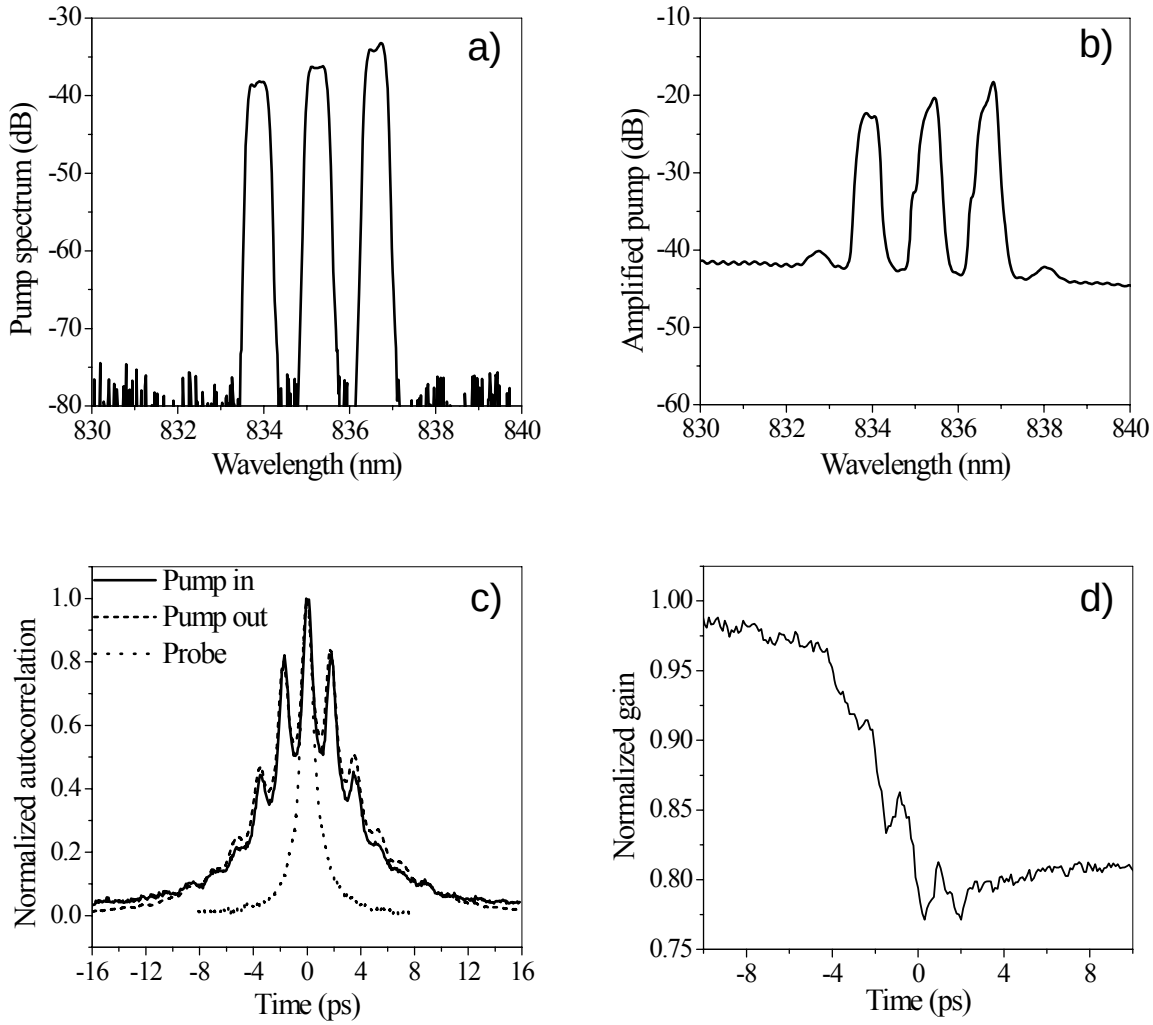

Figure 5.10: SOA gain dynamics for the amplification of dispersion compensated multiwavelength pulses. Pump spectrum a), pump spectrum after amplification b), pump, probe, and pump after amplification autocorrelations c), and time resolved gain dynamics d).

energy between wavelength channels, leading to a small spectral and temporal reshaping of the multiwavelength pulses. Figure 5.10c shows the pump and probe autocorrelations and Figure 5.10d plots the probe signal as a function of the delay between the pump and probe pulses, representing the evolution of the SOA gain dynamics as the multiwavelength pump is amplified. Fig. 5.10d shows an overall gain reduction due to stimulated emission, which recovers on a

nanosecond time scale. The rapid oscillation of the gain is caused by the periodic temporal nature of the phase coherent 3 wavelength channels. These gain transients are a result of carrier heating and carrier cooling effects triggered by the short pulses in the multiwavelength composite pulse profile.

The probe spectrum measured as a function of the delay between pump and probe is shown in Figure 5.11. As a result of the large coupling among gain, carrier concentration, and refractive index, the gain variations induce changes in the index of refraction and cause a phase modulation that couples to the probe pulse via degenerate cross phase modulation [69]. In Figure 5.11, the probe spectra are normalized with respect to the gain of the SOA to observe only the spectral changes, not the gain changes. Also, the probe spectra are normalized with respect to the unperturbed probe spectrum, to yield a flat top spectrum as a reference. Changes in the spectrum of the probe due to cross-phase modulation induced by the pump are observed, where a peak wavelength (or frequency) periodically alternates between long and short wavelengths as depicted by the white line in Figure 5.11. If this Figure is analyzed with care and compared with Fig. 5.10d, it can be observed that the long wavelength peaks correspond to times when the gain is decreasing (low frequency instantaneous frequency) and the short wavelength peaks correspond to times when the gain is recovering (high frequency instantaneous frequency). This plot clearly shows the temporal evolution of the phase modulation induced on a weak probe pulse by a strong multiwavelength pump pulse.

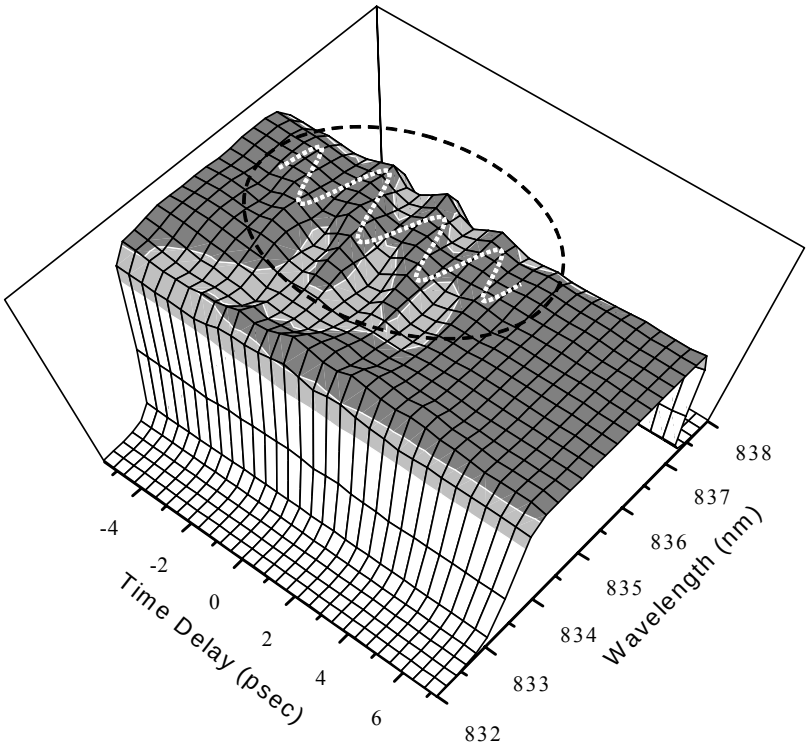

Figure 5.11: Probe spectrum measured as a function of the delay between pump and probe for the amplification of dispersion compensated multiwavelength pulses.

The measurement of the SOA gain dynamics under multiwavelength pulse amplification were repeated for chirped multiwavelength pulses. The chirped multiwavelength pulses were obtained by not compensating for the linear chirp impressed on the pulses generated from the external cavity semiconductor mode-locked laser used as the pulse source. In this case, the spectral filtering employed to create the pump pulse produces 3 mode-locked wavelength channels with a temporal skew, or delay, between wavelength channels. The composite pump

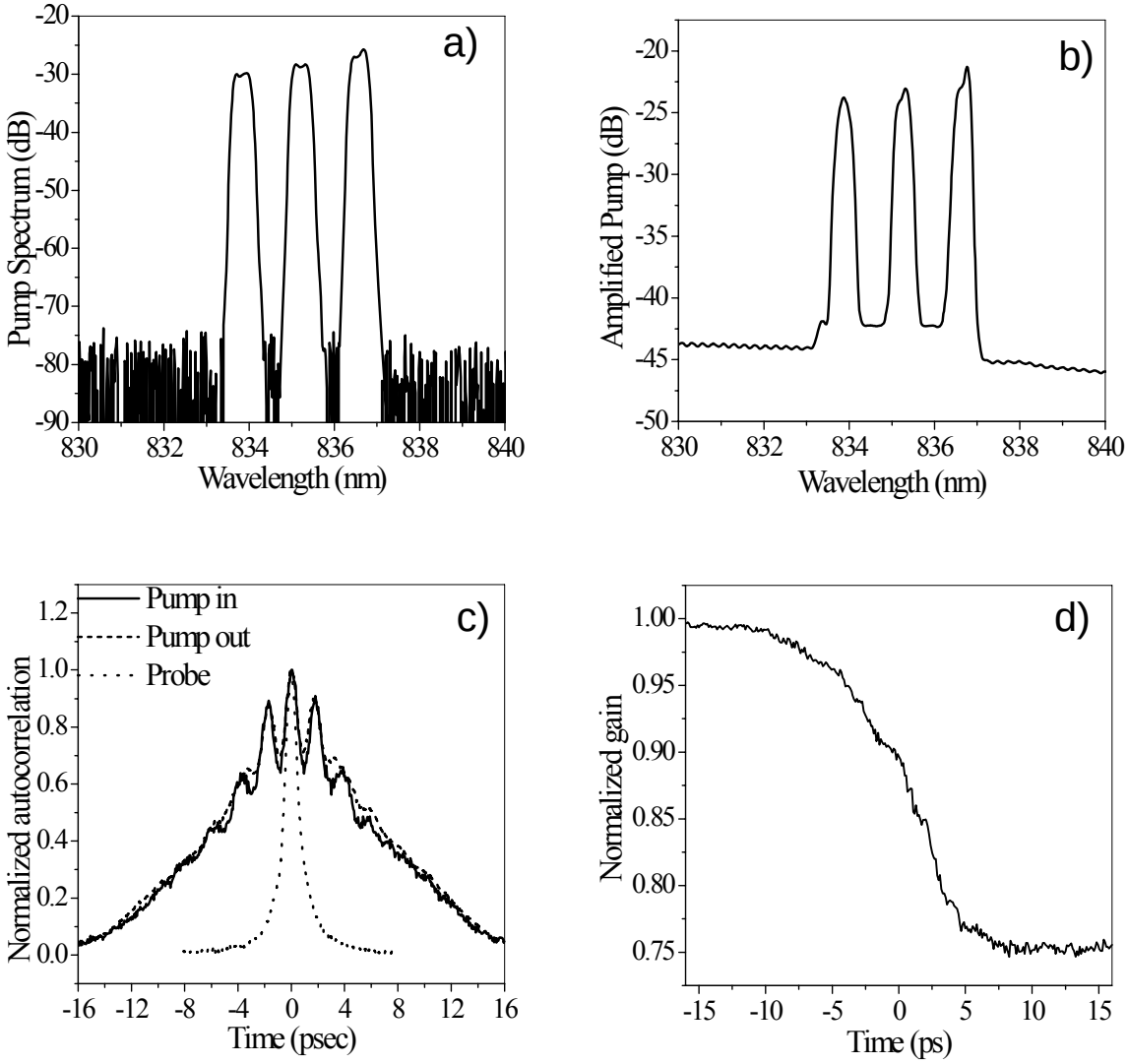

Figure 5.12: SOA gain dynamics for the amplification of non dispersion compensated multiwavelength pulses. Pump spectrum a), pump spectrum after amplification b), pump, probe, and pump after amplification autocorrelations c), and time resolved gain dynamics d).

pulse profile is therefore broader with less temporal beating. Figure 5.12 shows the input and output spectra, the intensity autocorrelations and the time resolved gain, and Figure 5.13 shows the time-resolved probe spectrum. In this case, the fast gain dynamics observed for the

amplification of dispersion compensated multiwavelength pulses are decreased, the extra wavelength channels product of four wave mixing effects on the SOA are greatly suppressed and the pump autocorrelation is broader with less temporal modulation owing to the temporal skew and the pulse broadening due to the pulse chirp. This leads to a slower gain depletion and results in the reduction of carrier heating and carrier cooling effects and a better power extraction from the SOA. In addition, the induced cross phase modulation effects are no longer evident when the probe spectrum is measured as a function of the delay between the pump and the probe as shown in Figure 5.13.

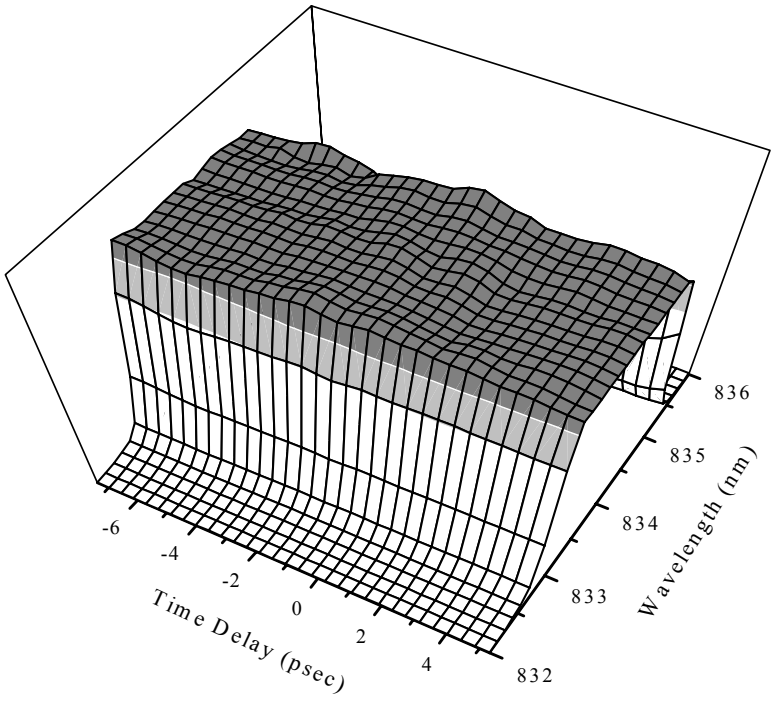

Figure 5.13: Probe spectrum measured as a function of the delay between pump and probe for the amplification of non dispersion compensated multiwavelength pulses.

In general, all the nonlinear effects were decreased when amplifying chirped multiwavelength pulses. This is owing to the fact that the composite pulse profile is broadened

and the temporal beating resulting from the coherent nature of the multiwavelength pulses is decreased as a result of the pulse chirp.

5.4 External cavity multiwavelength semiconductor hybrid mode-locked laser intracavity gain dynamics.

The measurement of the intracavity gain dynamics of an external cavity multiwavelength semiconductor hybrid mode-locked laser is presented in this section, revealing how multiwavelength semiconductor lasers avoid nonlinearities in the gain media thereby making multiwavelength operation feasible.

The experimental setup is depicted in Figure 5.14 and includes an external cavity multiwavelength semiconductor mode-locked laser (laser under investigation), a probe laser, a dispersion compensator and a spectral filter. The multiwavelength laser and the probe laser are external cavity semiconductor hybrid mode-locked lasers and are synchronized by carefully matching the cavity lengths of the two lasers and sharing the same RF source.

The probe laser shown in the upper part of Figure 5.14 has a linear cavity configuration and was hybridly mode-locked for a SOA dc bias current of 167 mA with 250 mW of radio frequency (RF) signal power at 450 MHz (second harmonic), yielding 2.2 mW of average output power. A dispersion compensator was used to compensate the linear dispersion of the probe pulses resulting in pulses of approximately 1 ps deconvolved from the autocorrelation. The probe spectrum and autocorrelation are plotted in Figure 5.15.

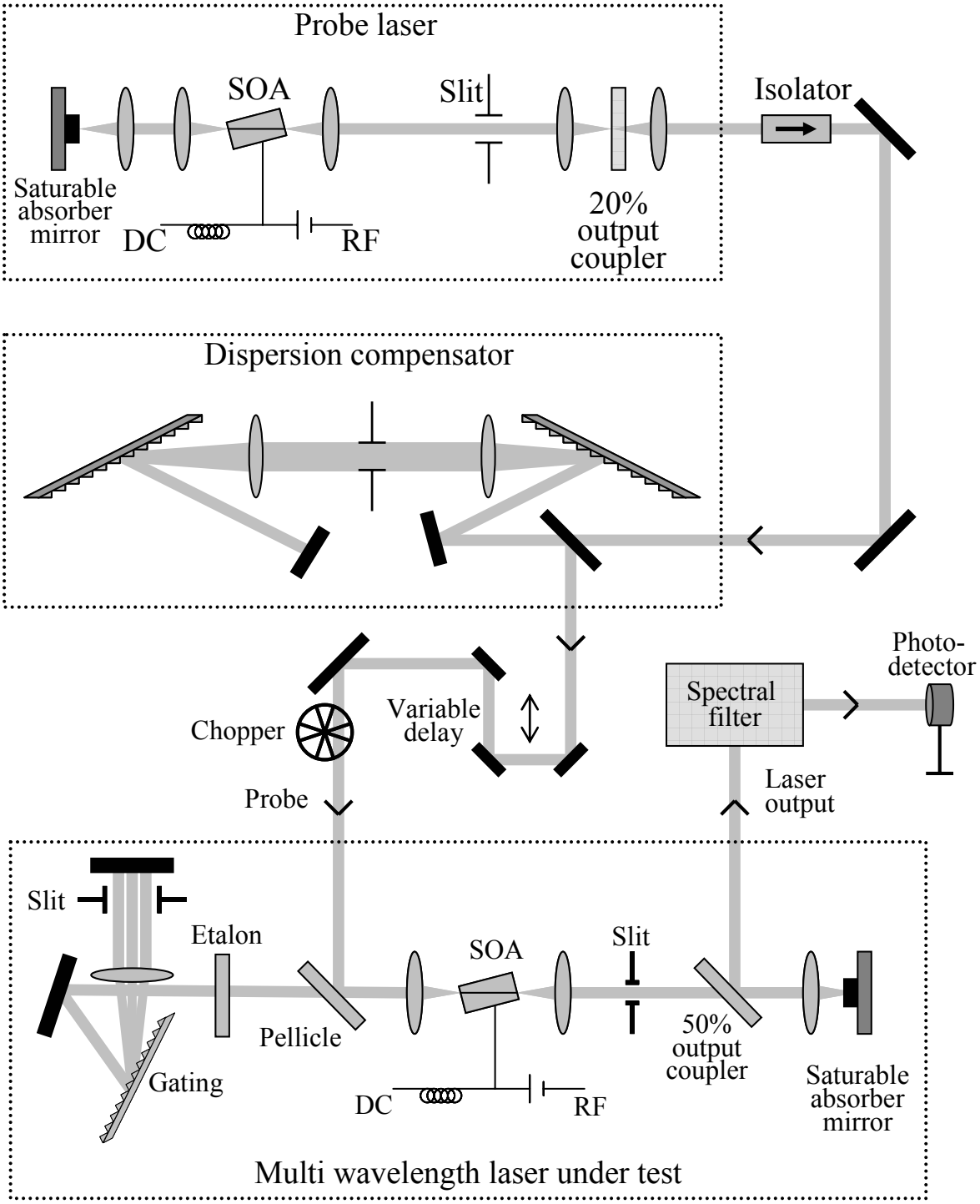

Figure 5.14: Experimental setup used to measure the intracavity gain dynamics of an external cavity multiwavelength semiconductor hybrid mode-locked laser

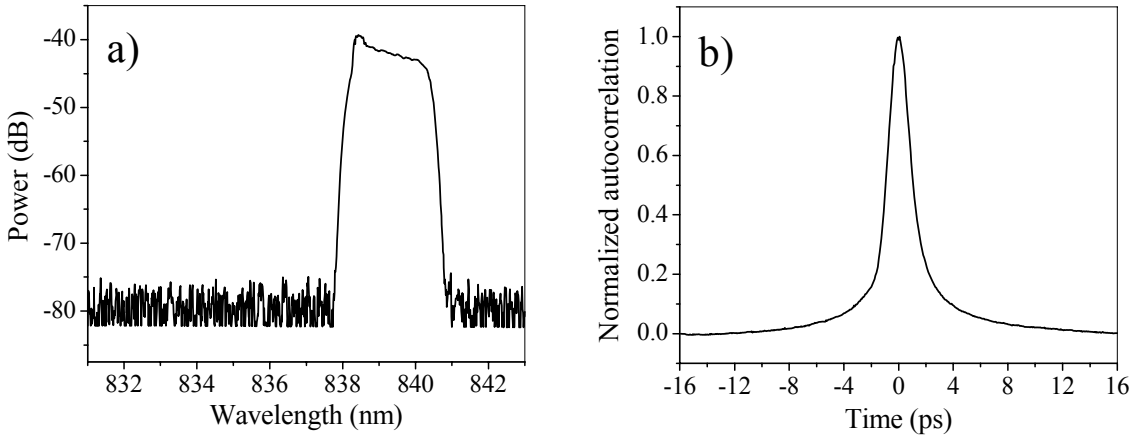

Figure 5.15: Probe pulse spectrum and autocorrelation

The multiwavelength laser in the lower part of Figure 5.14 has the same cavity configuration as the laser shown in Figure 5.3. The Fabry-Perot etalon in this case is a 0.5 mm thick solid glass etalon and its faces are 70% reflecting. The etalon transmission peaks are separated 0.48 nm at 835 nm and have a finesse of 8. Figure 5.l6 shows the calculated transmission spectrum of this etalon. The spectral filter in this laser is formed by an 1800 lines/mm grating, a 15 cm focal length lens and a mirror, located 15 cm from each other (lens' focal length). The slit in front of the mirror in the spectral filter allows 3 etalon transmission peaks around 835 nm (three mode-locked wavelength channels) to oscillate in the laser. Hybrid mode-locking was achieved for an SOA dc bias current of 150 mA with 250 mW of radio frequency (RF) signal power at 450 MHz (second harmonic), yielding 4 mW of average output power. Figure 5.17 shows the multiwavelength laser spectrum and the pulse train measured using a 15 GHz photo-detector and a sampling scope. Figure 5.18 shows the multiwavelength pulse

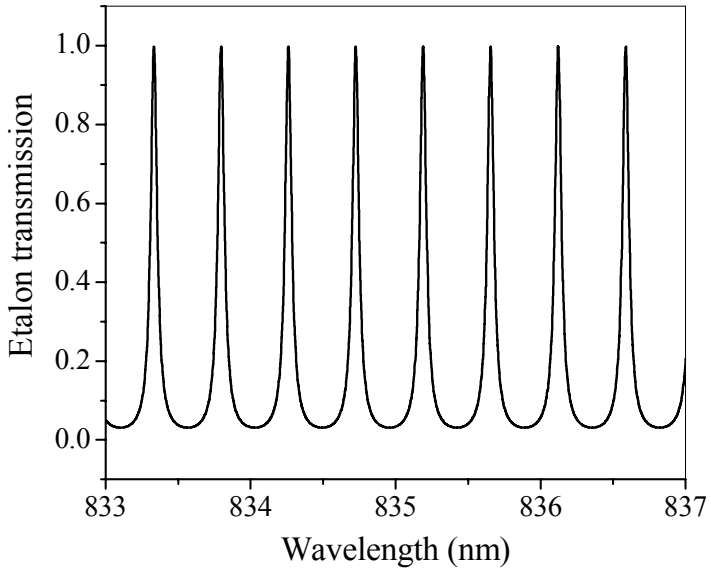

Figure 5.16: Transmission of a 0.5 mm tick solid glass etalon with 70% reflecting surfaces at normal incidence around 835 nm.

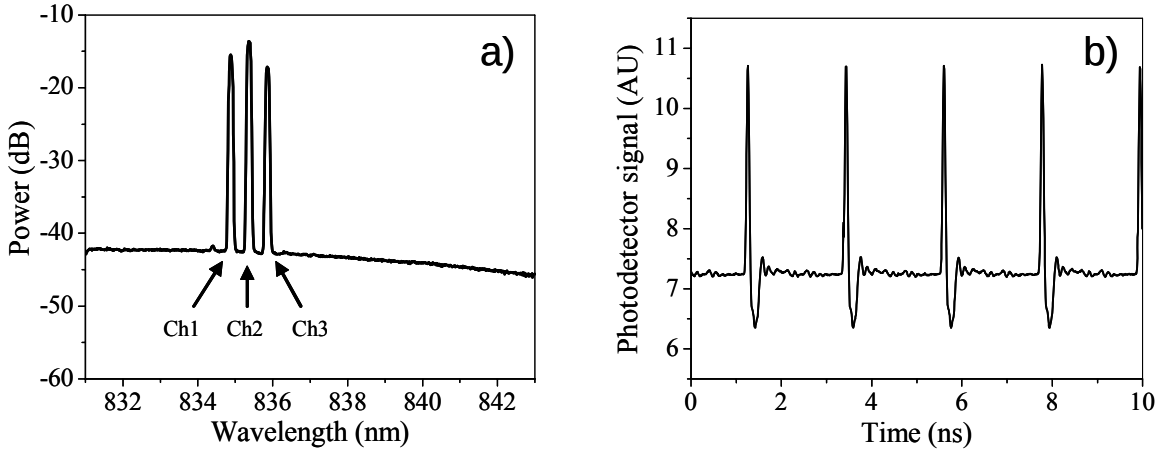

Figure 5.17: Multiwavelength laser spectrum and pulse train.

autocorrelation. As a result of the relatively long pulse duration and the limited time window of the autocorrelator, the complete autocorrelation could not be measured, thus an estimate of the pulse duration of the multiwavelength pulses can not be calculated. The modulation observed in the autocorrelation is an indication of the correlation between wavelength channels and the multi-pulse nature of the multiwavelength pulses.

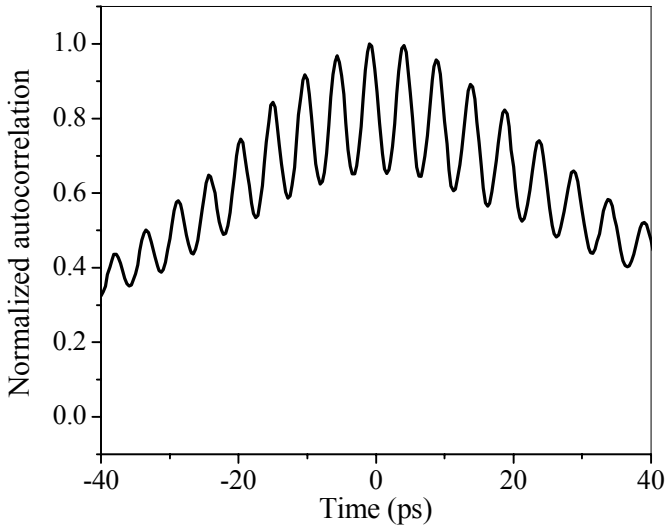

Figure 5.18: Multiwavelength pulse autocorrelation.

Each individual wavelength channel was selected using a spectral filter as the one depicted in Figure 5.2 and the autocorrelations of the pulses corresponding to each wavelength channel were measured. Also, each pulse was measured using a 15 GHz fast photo-detector and a sampling scope. Figure 5.19 shows the measured autocorrelations and the measured pulses corresponding to each individual wavelength channel. It can be observed in Figure 5.19b that the pulses corresponding to different wavelength channels do not temporarily coincide. These pulses are chirped and have a time duration several times the Fourier transform limit. The intensity and

the relative temporal pulse position of each channel are determined by the laser gain and dispersion. Note that the negative signal values in Fig. 5.19bc are an artifact from the impulse response of the photo-detector. In Figs. 5.19a and 5.19b channel one refers to the wavelength channel with the shortest wavelength, channel 2, to the wavelength channel in the middle, and channel 3, to the wavelength channel with the longest wavelength.

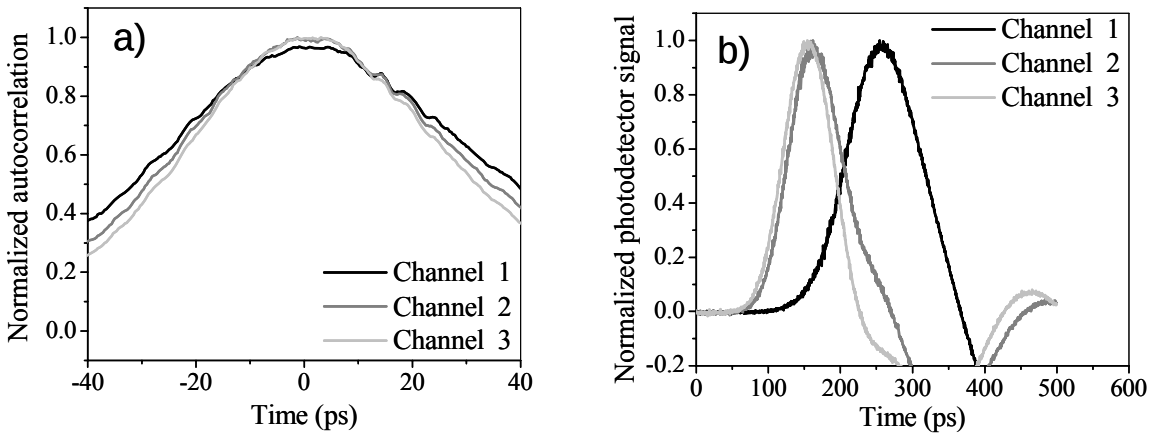

Figure 5.19: Individual wavelength channels autocorrelations a) and relative pulse positions b).

To measure the temporal evolution of the SOA gain in the multiwavelength laser, the probe pulses were introduced into the multiwavelength laser cavity using a pellicle beam splitter, as shown in Figure 5.14. The probe power coupled into the multiwavelength laser (a few micro watts averaged power), is sufficiently low to avoid disturbing the multiwavelength operation of the laser. A variable delay stage changes the relative delay between the probe and the multiwavelength pulses in the multiwavelength laser cavity. The probe pulses measure the SOA gain as a function of the delay between the probe and the multiwavelength pulses, representing

the temporal evolution of the SOA gain. A chopper and a lock-in amplifier were used on the probe to obtain clean measurements.

The laser output contains the probe pulses after measuring the SOA gain and the multiwavelength pulses; however the probe and the multiwavelength laser spectra do not overlap, facilitating their separation via spectral filtering. Figure 5.20a shows the measured temporal evolution of the SOA gain. The gain changes resulting from the gain depletion induced by the amplification of the multiwavelength pulses and the gain recovery are superimposed on a gain that is modulated by the bias current. By measuring the temporal evolution of the gain while blocking the laser feedback, the modulated gain was measured, and it was used as a reference to normalize the measured gain under multiwavelength operation. The modulated gain is shown in Fig. 5.20b and the normalized gain is shown in Fig. 5.20c. The chosen time window in Figs. 5.20a, 5.20b and 5.20c is sufficient to observe the important gain dynamics during one cavity round trip. Times beyond this window correspond to a slow gain recovery between the amplification of consecutive pulses. Due to the multiwavelength laser cavity configuration, the multiwavelength pulses pass through the SOA twice per cavity round trip, traveling in opposite directions each time, while the probe pulses pass through the SOA in only one direction measuring the SOA gain. Two gain depletion regions can be observed in Fig. 5.20c. The first corresponds to the multiwavelength and the probe pulses passing through the SOA in opposite directions and the second corresponds to multiwavelength and probe pulses passing through the SOA in the same direction. A close-up of the second gain depletion is shown in Fig. 5.20d, where the important feature is that the SOA gain is slowly depleted avoiding nonlinearities in the SOA during the amplification process.

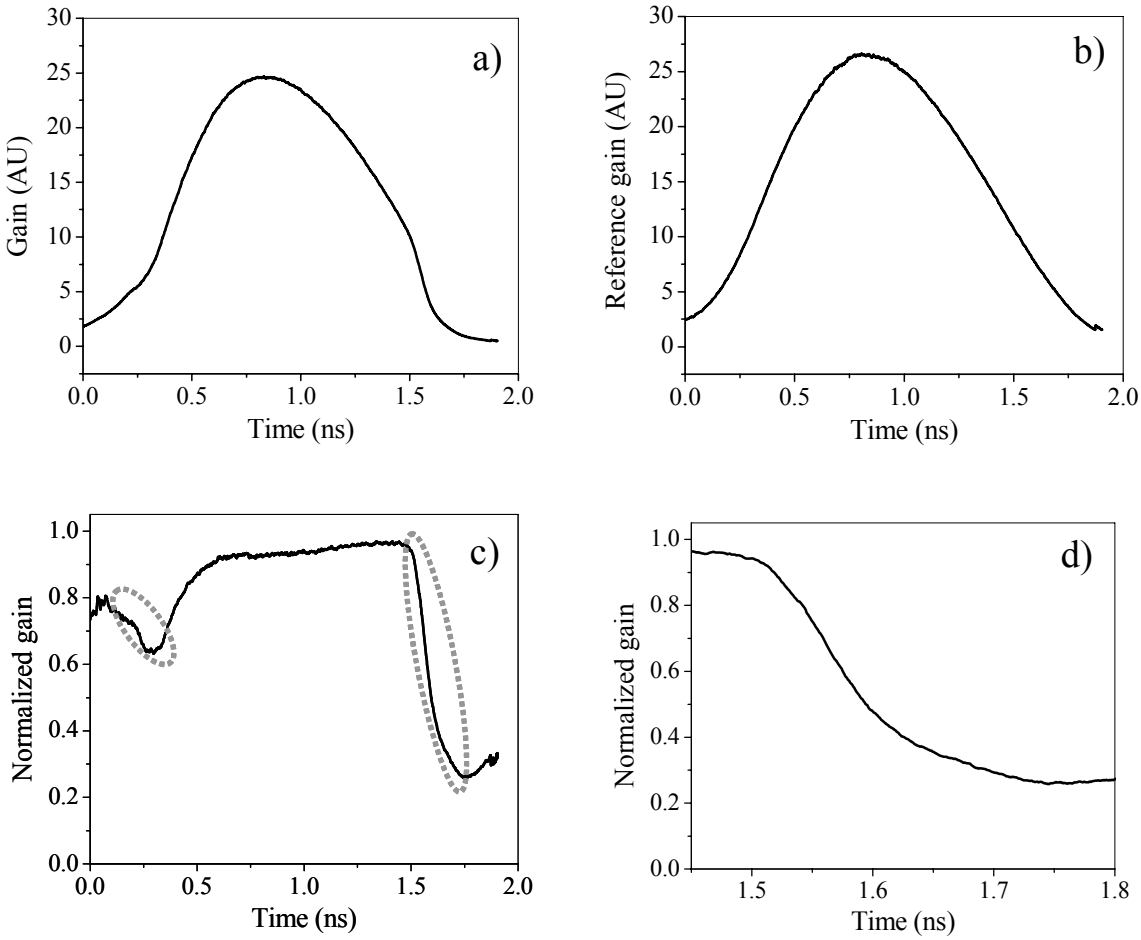

Figure 5.20: Temporal evolution of the SOA gain a), gain modulated by the bias current b), normalized gain (the gain depletions due to the amplification of the multiwavelength pulses are circled) c), and gain depletion close-up d).

In order to assure that these measurements are not limited by the timing jitter between the probe laser and the multiwavelength laser, the relative timing jitter between lasers was measured. The timing jitter between lasers was calculated from the measurement of the cross-correlation of pulses from the multiwavelength laser with pulses from the probe laser. The timing jitter is equal to the broadening of the cross-correlation over the theoretical width of the cross-correlation calculated from the autocorrelation of each pulse [70]. For this measurement, the

multiwavelength laser was temporarily configured to obtain short pulses by removing the etalon and adjusting the spectral filter to allow for a broader spectral bandwidth, producing pulses of approximately 1 ps after dispersion compensation. The spectrum and autocorrelation of these pulses are showed in Figure 5.21. To measure the cross-correlation, the pulses from the probe laser were delayed 19 ps with respect to the pulses from the multiwavelength laser, then the pulses from both lasers were combined using a 50% beam splitter and the autocorrelation of this pulse combination was measured and is shown in Figure 5.22. The autocorrelation has three peaks, the two lateral peaks are the cross-correlation of the probe pulses with the pulses from the multiwavelength laser and the center peak is the sum of the autocorrelations of each pulse. The calculated timing jitter is 2 ps.

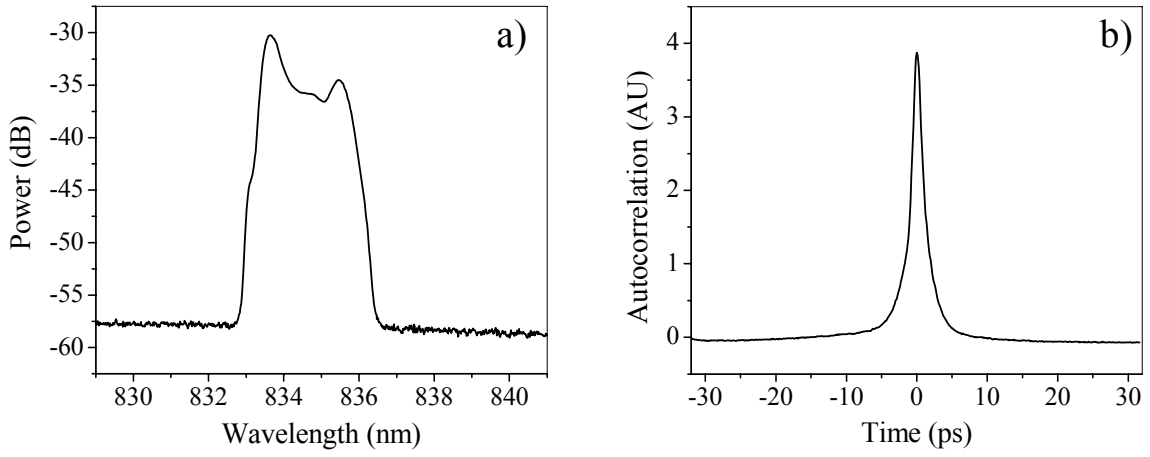

Figure 5.21: Multiwavelength laser temporarily configured as a short pulse laser. Pulse spectrum a) and pulse autocorrelation after dispersion compensation b).

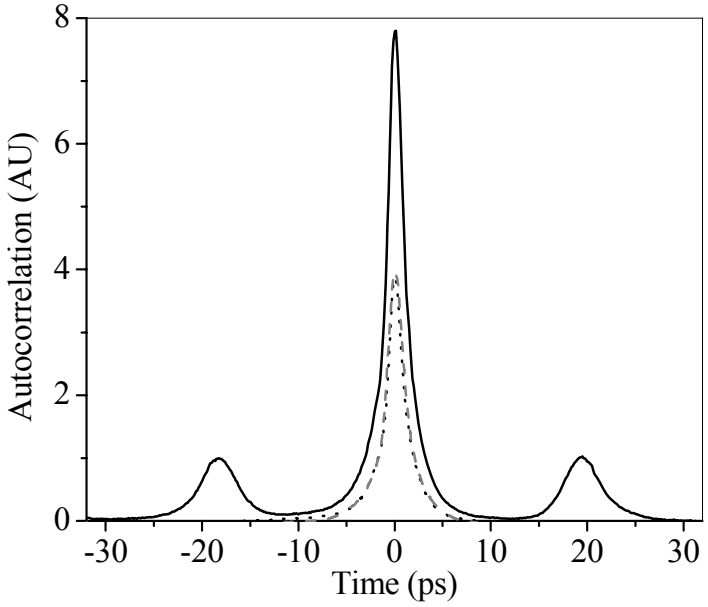

Figure 5.22: Autocorrelations of the pulses from the probe laser (---), pulses from the multiwavelength laser configured as a short pulse laser (…) and delayed combination of these two pulses (──).

A second method was used to measure the timing jitter between the probe and the multiwavelength lasers to verify the previous timing jitter measurement. A 25 GHz photo-detector was used to detect the pulses from the multiwavelength laser and a 15 GHz photo-detector was used to detect the probe pulses. The signal from the 25 GHz photo-detector was used to trigger a sampling scope measuring the probe pulses detected by the 15 GHz photo-detector. Figure 5.20 shows a picture of the sampling scope performing this measurement with a measured timing jitter between lasers of 1.87 ps, agreeing with the jitter measurement obtained from the cross correlation between pulses. It should be noted that that the measured probe pulse shown in Figure 5.20 is up side down, but this does not affect the results.

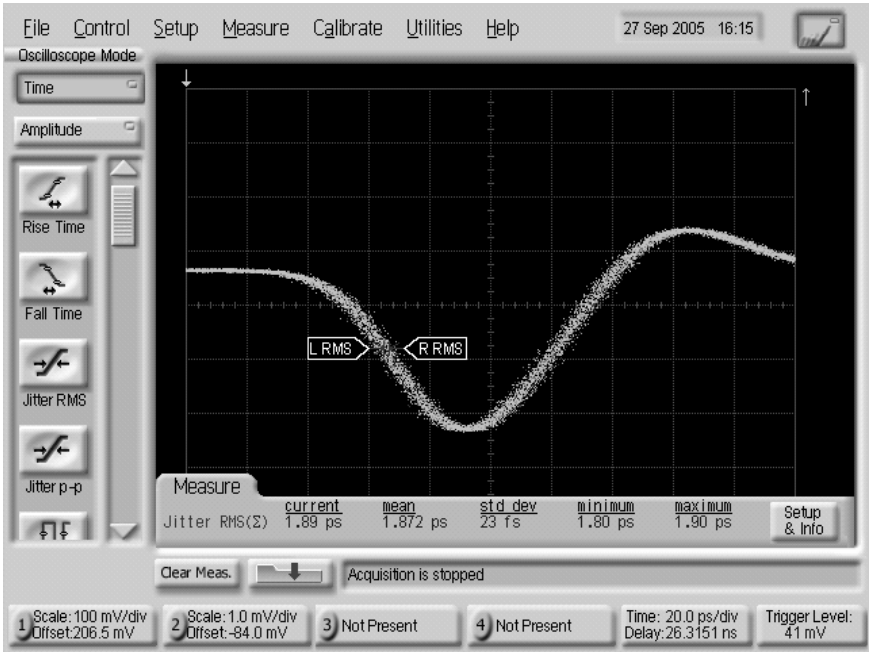

Figure 5.23: Relative time jitter between pulses from the probe and the multiwavelength lasers.

The temporal beating of the multiwavelength pulse resulting from the phase correlation between wavelength channels has a period defined by the separation of the wavelength channels. For the three wavelength case presented in this section, the beat period of the composite pulses is approximately 5 ps as can be observed from the autocorrelation shown in Figure 5.18. It should be noted that the timing jitter between the probe laser and the multiwavelength laser is smaller than the temporal beat period of the multiwavelength pulses and it should allow the resolution of fast gain dynamics if present.

CHAPTER SIX:
NUMERICAL SIMULATIONS

6.1 Numerical approach

Numerical simulations of the gain dynamics of a semiconductor optical amplifier were performed for the five different SOA gain dynamics measurements presented in this dissertation. The first one is the SOA gain dynamics measurement for the amplification of 750 fs pulses (Section 3.3), the second is the SOA gain dynamics measurement for the amplification of 6.5 ps pulses (Section 3.3), the third is the SOA gain dynamics measurement for amplification of dispersion compensated multiwavelength pulses (Section 5.3), the fourth is the SOA gain dynamics measurement for the amplification of non-dispersion compensated multiwavelength pulses (Section 5.3), and the fifth is the intracavity gain measurement of a external cavity multiwavelength semiconductor hybrid mode-locked laser (Section 5.4). The numerical approach used for the simulations is described next.

The SOA gain change $\Delta g(t)$ resulting from the amplification of a particular pulse was simulated by calculating the convolution of the intensity pulse profile $I_{pump}(t)$ and the SOA impulse response $h(t)$:

$$\Delta g(t) = \int_{-\infty}^{\infty} h(t - t_1) I_{pump}(t_1) dt_1 \tag{6.1}$$

The SOA impulse response function was calculated using the formula [54]:

$$h(t) = u(t)[a_0 e^{-(t/T_0)} + a_1(1 - e^{-(t/T_{1a})})e^{-(t/T_{1b})} + a_2 e^{-(t/T_2)}] + a_3\delta(t) \tag{6.2}$$

where: $u(t)$ is the unit step function ensuring casualty, $a_0 e^{-(t/T_0)}$ is the long lived stimulated carrier density change with a recovery time T_0 of approximately 1 ns, $a_1(1 - e^{-(t/T_{1a})})e^{-(t/T_{1b})}$ is the carrier heating response with a carrier heating delay T_{1a} of approximately 100 fs and a carrier cooling time T_{1b} of approximately 1 ps, $a_2 e^{-(t/T_2)}$ is the spectral hole burning with a carrier redistribution time T_2 of approximately 100 fs and $a_3\delta(t)$ represents the instantaneous processes.

The parameters used to generate the SOA impulse response function were obtained from previous simulations [54], and adjusted until the simulated gain dynamics matched the experimental results obtained for the amplification of the750 fs presented in Section 3.3.

An approximation of the intensity pulse profile was obtained for each case from the measured spectra and autocorrelations. The square root of the measured pulse spectrum is calculated, representing the spectral field for Fourier transform limited pulses, then quadratic and cubic phase are added to the spectral field to broaden the pulses. The modified spectral field is inverse Fourier transformed and multiplied by its complex conjugate obtaining the simulated temporal pulse profile. The autocorrelation of the simulated pulse is calculated and compared with the measured autocorrelation, and the spectral phase is modified until a satisfactory fit is obtained.

In the pump-probe measurements the probe power was measured using a slow photo-detector which averages the probe power over time, thus the probe power measured as a function of the delay between pump and probe $S(\tau)$ is equivalent to the cross-correlation of the probe pulse intensity profile $I_{probe}(t)$ and the gain changes induced by the pump pulses $\Delta_g(t)$ [54]:

$$S(\tau) = \int_{-\infty}^{\infty} I_{probe}(t-\tau)\Delta_g(t)dt \tag{6.3}$$

The SOA gain change induced by the pump pulses $\Delta_g(t)$ and the simulation of the measured gain dynamics taking into account the duration of the probe pulses $S(\tau)$ are computed for each case.

It is important to emphasize that this simulations represent an approximation and not an exact fit of the experimental results.

6.2 Numerical simulation of the impulse response function of a SOA and the SOA gain dynamics for the amplification of 750 fs pulses

The experimental results of the measurement of the gain dynamics of a semiconductor optical amplifier for the amplification of 750 fs pulses were used to adjust the parameters of the impulse response function calculated using the formula 6.1 to match the experimental results. In this case the pump and probe pulses were identical and were experimentally obtained by compensating the linear chirp (quadratic phase) of the pulses from the laser source (Section 3.3).

Since the quadratic phase was compensated, the residual phase must contain only higher order phase terms, hence the pulse profile was simulated by adding only cubic spectral phase to the pulse spectral field. Figure 6.1 shows the resulting simulated SOA impulse response. Figure 6.2 shows the measured spectrum, the measured autocorrelation, the simulated pulse profile, the simulated autocorrelation, the measured SOA gain dynamics and the simulated measured SOA gain dynamics. The sign of the spectral cubic phase added was such that the simulated pulse has a sharp leading edge and a slow trailing one as can be observed in Figure 6.2c. This follows the temporal pulse profile of pulses from external cavity semiconductor mode-locked lasers as previously investigated in our research group [22, 59]. The parameters and the MATLAB programs used to calculate the impulse response, the pulse profile, the autocorrelation and the gain dynamics for this and the following simulations are presented in the Appendix.

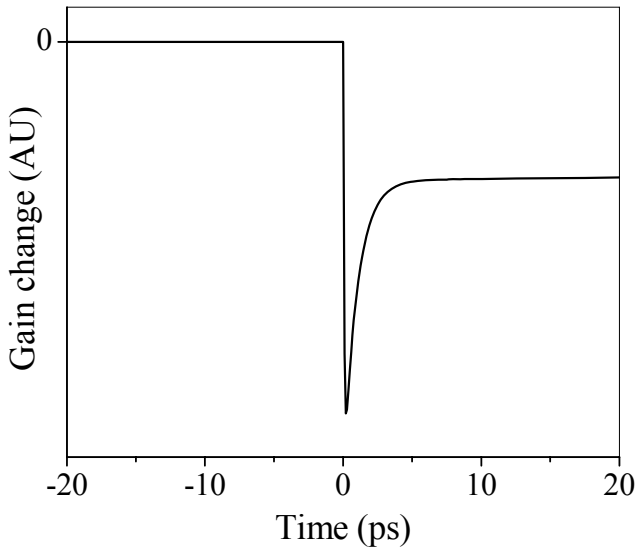

Figure 6.1: SOA impulse response.

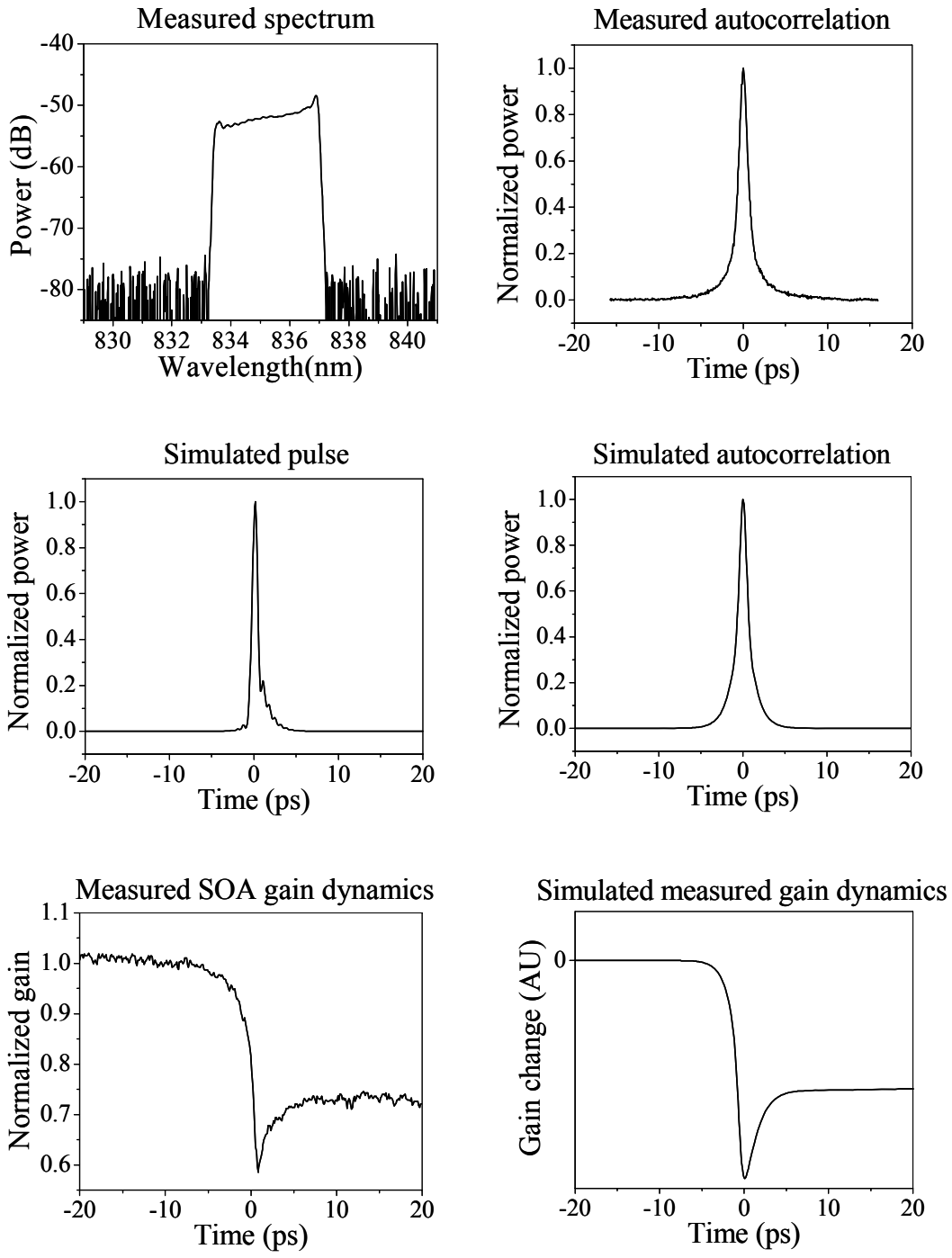

Figure 6.2: Measured spectrum a), measured autocorrelation b), simulated pulse profile c), simulated autocorrelation d), measured SOA gain dynamics e), and simulated measured SOA gain dynamics f) for the amplification of 750 fs pulses.

The simulation of the measured SOA gain dynamics for the amplification of the 750 fs pulses using a 750 fs probe is shown in Figure 6.2f. This is the result of the cross correlation of the probe intensity $I_{probe}(t)$ and the SOA gain change induced by the 750 fs pump $\Delta_g(t)$. Figure 6.3 compares the simulated SOA gain change $\Delta_g(t)$ and the simulated measured SOA gain dynamics $S(\tau)$. It can be observed in this Figure that the finite temporal duration of the probe smoothes the fast gain changes induced by the pump, but the measured gain dynamics is still good enough to resolve these fast gain changes.

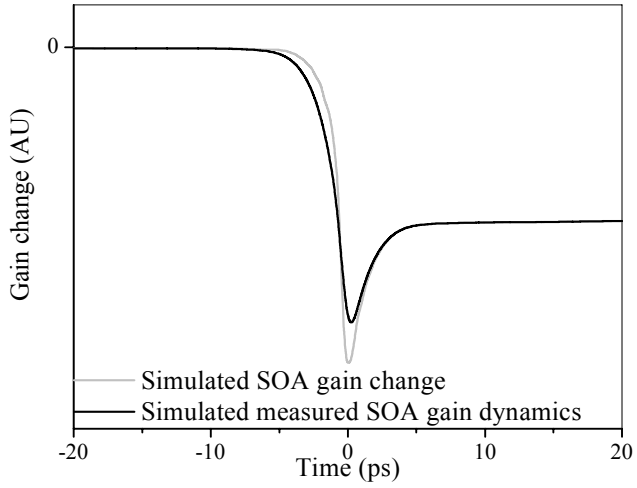

Figure 6.3: Simulated SOA gain change induced by the amplification of 750 fs pulses and the corresponding simulated measured SOA gain dynamics using a 750 fs probe.

For all the simulations in this chapter, the SOA impulse response plotted in Figure 6.1 was used to calculate the SOA gain change induced by the pump pulses $\Delta_g(t)$ and the pulse profile shown in Figure 6.2c was used as the probe pulse used to simulate the measured SOA gain dynamics $S(\tau)$.

6.3 Numerical simulation of the SOA gain dynamics for the amplification of 6.5 ps pulses

This section shows the numerical simulations for the amplification of 6.5 ps pulses presented in Section 3.3. In the experiment, the 6.5 ps pump pulses were obtained directly from an external cavity semiconductor mode-locked laser and were primary linearly chirped. The simulated pulse profile of the 6.5 ps pulses was calculated by adding linear dispersion to the simulated 750 fs pulses of Section 6.2. The amount of linear dispersion added is such that the measured and simulated autocorrelations of the 6.5 ps pulses are well matched. Figure 6.4 shows the measured spectrum, the measured autocorrelation, the simulated pulse profile, the simulated autocorrelation, the measured SOA gain dynamics and the simulated measured SOA gain dynamics. Figure 6.5 plots the simulated SOA gain change $\Delta_g(t)$ and the simulated measured SOA gain dynamics.

6.4 Numerical simulation of the SOA gain dynamics for the amplification of dispersion compensated multiwavelength pulses.

This section shows the numerical simulations for the amplification of dispersion compensated multiwavelength pulses. The measured gain dynamics for the amplification of these pulses is presented in Section 5.3. In the experiment, the dispersion compensated multiwavelength pulses where obtained by spectrally filtering the 750 fs obtained by dispersion compensating the pulses from the mode-locked laser pulse source.

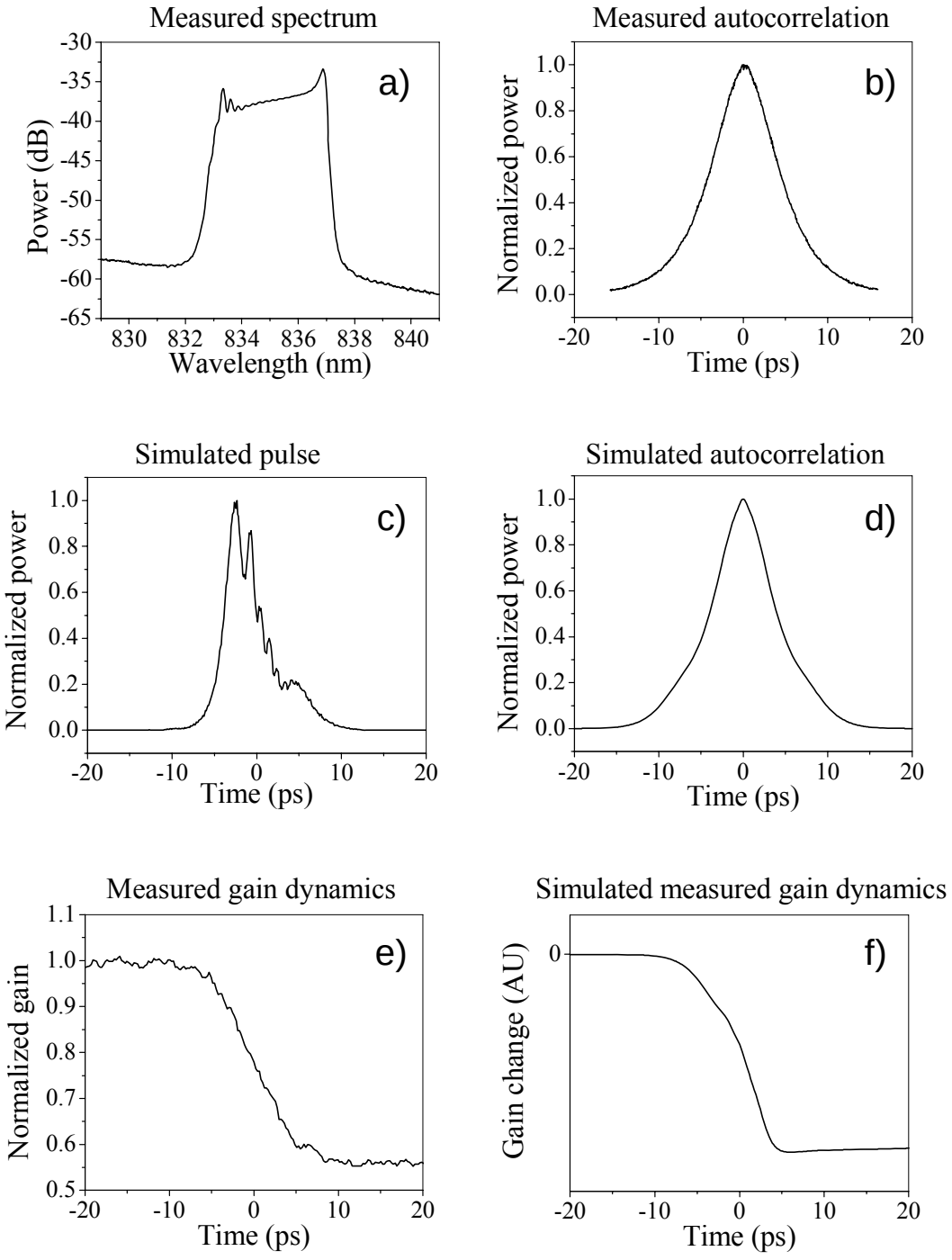

Figure 6.4: Measured spectrum a), measured autocorrelation b), simulated pulse profile c), simulated autocorrelation d), measured SOA gain dynamics e), and simulated measured SOA gain dynamics f) for the amplification of 6.5 ps pulses.

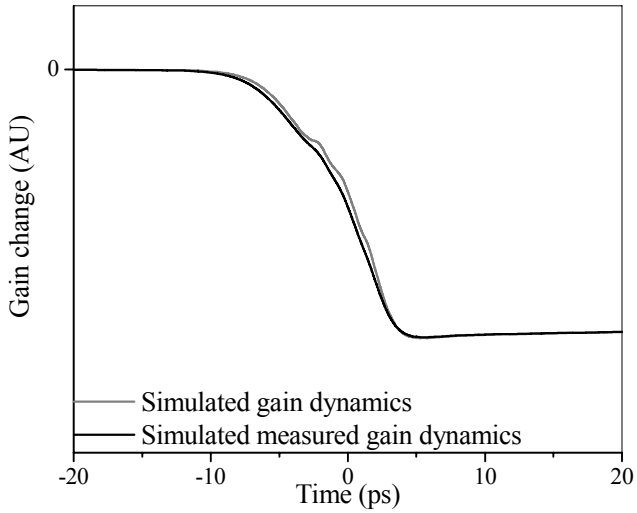

Figure 6.5: Simulated SOA gain change induced by the amplification of 6.5ps pulses and the corresponding simulated measured SOA gain dynamics using a 750 fs probe.

To simulate the pulse profile of the dispersion compensated multiwavelength pulses, the square root of the measured multiwavelength spectrum shown in Figure 5.10a is calculated and the same phase added to the 750 fs pulses of Section 6.2 is added to the calculated spectral field. The measured spectrum, the measured autocorrelation, the simulated pulse profile, the simulated autocorrelation, the measured SOA gain dynamics and the simulated measured SOA gain dynamics are shown in Figure 6.6. Figure 6.7 plots the simulated SOA gain change $\Delta_g(t)$ and the simulated measured SOA gain dynamics showing the smoothing effects of the finite probe in the gain dynamics measurements.

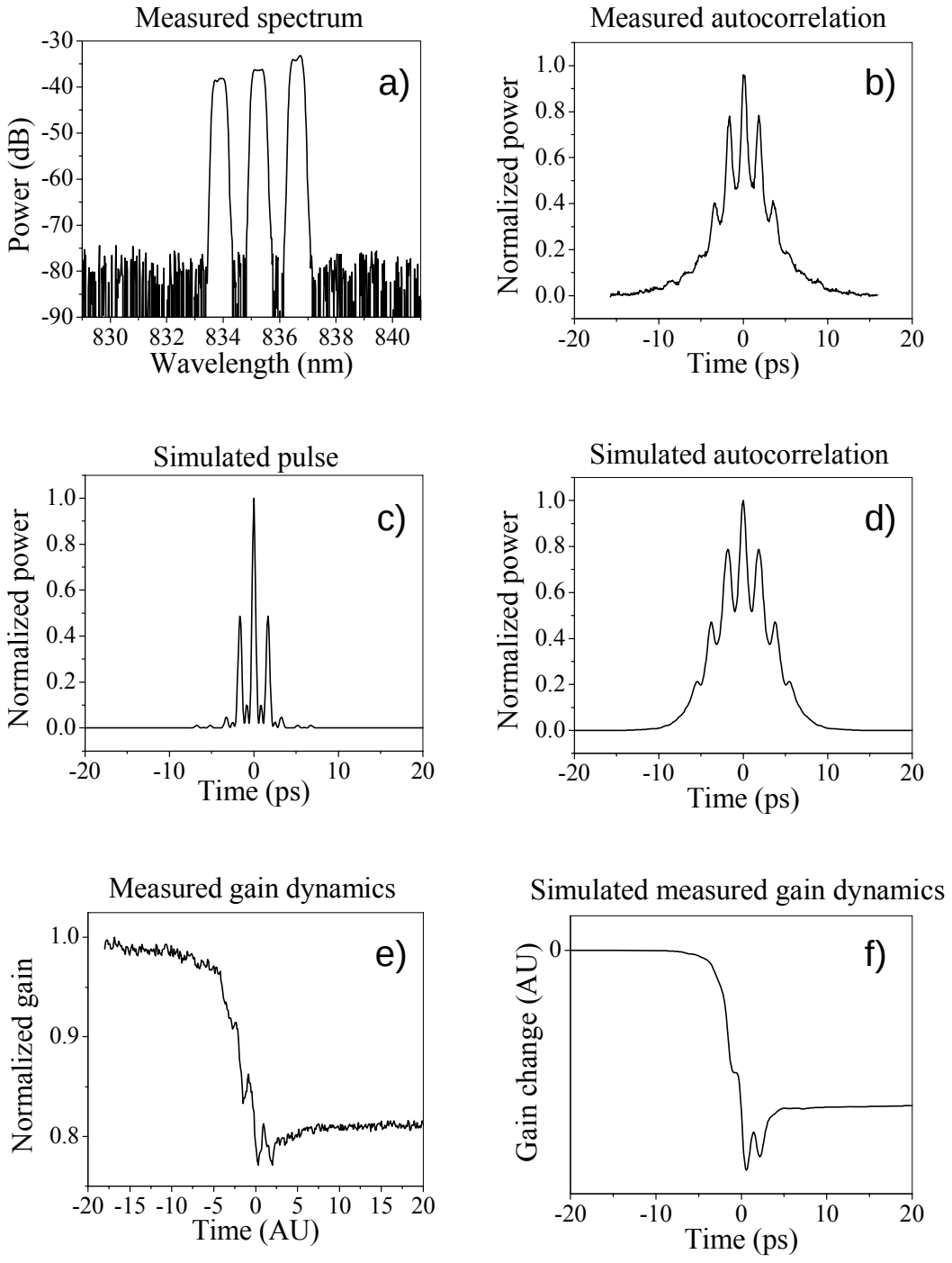

Figure 6.6: Measured spectrum a), measured autocorrelation b), simulated pulse profile c), simulated autocorrelation d), measured SOA gain dynamics e), and simulated measured SOA gain dynamics f) for the amplification of dispersion compensated multiwavelength pulses.

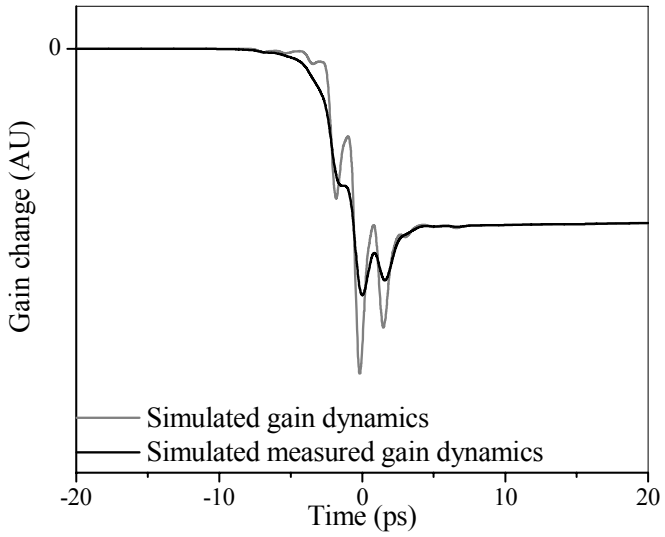

Figure 6.7: Simulated SOA gain change induced by the amplification of dispersion compensated multiwavelength pulses and the corresponding simulated measured SOA gain dynamics using a 750 fs probe.

6.5 Numerical simulation for the SOA gain dynamics for the amplification of non dispersion compensated multiwavelength pulses.

This section shows the numerical simulations for the amplification of non dispersion compensated multiwavelength pulses. The measured gain dynamics for the amplification of these pulses is presented in Section 5.3. In the experiment, the non dispersion compensated multiwavelength pulses where obtained by spectrally filtering the pulses obtained from the mode-locked laser pulse source. To simulate the pulse profile of the non dispersion compensated multiwavelength pulses, the square root of the measured multiwavelength spectrum shown in Figure 5.12a was calculated and the same phase added to the 6.5 fs pulses of Section 6.3 is added

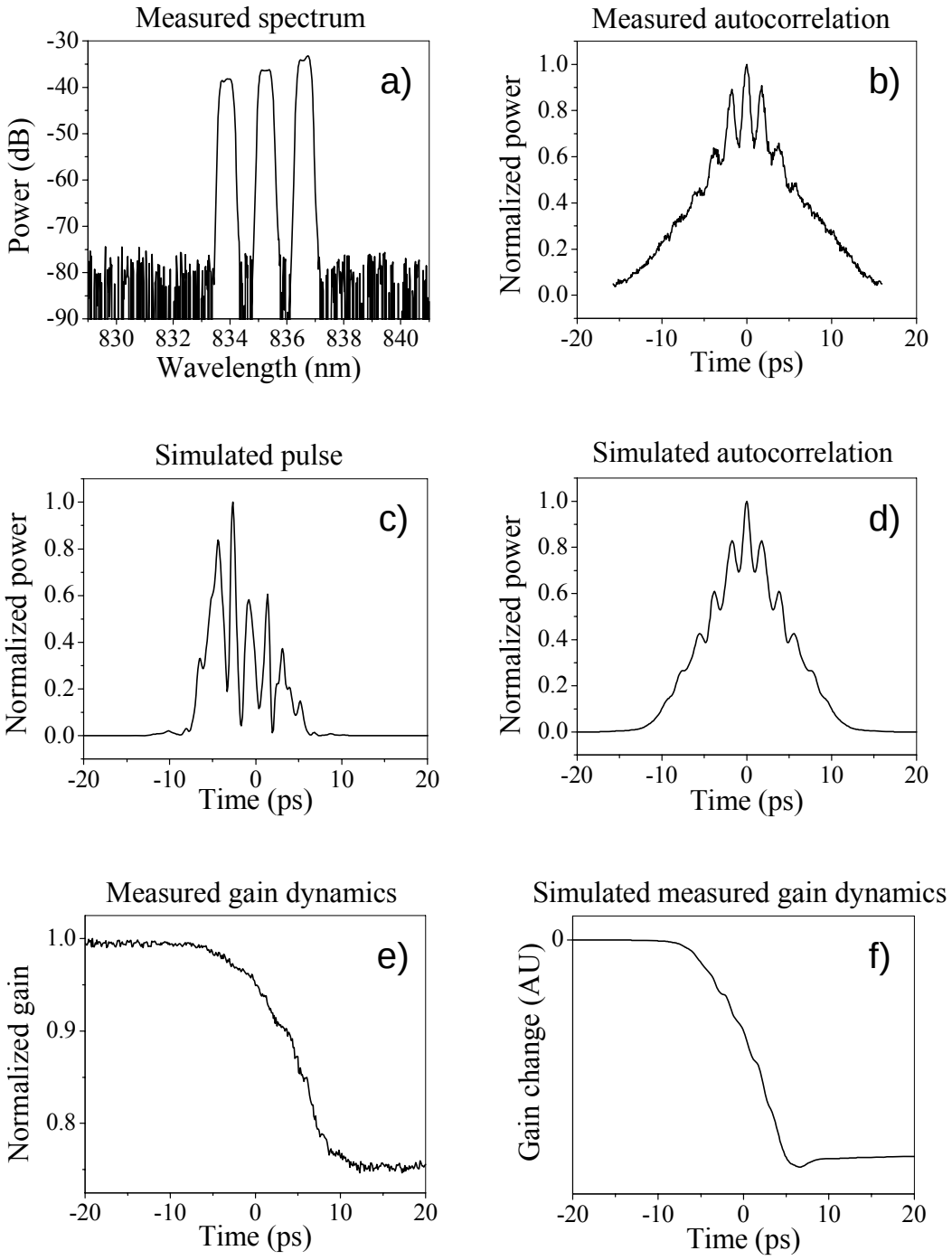

Figure 6.8: Measured spectrum a), measured autocorrelation b), simulated pulse profile c), simulated autocorrelation d), measured SOA gain dynamics e), and simulated measured SOA gain dynamics f) for the amplification of non dispersion compensated multiwavelength pulses.

to the calculated spectral field. The measured spectrum, the measured autocorrelation, the simulated pulse profile, the simulated autocorrelation, the measured SOA gain dynamics and the simulated measured SOA gain dynamics are shown in Figure 6.8. Figure 6.9 compares the simulated SOA gain change $\Delta_g(t)$ and the simulated measured SOA gain dynamics.

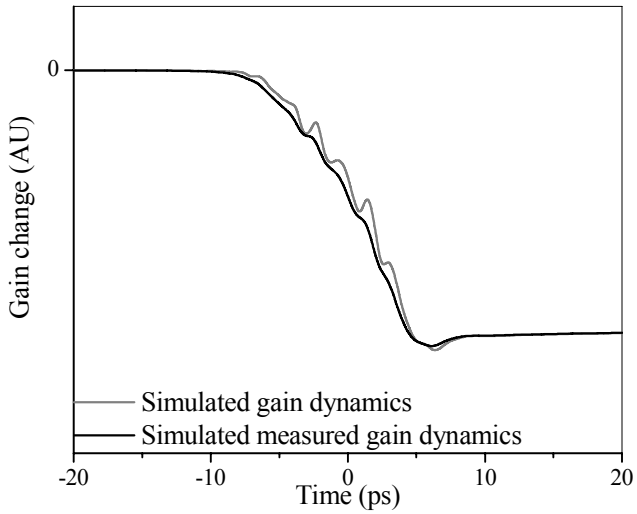

Figure 6.9: Simulated SOA gain change induced by the amplification of non dispersion compensated multiwavelength pulses and the corresponding simulated measured SOA gain dynamics using a 750 fs probe.

6.6 Numerical simulation for the intracavity gain dynamics measurements of an external cavity multiwavelength semiconductor hybrid mode-locked laser.

To simulate the intracavity gain dynamics of the multiwavelength laser presented in Section 5.4, the intracavity pulses were simulated by taking the square root of the measured spectrum, then by adjusting the spectral phase of each wavelength channel, the corresponding

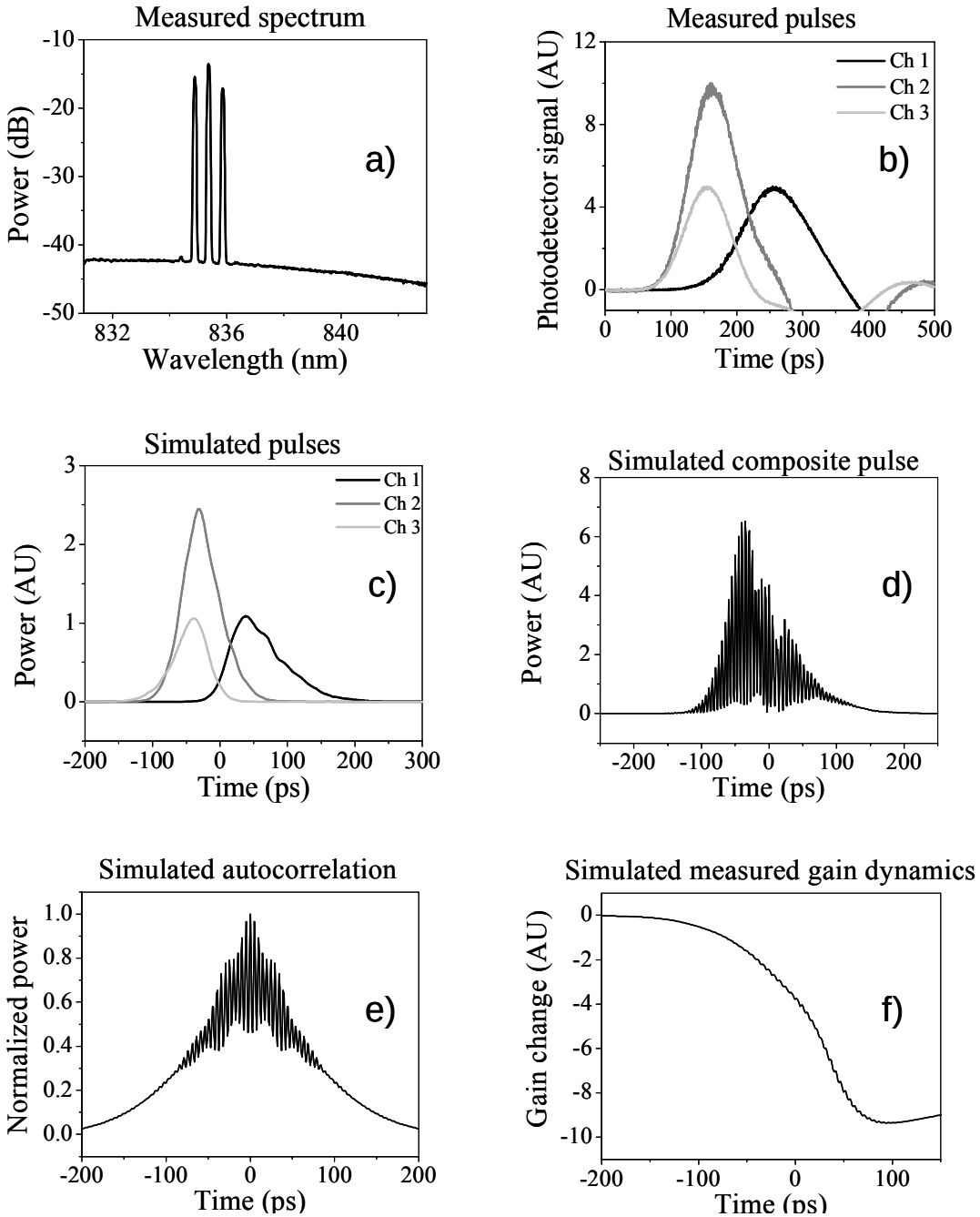

Figure 6.10: Measured spectrum a), measured pulses corresponding to each wavelength channel b) ,simulated pulses corresponding to each wavelength channel c), simulated composite pulse profile d), simulated autocorrelation e), and simulated measured SOA gain dynamics f) for the intracavity amplification of multiwavelength pulses.

pulses were broadened and temporally skewed to match the measured ones. Figure 6.10 shows the measured spectrum, the measured pulses corresponding to each wavelength channel, the simulated pulses, the composite pulse profile resulting from the combination of the three phase correlated wavelength channels, the simulated autocorrelation and the simulated gain dynamics. It can be observed in Figure 16f that the simulated gain dynamics is characterized by a slow gain depletion with no significant fast gain changes observed. Figure 6.9 compares the simulated SOA gain change $\Delta_g(t)$ and the simulated measured SOA gain dynamics.

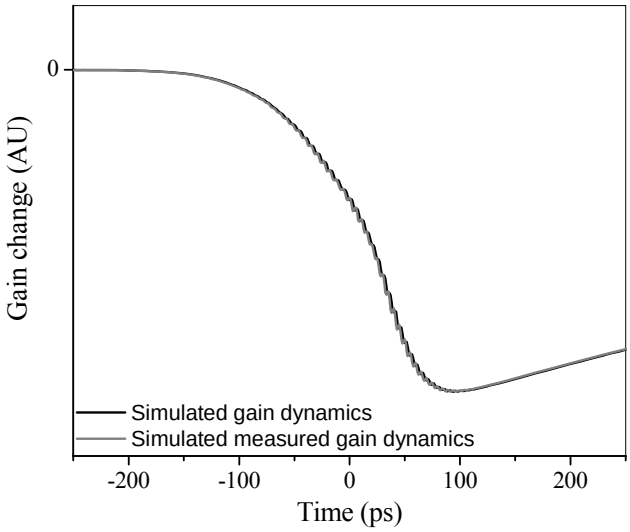

Figure 6.11: Simulated SOA gain change induced by the amplification of the intracavity multiwavelength pulses and the corresponding simulated measured SOA gain dynamics using a 750 fs probe.

The numerical simulations results agree well with the experimental ones, constituting theoretical support for the experimental conclusions derived from this work.

CHAPTER SEVEN:
SUMMARY AND CONCLUSIONS

The main goal of this dissertation was to understand the mechanisms that support the multiwavelength operation of external cavity multiwavelength semiconductor mode-locked lasers, and the knowledge acquired can be used for the future improvement of these lasers.

Semiconductor optical amplifiers (SOAs) are used as the gain media of external cavity semiconductor lasers and saturable absorbers (SAs) are used to passively or hybridly mode-locked these lasers. The SOA and the SA are the main elements of external cavity semiconductor mode-locked lasers and govern the pulse evolution in the laser. Pump-probe techniques were used to measure the absorption dynamics of a SA, the gain dynamics of a SOA for the amplification of diverse pulses and the intracavity gain dynamics of an external cavity semiconductor mode-locked laser in a multiwavelength configuration.

The absorption dynamics of the multiple quantum well saturable absorber were measured using sub-picosecond pulses as pump and probe and in an operating external cavity semiconductor laser where the saturable absorber was used to hybridly mode-locked the laser. The contribution of the SA to the pulse shaping and evolution in this kind of lasers was also studied.

The gain dynamics of the SOA were measured for the amplification of sub-picosecond pulses, pulses of several picoseconds, dispersion compensated multiwavelength pulses and multiwavelength pulses containing the dispersion of the pulses from the external cavity

semiconductor mode-locked laser used as the pulse source. It was proven that semiconductor optical amplifiers do not support the amplification of short pulses (sub-picosecond pulses). When a short pulse is amplified in a SOA, carrier heating, carrier cooling and fast gain changes take place changing the index of refraction and modulating the temporal phase of the pulses. This results in a spectral reshaping and a nonlinear chirp imparted on the amplified pulse with a corresponding pulse broadening. Pulses from external cavity semiconductor mode-locked lasers are inherently chirped and far from Fourier transform limit with time durations of several picoseconds. The pulse duration and chirp are determined by the SOA gain dynamics, the SA absorption dynamics and the dispersion of the intracavity elements. The relatively long pulses result in a slow SOA gain depletion that avoids nonlinearities and decreases shelf-phase modulation effects leading to a stable mode-locked operation. The best approach for the production of short pulses from external cavity semiconductor mode-locked laser systems is the production of long linearly chirped pulses from the laser followed by the pulse compression by dispersion compensation.

Carrier heating, carrier cooling and four wave mixing effects were observed for the amplification of dispersion compensated multiwavelength pulses. In this case, the carrier heating and carrier cooling triggered by the short pulses in the composite pulse profile modulate the gain resulting in an oscillating instantaneous frequency imparted on the amplified multiwavelength pulses. In the ideal case of a Fourier transform limited multiwavelength pulse, the duration of the pulses in the pulse burst is inversely proportional to the bandwidth of the envelope of the spectrum encompassing all the wavelength channels. These short pulses can trigger fast gain dynamics and nonlinear effects in the SOA. In external cavity semiconductor mode-locked lasers the pulses are chirped and far from Fourier transform limit thereby avoiding the nonlinearities.

The results for the amplification of multiwavelength pulses containing the chirp of the laser source show a broad composite pulse with a decreased temporal modulation due to the pulse chirp and as a consequence, the fast gain changes and nonlinearities observed for the amplification of the dispersion compensated multiwavelength pulses are avoided.

The measurement of the intracavity gain dynamics of an external cavity multiwavelength semiconductor mode-locked laser revealed chirped pulses with a temporal skew among the pulses corresponding to the different wavelength channels. The temporal skew and pulse chirp broaden the composite pulse profile and decrease the temporal beating due to the phase correlation between wavelength channels, avoiding fast gain dynamics and nonlinearities, decreasing the gain competition among wavelength channels and supporting the multiwavelength operation of the laser.

Numerical simulations were made for the measurements of the SOA gain dynamics presented in this dissertation using a simple impulse function model and the results support the experimental results of this dissertation.

APPENDIX:
MATLAB SIMULATION PROGRAMS

MATLAB program used to simulate the probe pulses, the 750 fs pulses and the dispersion compensated multiwavelength pulses

```
close all; clear all; format long;
spectrumT=importdata('spectrum.xls');          %import spectrum
spectrum=spectrumT';                           %transpose vector

m=1024;                                        %vector length
i=1:m;                                         %index
center=m/2+1;                                  %index center
fstep=0.01*10^12;                              %frequency step
f=(i-center)*fstep;                            %frequency vector
tspan=1/fstep;                                 %time span
tstep=1/(m*fstep);                             %time step
t=(i-center)*tstep;                            %time vector

Ef0=sqrt(spectrum);                            %spectral field with no phase
Et0=ifft(Ef0);                                 %temporal field
It0=Et0.*conj(Et0);                            %temporal intensity
It0s=fftshift(It0);                            %temporal intensity shifted to center

qua=0*10^-6;                                   %quadratic phase coefficient
cub=1.0*10^-6;                                 %cubic phase coefficient
four=0*10^-6;                                  %quartic phase coefficient
PH2=exp(-j*qua*(i-center).^2);                 %quadratic phase
PH3=exp(-j*cub*(i-center).^3);                 %cubic phase
PH4=exp(-j*four*(i-center).^4);                %quartic phase

Ef1=Ef0.*PH2.*PH3.*PH4;                        %spectral field including phase
Et1=ifft(Ef1);                                 %temporal field
It1=Et1.*conj(Et1);                            %temporal intensity
It1s=fftshift(It1);                            %temporal intensity shifted to center
It1sT=It1s';

%save temporal profile
save('c:\archu\publications\simulations\Gaindynamics\probe\temporalprofile','It1s','-ASCII');
save('c:\archu\publications\simulations\Gaindynamics\probe\temporalprofileT','It1sT','-ASCII');

%plot spectrum and pulse profile
figure(1)
subplot(1,2,1)
plot(f,spectrum);
```

```
title('Spectrum');
xlabel('Frequency (Hz)');
ylabel('Power(AU)');
subplot(1,2,2)
plot(t,It0s,t,It1s);
title('Pulse profile, no phase and high order phase');
xlabel('Time (s)');
ylabel('Power(AU)');

   %Autocorrelation

   %       %decrease vector size to perform fast autocorrelation
   %       m=256;
   %       for k=1:m
   %          It1sa(k)=It1s(384+k);
   %          ta(k)=t(384+k);
   %       end
   %       It1s=It1sa;
   %       t=ta;

   It=zeros(1,3*m);
   ItT=zeros(1,3*m);
   for k=1:m
      It(k)=0;
      It(m+k)=It1s(k);
      It(2*m+k)=0;
      ItT(k)=It1s(k);
   end
   i2=1:3*m;
   for k=1:2*m
      for p=3*m:-1:2
         ItT(p)=ItT(p-1);
      end
      ItT(1)=0;
      int=0;
      for q=1:3*m
         int=int+(It(q).*ItT(q));
      end
      autocorr(k)=int;
   end

   for k=1:m
      autocorrelation(k)=autocorr(k-1+m/2);
   end
   autocorrelation=autocorrelation/max(autocorrelation);
```

```
   autocorrelationT=autocorrelation';

%save simulated autocorrelation
save('c:\archu\publications\simulations\Gaindynamics\probe\simautocorr','autocorrelationT','-
ASCII');

measautocorrT=importdata('autocorrelation.xls');          %import measured autocorrelation
measautocorr=measautocorrT;                               %transpose vector
timeautocorrT=importdata('timeautocorrelation.xls');      %import time vector for measured
autocorrelation
timeautocorr=timeautocorrT*1*10^-12;                      %transpose vector

%plot measured and simulated autocorrelations
figure(2)
plot(timeautocorr,measautocorr,t,autocorrelation);
title('Autocorrelation, experimental and simulated');
xlabel('Time (s)');
ylabel('Normalized power');
```

MATLAB program used to simulate the 6.5 ps pulses and the non dispersion compensated multiwavelength pulses

```
close all; clear all; format long;
spectrumT=importdata('spectrum.xls');          %import spectrum
spectrum=spectrumT';                           %transpose vector

m=1024;                                        %vector length
i=1:m;                                         %index
center=m/2+1;                                  %index center
fstep=0.01*10^12;                              %frequency step
f=(i-center)*fstep;                            %frequency vector
tspan=1/fstep;                                 %time span
tstep=1/(m*fstep);                             %time step
t=(i-center)*tstep;                            %time vector

Ef0=sqrt(spectrum);                            %spectral field with no phase
Et0=ifft(Ef0);                                 %temporal field
It0=Et0.*conj(Et0);                            %temporal intensity
It0s=fftshift(It0);                            %temporal intensity shifted to center

qua=1800*10^-6;                                %quadratic phase coefficient
cub=1.0*10^-6;                                 %cubic phase coefficient
four=0*10^-6;                                  %quartic phase coefficient
PH2=exp(-j*qua*(i-center).^2);                  %quadratic phase
PH3=exp(-j*cub*(i-center).^3);                  %cubic phase
PH4=exp(-j*four*(i-center).^4);                 %quartic phase

Ef1=Ef0.*PH2.*PH3.*PH4;                        %spectral field including phase
Et1=ifft(Ef1);                                 %temporal field
It1=Et1.*conj(Et1);                            %temporal intensity
It1s=fftshift(It1);                            %temporal intensity shifted to center
It1sT=It1s';

%save temporal profile
save('c:\archu\publications\simulations\Gaindynamics\probe\temporalprofile','It1s','-ASCII');
save('c:\archu\publications\simulations\Gaindynamics\probe\temporalprofileT','It1sT','-ASCII');

%plot spectrum and pulse profile
figure(1)
subplot(1,2,1)
plot(f,spectrum);
```

```
title('Spectrum');
xlabel('Frequency (Hz)');
ylabel('Power(AU)');
subplot(1,2,2)
plot(t,It0s,t,It1s);
title('Pulse profile, no phase and high order phase');
xlabel('Time (s)');
ylabel('Power(AU)');

   %Autocorrelation

   %       %decrease vector size to perform fast autocorrelation
   %       m=256;
   %       for k=1:m
   %          It1sa(k)=It1s(384+k);
   %          ta(k)=t(384+k);
   %       end
   %       It1s=It1sa;
   %       t=ta;

   It=zeros(1,3*m);
   ItT=zeros(1,3*m);
   for k=1:m
      It(k)=0;
      It(m+k)=It1s(k);
      It(2*m+k)=0;
      ItT(k)=It1s(k);
   end
   i2=1:3*m;
   for k=1:2*m
      for p=3*m:-1:2
         ItT(p)=ItT(p-1);
      end
      ItT(1)=0;
      int=0;
      for q=1:3*m
         int=int+(It(q).*ItT(q));
      end
      autocorr(k)=int;
   end

   for k=1:m
      autocorrelation(k)=autocorr(k-1+m/2);
   end
   autocorrelation=autocorrelation/max(autocorrelation);
```

```
   autocorrelationT=autocorrelation';

%save simulated autocorrelation
save('c:\archu\publications\simulations\Gaindynamics\probe\simautocorr','autocorrelationT','-
ASCII');

measautocorrT=importdata('autocorrelation.xls');          %import measured autocorrelation
measautocorr=measautocorrT;                               %transpose vector
timeautocorrT=importdata('timeautocorrelation.xls');      %import time vector for measured
autocorrelation
timeautocorr=timeautocorrT*1*10^-12;                      %transpose vector

%plot measured and simulated autocorrelations
figure(2)
plot(timeautocorr,measautocorr,t,autocorrelation);
title('Autocorrelation, experimental and simulated');
xlabel('Time (s)');
ylabel('Normalized power');
```

MATLAB program used to simulate the intracavity multiwavelength pulses

```
close all; clear all; format long;
spectrumT=importdata('spectrum.xls');          %import spectrum
spectrum=spectrumT';                           %transpose vector

m=1024;                                        %vector length
i=1:m;                                         %index
center=m/2+1;                                  %index center
fstep=0.001*10^12;                             %frequency step
wavestep=fstep*(835*10^-9)^2/3E8;              %wavelength step
wavespan=wavestep*m;                           %wavelength span
f=(i-center)*fstep;                            %frequency vector
tspan=1/fstep;                                 %time span
tstep=1/(m*fstep);                             %time step
t=(i-center)*tstep;                            %time vector

Ef0=sqrt(spectrum);                            %spectral field with no phase
Ef0=Ef0-Ef0(612);
Et0=ifft(Ef0);                                 %temporal field
It0=Et0.*conj(Et0);                            %temporal intensity
It0s=fftshift(It0);                            %temporal intensity shited to center

figure(4)
plot(i,It0s)

r=1:200;

%phase channel 1
lina=2*pi*0.001E12*50E-12;                     %linear phase coeficient
quaa=8000*10^-6;                               %quadratic phase coeficient
cuba=10*10^-6;                                 %cubic phase coeficient
foura=0*10^-6;                                 %quartic phase coeficient
PH1a=exp(-j*lina*(r-100));                     %linear phase
PH2a=exp(-j*quaa*(r-100).^2);                  %quadratic phase
PH3a=exp(-j*cuba*(r-100).^3);                  %cubic phase
PH4a=exp(-j*foura*(r-100).^4);                 %quartic phase

%phase channel 2
linb=2*pi*0.001E12*(-50E-12);                  %linear phase coeficient
quab=8000*10^-6;                               %quadratic phase coeficient
```

```
cubb=10*10^-6;                          %cubic phase coeficient
fourb=0*10^-6;                          %quartic phase coeficient
PH1b=exp(-j*linb*(r-100));              %linear phase
PH2b=exp(-j*quab*(r-100).^2);           %quadratic phase
PH3b=exp(-j*cubb*(r-100).^3);           %cubic phase
PH4b=exp(-j*fourb*(r-100).^4);          %quartic phase

%phase channel 3
linc=2*pi*0.001E12*(-60E-12);           %linear phase coeficient
quac=8000*10^-6;                        %quadratic phase coeficient
cubc=10*10^-6;                          %cubic phase coeficient
fourc=0*10^-6;                          %quartic phase coeficient
PH1c=exp(-j*linc*(r-100));              %linear phase
PH2c=exp(-j*quac*(r-100).^2);           %quadratic phase
PH3c=exp(-j*cubc*(r-100).^3);           %cubic phase
PH4c=exp(-j*fourc*(r-100).^4);          %quartic phase

Ef1a=zeros(1,1024);
Ef1b=zeros(1,1024);
Ef1c=zeros(1,1024);
for k=1:200;
   Ef1a(center+100+k)=Ef0(center+100+k).*PH1a(k).*PH2a(k).*PH3a(k).*PH4a(k);
        %spectral field including phase
   Ef1b(center-100+k)=Ef0(center-100+k).*PH1b(k).*PH2b(k).*PH3b(k).*PH4b(k);
        %spectral field including phase
   Ef1c(center-300+k)=Ef0(center-300+k).*PH1c(k).*PH2c(k).*PH3c(k).*PH4c(k);
        %spectral field including phase
end

%channel 1
Et1a=ifft(Ef1a);                        %temporal field
It1a=Et1a.*conj(Et1a);                  %temporal intensity
It1sa=fftshift(It1a);                   %temporal intensity shited to center

%channel2
Et1b=ifft(Ef1b);                        %temporal field
It1b=Et1b.*conj(Et1b);                  %temporal intensity
It1sb=fftshift(It1b);                   %temporal intensity shited to center

%Channel 3
Et1c=ifft(Ef1c);                        %temporal field
It1c=Et1c.*conj(Et1c);                  %temporal intensity
It1sc=fftshift(It1c);                   %temporal intensity shited to center

figure(3)
```

```
plot(i,abs(It1sa),i,abs(It1sb),i,abs(It1sc))

Ef1=Ef1a+Ef1b+Ef1c;
Et1=ifft(Ef1);
It1=Et1.*conj(Et1);
It1s=fftshift(It1);

figure(5)
plot(It1s)

%save temporal profile
save('c:\archu\publications\simulations\Gaindynamics\MWintracavity\temporalprofile','It1s','-
ASCII');


%plot spectrum and pulse profile
figure(1)
subplot(1,2,1)
plot(f,spectrum);
title('Spectrum');
xlabel('Frequency (Hz)');
ylabel('Power(AU)');
subplot(1,2,2)
plot(t,It0s,t,It1s);
title('Pulse profile, no phase and high order phase');
xlabel('Time (s)');
ylabel('Power(AU)');

%Autocorrelation

      %decrease vector size to perform fast autocorrelation
%       m=256;
%       for k=1:m
%         It1sa(k)=It1s(384+k);
%         ta(k)=t(384+k);
%       end
%       It1s=It1sa;
%       t=ta;

   It=zeros(1,3*m);
   ItT=zeros(1,3*m);
   for k=1:m
      It(k)=0;
      It(m+k)=It1s(k);
      It(2*m+k)=0;
```

```
    ItT(k)=It1s(k);
  end
  i2=1:3*m;
  for k=1:2*m
    for p=3*m:-1:2
      ItT(p)=ItT(p-1);
    end
    ItT(1)=0;
    int=0;
    for q=1:3*m
      int=int+(It(q).*ItT(q));
    end
    autocorr(k)=int;
  end

  for k=1:m
    autocorrelation(k)=autocorr(k-1+m/2);
  end
  autocorrelation=autocorrelation/max(autocorrelation);
  autocorrelationT=autocorrelation';
  figure(2)
  plot(autocorrelation)

%save simulated autocorrelation
save('c:\archu\publications\simulations\Gaindynamics\MWintracavity\simautocorr','autocorrelati
onT','-ASCII');

%plot simulated autocorrelations
figure(2)
plot(t,autocorrelation);
title('Similated autocorrelation');
xlabel('Time (s)');
ylabel('Normalized power');
```

MATLAB program used to simulate the SOA impulse response and the SOA gain dynamics

```
close all; clear all; format long;

m=1024;                                          %vector length
i=1:m;                                           %index
center=m/2+1;                                    %index center

fstep=0.01*10^12;                                %frequency step
f=(i-center)*fstep;                              %frequency vector
tspan=1/fstep;                                   %time span
tstep=1/(m*fstep);                               %time step
t=(i-center)*tstep;                              %time vector

autocorrelationT=importdata('simautocorr');      %import simulated autocorrelation
autocorrelation=autocorrelationT';               %transpose vector

%plot simulated autocorrelation
figure(1)
plot(t,autocorrelation);
title('Simulated autocorrelation');
xlabel('Time (s)');
ylabel('Normalized power');

%impulse response function

   a0=-0.40;                                     %long lived stimulated carrier density change
   T0=1*10^-9;                                   %1 ns gain recovery
   a1=-.8;                                       %carrier heating response
   T1a=100*10^-15;                               %100 fs delay in heating of carriers
   T1b=1000*10^-15;                              %1000 fs cooling back to equilibrium
   a2=-0.5;                                      %spectral hole burning
   T2=120*10^-15;                                 %120 fs spectral hole burning recovery
   a3=-1;                                        %instantaneous response

   ut=zeros(1,m);                                %step function
   for k=center:m
      ut(k)=1;
   end

   SE=a0*exp(-(t/T0));                           %stimulated emision
   CH=a1*(1-exp(-(t/T1a))).*exp(-(t/T1b));       %carrier heating
```

```
   SHB=a2*exp(-(t/T2));                    %spectral hole burning

   IR=ut.*(SE+CH+SHB);                     %impulse response

%plot impulse response
figure(2)
plot(t,IR)
title('Impulse response');
xlabel('Time (s)');
ylabel('Normalized power')
IRT=IR';

%impulse function and intensity pulse profile convolution

I1=IR;
I2=importdata('temporalprofile');
I3=importdata('probetemporalprofile');

%    %decrease vector size to perform convolution
%    m=256;
%    for k=1:m
%      I1a(k)=I1(384+k);
%       I2a(k)=I2(384+k);
%       I3a(k)=I3(384+k);
%       ta(k)=t(384+k);
%    end
%    I1=I1a;
%    I2=I2a;
%    I3=I3a;
%    t=ta;

   %time inversion
   for k=1:m
      I2T(k)=I2(m-k+1);
   end

   convol=zeros(1,2*m);
   It1=zeros(1,3*m);
   It2T=zeros(1,3*m);
   for a=1:m
      It1(a)=I1(1);
      It1(m+a)=I1(a);
      It1(2*m+a)=I1(m);
      It2T(a)=I2(a);
   end
```

```
    i2=1:3*m;

    for b=1:2*m
       for d=3*m:-1:2
          It2T(d)=It2T(d-1);
       end
       It2T(1)=0;
       int=0;
       for e=1:3*m
          int=int+(It1(e).*It2T(e));
       end
       convol(b)=int;
    end

    for g=1:m
       convolution(g)=convol(g+m/2-3)+a3*I2(g);
    end
    convolutionT=convolution';

%correlation of convolution and probe intensity pulse profile

    I4=convolution;
    correl=zeros(1,2*m);
    It3T=zeros(1,3*m);
    It4=zeros(1,3*m);
    for a=1:m
       It4(a)=I4(1);
       It4(m+a)=I4(a);
       It4(2*m+a)=I4(m);
       It3T(a)=I3(a);
    end
    i2=1:3*m;
    for b=1:2*m
       for d=3*m:-1:2
          It3T(d)=It3T(d-1);
       end
       It3T(1)=0;
       int=0;
       for e=1:3*m
          int=int+(It4(e).*It3T(e));
       end
       correl(b)=int;
    end
    for g=1:m
```

```
    correlation(g)=correl(g+m/2-3);
  end
  correlationT=correlation';

%save gain dynamics and cross correlation
save('c:\archu\publications\simulations\Gaindynamics\lasercompressed\impulsefunction','IRT','-
ASCII');
save('c:\archu\publications\simulations\Gaindynamics\lasercompressed\gaindynamics','convoluti
onT','-ASCII');
save('c:\archu\publications\simulations\Gaindynamics\lasercompressed\crosscorrelation','correlat
ionT','-ASCII');

time=1*10^-12*importdata('timegain.xls');          %import time vector for measured gain
dynamics
gaindynamics=importdata('gain.xls');               %import measured gain dynamics

%plot measured and simulated gain dynamics
figure(3)
plotyy(time,gaindynamics./(-min(gaindynamics)),t,convolution./(-min(convolution)));
title('Gain dynamics, measured and simulated');
xlabel('Time (s)');
ylabel('probe transmission change (AU)');
figure(4)
plotyy(time,gaindynamics./(-min(gaindynamics)),t,correlation./(-min(correlation)));
title('Gain dynamics, measured and simulated');
xlabel('Time (s)');
ylabel('probe transmission change (AU)');
```

REFERENCES

1. R. N. Hall, G. E. Fenner, J. D. Kingsley, T. J. Soltys, and R. O. Carlson, “Coherent light emission from GaAs junctions,” Phys. Rev. Lett., 9, 366-369 (1962).

2. M. I. Nathan, W. Dumke, G. Burns, F. H. Dill Jr., and G. Lasher, “Stimulated emission of radiation from GaAs p-n junctions,” Appl. Phys. Lett., 1, 62-64 (1962).

3. N. Holonyak Jr. and S. F. Bevacqua, “Coherent (visible) light emission from Ga(As1–xPx) junctions,” Appl. Phys. Lett., 1, 82-83 (1962).

4. T. M. Quist, R. H. Rediker, R. J. Keyes, W. E. Krag, B. Lax, A. L., McWhorter, and H. J. Zeigler, “Semiconductor maser of GaAs,” Appl. Phys. Lett., 1, 91-92 (1962).

5. Hayashi, M. B. Panish, W. Foy, and S. Sumski, Appl. Phys. Lett., “Junction lasers which operate continuously at room temperature,” 17, 109-111 (1970).

6. Zh. I. Alferov, V. M. Andreev, D. Z. Garbuzov, Yu. V. Zhilyaev, E. P. Morozov, E. L. Portnoi, and V. G. Trofim, “Effect of heterostructure parameters on the laser threshold current and the realization of continuous generation at room temperature,” Sov. Phys. Semicond., 4, 1573–1575 (1970).

7. J. P. van der Ziel, R. Dingle, R. C. Miller, W. Wiegmann, and W. A. Nordland, Jr., "Laser oscillation from quantum states in very thin GaAs-Al0.2Ga0.8As multilayer structure," Appl. Phys. Lett,. 26, 463-465 (1975).

8. H. Hirayama, K. Matsunaga, M. Asada, and Y. Suematsu, “Lasing action of GaInAs/GaInAsP/InP tensile-strained quantum-box lasers,” Electron. Lett., 30, 142-143, (1994).

9. Drozhbin, Yu. A.; Zakharov, Yu. P.; Nikitin, V. V.; Semenov, A. S.; Yakovlev, V. A., “Generation of ultrashort light pulses with a GaAs semiconductor laser,” Journal of Experimental and Theoretical Physics Letters,” 5, 14-17 (1967).

10. P.-T. Ho, L. A. Glasser, E. P. Ippen, and H. A. Haus, “Picosecond pulse generation with a CW GaAlAs laser diode,” Appl. Phys. Lett., 33, pp. 241-243 (1978).

11. P. T. Ho, “Coherent pulse generation with a GaAlAs laser by active mode-locking,” Electron. Lett., 15, 526-527 (1979).

12. J. P. Van der Ziel, “Active mode-locking of double heterostructure lasers in an external cavity,” J. Appl. Phys., 52, 4435-4446 (1981).

13. J. E. Bowers, P. A. Morton, A. Mar, and S. W. Corzine, “Actively mode-locked semiconductor lasers,” IEEE J. Quantum Electron., 25, 1426-1439 (1989).

14. P. A. Morton, R. J. Helkey, and J. E. Bowers, “Dynamic detuning in actively mode-locked semiconductor lasers,” IEEE J. Quantum Electron., 25, 2621-2633 (1989).

15. M. Schell, A. G. Weber, E. Scholl, and D. Bimberg, “Fundamental limits of sub-ps pulse generation by active mode locking of semiconductor lasers: the spectral gain width and the facet reflectivities,” IEEE J. Quantum Electron., 27, 1661-1668 (1991).

16. M. Schell, A. G. Weber, E. H. Bottcher, E. Scholl, and D. Bimberg, “Theory of subpicosecond pulse generation by active modelocking of a semiconductor laser amplifier in an external cavity: Limits for the pulse width,” IEEE J. Quantum Electron., 27, 402-409 (1991).

17. E. P. Ippen, D. J. Eichenberger, and R. W. Dixon, “Picosecond pulse generation by passive modelocking of diode lasers,” Appl. Phys. Lett., 37, 267-269 (1980).

18. J. P. v. d. Ziel, W. T. Tsang, R. A. Logan, R. M. Mikulyak, and W. M. Augustyniak, “Subpicosecond pulses from a passively modelocked GaAs buried optical guide semiconductor lasers,” Appl. Phys. Lett., 39, 525-527 (1981).

19. H. Yokoyama, H. Ito, and H. Inaba, “Generation of subpicosecond coherent optical pulses by passive mode locking of an AlGaAs diode laser,” Appl. Phys. Lett., 40, 105-107 (1982).

20. Y. Silberberg, P. W. Smith, D. J. Eilenberger, D. A. B. Miller, A. C. Gossard, and W. Wiegmann, "Passive modelocking of a semiconductor diode laser," Opt. Lett., 9, 507-509 (1984).

21. P. J. Delfyett, L. Florez, N. Stoffel, T. Gmitter, N. Andreadakis, G. Alphonse, and W. Ceislik, "200-fs optical pulse generation and intracavity pulse evolution in a hybrid mode-locked semiconductor diode-laser/amplifier system", Opt. Lett. 17, 670-672 (1992).

22. B. Resan, L. Archundia, and P. J. Delfyett, Jr., "FROG measured high-power 185 fs pulses generated by down chirping of the dispersion-managed breathing-mode semiconductor mode-locked laser," IEEE Photonics Technology Letters, 17, 1384-1386 (2005).

23. Y. J. Chai, "1.36-Tb/s Spectral Slicing Source Based on a Cr4+-YAG Femtosecond Laser," J. Lightwave Technol., 23, 1319-1324 (2005).

24. J.-P. Blondel, "Massive WDM systems: recent developments and future prospects", in proceedings of IEEE 27th European Conference on Optical Communications, 50-53. (2001).

25. B. Mukherjee, "WDM optical communication networks: progress and challenges," IEEE J. Sel. Area Comm., 18, 1810-1824 (2000).

26. M. H. Reeve, A. R. Hunwicks, W. Zhao, S. G. Methley, L. Bickers, and S. Hornung, "LED spectral slicing for single-mode local loop applications," Electron. Lett., 24, 389–390 (1988).

27. S. S. Wagner and T. E. Chapuran, "Broadband high-density WDM transmission using superluminescent diodes", Electron. Lett., 26, 696-697 (1990).

28. J. S. Lee, Y. C. Chung, and D. J. DiGiovanni, "Spectrum-sliced fiber amplifier light source for multichannel WDM applications", IEEE Photonic. Tech. L., 5, 1458-1461 (1993).

29. S. Kawanishi, H. Takara, T. Morioka, O. Kamatani, and M. Saruwatari, "200 Gbit/s, 100 km time-division multiplexed optical transmission using supercontinuum pulses with prescaled PLL timing extraction and all-optical demultiplexing," Elecron. Lett., 31, 816-817 (1995).

30. T. Morioka, H. Takara, S. Kawanishi, O. Kamatani, K. Takiguchi, K. Uchiyama, M. Saruwatari, H. Takahashi, M. Yamada, T. Kanamori, and H. Ono, "1 Tbit/s (100Gbit/s x 10 channel) OTDM/WDM transmission using a single supercontinuum WDM source," Electron. Lett., 32, 906-907 (1996).

31. O. Boyraz, J. Kim, M. N. Islam, F Coppinger and B. Jalali, J, "10 Gb/s Multiple wavelength, coherent short pulse source based on spectral carving of supercontinuum generated in fibers", J. Lightwave Technol., 18, 2167-2175 (2000).

32. E. A. D. Souza, M. C. Nuss, W. H. Knox, and D. A. B. Miller, "Wavelength-division multiplexing with femtosecond pulses," Opt. Lett., 20, 1166-1168 (1995).

33. L. Boivin, M. C. Nuss, W. H. Knox, and J. B. Stark, "206-channel chirped-pulse wavelength-division multiplexed transmitter," Electron. Lett., 33, 827-829 (1997).

34. L. Boivin, M. Wegmueller, M. C. Nuss and W. H. Knox, "110Channels X 2.35 Gbs from a single femtosecond laser," IEEE Photonic. Tech. L., 11, 466-468 (1999).

35. H. Shi, J. Finaly, G. A. Alphonse, J.C. Connolly, and P.J. Delfyett, "Multiwavelength 10-GHz Picosecond Pulse Generation from a Single-Stripe Semiconductor Diode Laser," IEEE Photonic. Tech. L., 9, 1439-1441 (1997).

36. Nitta, J. Abeles, and P. J. Delfyett, "Hybrid wavelength-division and optical time-division multiplexed multiwavelength mode-locked semiconductor laser", Appl. Optics. 39, 6799-6805 (2000).

37. P. J. Delfyett, C. DePriest, and T. Yilmaz, "Signal processing at the speed of lightwaves", IEEE Circuit. Devic., 18, 28-35 (2002).

38. M. Mielke, G. A. Alphonse and P. J. Delfyett, "168 Channels X 6 GHz From a Multiwavelength mode-locked semiconductor laser," IEEE Photonic. Tech. L. 15, 501-503 (2003).

39. D. Marcuse, "Reflection loss of laser mode from tilted end mirror," J. Lightwave Technol., 7, 336-339 (1989).

40. G. A. Alphonse, D. B. Gilbert, M. G. Harvey and M. Ettenberg, "High power superluminescent diodes," IEEE J. Quantum Elect., 24, 2454-2457 (1988).

41. N. K. Dutta and P. P. Deimel, "Optical properties of a GaAlAs superluminescent diode," IEEE J. Quantum Electron. 19, 469–498 (1983).

42. D. S. Chemla, D. A. B. Miller, P. W. Smith, A. C. Gossard, and W. Wiegmann, "Room temperature excitonic nonlinear absorption and refraction in GaAs/AlGaAs multiple quantum well structures," IEEE J. Quantum Electron., 20, 265-275, (1984).

43. D. S. Chemla and D. A. B. Miller," Room-temperature excitonic nonlinear-optical effects in semiconductor quantum-well structures" J. Opt. Soc. Am. B 2, 1155-1173 (1985).

44. E. Yablonovitch, T. Gmitter, J. P. Harbison, and R. Bhat, "Extreme selectivity in the lift-off of epitaxial GaAs films," Appl. Phys. Lett., 51, 2222-2224 (1987).

45. E. Yablonovitch, D. M. Hwang, T. J. Gmitter, L. T. Florenz, and J. P. Harbison, "Van der Waals bonding of GaAs epitaxial liftoff films onto arbitrary substrates," Appl. Phys. Lett., 56, 2419-2421 (1990).

46. P. J. Delfyett, A. Dienes, J. P. Heritage, M. Y. Hong, and Y. H. Chang, "Femtosecond hybrid mode-locked semiconductor laser and amplifier dynamics," Appl. Phys. B, 58, 183–195 (1994).

47. P. W. Smith, Y. Silberberg, and D. A. B. Miller, "Mode locking of semiconductor diode lasers using saturable excitonic nonlinearities," J. Opt. Soc. Amer. B, 2, 1228-1236 (1985).

48. P. J. Delfyett, L. T. Florez, N. Stoffel, T. Gmitter, N. C. Andeadakis, Y. Silberberg, J. P. Heritage, and G. A. Alphonse, “High-power ultrafast laser diodes,” IEEE J. Quantum Electron., 28, 2203–2219 (1992).

49. H. A. Haus and Y. Silberberg, ‘‘Theory of mode-locking of a laser diode with a multiple-quantum-well structure,’’ J. Opt. Soc. Am. B, 2, 1237–1243 (1985).

50. H. A. Haus, “Theory of mode locking with a slow saturable absorber,” IEEE J. Quantum Electron., 11, 736-7461 (1975).

51. E. B. Treacy, “Optical pulse compression with diffraction gratings”, IEEE Journal of Quantum Electronics, 5, 454-458 (1969).

52. Ultrafast laser pulse phenomena. Fundamentals, techniques, and applications on a femtosecond time scale, Jean-Claude Diels, and Wolfgang. Rudolph, San Diego, California, Academic Press (1996).

53. O. E. Martinez, “Grating and prism compressors in the case of finite beam size,” J. Opt. Soc. Amer. B, vol. 3, pp. 929-934, 1986.

54. K. L. Hall, G. Lenz, A. M. Darwish, and E. P. Ippen, “Subpicosecond gain and index nonlinearities in InGaAsP diode lasers,” Opt. Commun., 111, 589-612 (1994).

55. K. L. Hall, E. R. Thoen, and E. P. Ippen, “Nonlinearities in active media,” in Nonlinear optics in semiconductors II, E. Garmire and A. Kost, Eds., San Diego, CA: Academic (1999).

56. J. Mork, M. L. Nielsen, and T. W. Berg, “The dynamics of semiconductor optical amplifiers, modeling and applications,” Opt. Photon. News, 42-48 (July 2003).

57. R. R. Alfano and P. P. Ho, ‘‘Self-, cross-, and induced-phase modulations of ultrashort laser pulse propagation,’’ IEEE J. Quantum Electron. 24, 351–364 (1988).

58. P. J. Delfyett, Y. Silberberg, and G. A. Alphonse, “Hot-carrier thermalization induced self-phase modulation in semiconductor traveling wave amplifiers,” Appl. Phys. Lett., 59, 10-12 (1991).

59. S. Gee, R. Coffie, and P. J. Delfyett, “Intracavity gain and absorption dynamics of hybrid modelocked semiconductor lasers using multiple quantum well saturable absorbers,” Appl. Phys. Lett., 71, 2569-2571 (1997).

60. L. Lepetit, G. Che´riaux, and M. Joffre, ‘‘Linear techniques of phase measurement by femtosecond spectral interferometry for applications in spectroscopy,’’ J. Opt. Soc. Am. B, 12, 2467–2474 (1995).

61. W. H. Knox, R. L. Fork, M. C. Downer, D. A. B. Miller, D. S. Chemla, and C. V. Shank, “Femtosecond dynamics of resonantly excited excitons in room-temperature GaAs quantum wells”, Phys. Rev. Lett., 54, 1306-1309 (1985).

62. W. H. Knox, C. Hirlimann, D. A. Miller, J. Shah, D. C. Chemla, and C. V. Shank, “Femtosecond excitation of nonthermal carrier populations in GaAs quantum wells,” Phys. Rev. Lett., 56, 1191-1193 (1986).

63. M. Mielke, G. A. Alphonse, and P. J. Delfyett, “60 channel WDM transmitter using multiwavelength modelocked”, Electron. Lett., 38, 368-370 (2002).

64. P. J. Delfyett, H. Shi, S. Gee, C. P. J. Barty, G. Alphonse, and J. Connolly, “Intracavity spectral shaping in external cavity mode-locked semiconductor diode lasers,” IEEE J. Selected Topics Quantum Electron., 4, 216–223 (1998).

65. M. Mielke, G. A. Alphonse, and P. J. Delfyett, “Suppression of mode partition noise in a multiwavelength semiconductor laser through hybrid mode locking,” Opt. Lett., 27, 1064–1066 (2002).

66. J. Zhou, N. Park, J. W. Dawson, and K. L. Vahala, “Highly nondegenerate four wavemixing and gain nonlinearity in a strained multiple quantum well optical amplifier,” Appl. Phys. Lett., 62, 301-2303 (1993).

67. A. Mecozzi, S. Scotti, A. D'Ottavi, E. Iannone, and P. Spano, “Four-wave mixing in traveling-wave semiconductor amplifiers,” IEEE J. Quantum Electron., 31, 689-699 (1995).

68. H. Shi, I. Nitta, A. Schober, P. J. Delfyett, G. Alphonse, and J. Connolly, ‘‘Demonstration of phase correlation in multiwavelength mode-locked semiconductor diode lasers,’’ Opt. Lett., 24, 238–240 (1999).

69. M. Y. Hong, Y. H. Chang, A. Dienes, J. P. Heritage, P. J. Delfyett, S. Dijaili, and F. G. Patterson, “Femtosecond self- and cross-phase modulation in semiconductor laser amplifiers,” IEEE J. Select. Topics Quantum Electron., 2, 523-539 (1996)

70. L. A. Jiang, S. T. Wong, M. E. Grein, E. P. Ippen, and H. A. Hauss, “Measuring timing jitter with optical cross correlations”, IEEE J. Quantum Electron., 38, 1047-1052 (2002).